Nd ISOTOPIC MAPPING OF THE CENTRAL GRENVILLE PROVINCE IN THE LAC ST. JEAN REGION, QUEBEC

Nd ISOTOPIC MAPPING OF THE CENTRAL GRENVILLE PROVINCE IN THE LAC ST. JEAN REGION, QUEBEC

BY

CHRISTOPHER MARTIN, B.Sc.(HON.)

A Thesis

Submitted to the School of Graduate Studies

in Partial Fulfilment of the Requirements

for the Degree

Master of Science

McMaster University

September, 1995

MASTER OF SCIENCE (1995) McMASTER UNIVERSITY

(Geology) Hamilton,

Ontario

TITLE : Nd Model Age Mapping of the Central Grenville Province in the Lac St. Jean Region, Quebec.

AUTHOR : Christopher L. Martin

B. Sc. Honours (McMaster University)

SUPERVISOR : Dr. A.P. Dickin

NUMBER OF PAGES : xiv, 160

Abstract

Detailed Neodymium (Nd) and Lead (Pb) isotopic mapping was performed on gray gneisses from the Lac St. Jean region of Quebec, in the Central Grenville Province. The Nd model ages determined were based upon the Depleted Mantle Model of DePaolo (1981c). The use of this model is justified by a Sm-Nd whole-rock isochron as well as common Pb-Pb whole-rock dating.

The field area was divided up into three sections: Western, Central, and Eastern. The boundaries of these divisions corresponded to abrupt changes in Nd model ages. The Western section was located in the Parautochthonous Belt of Rivers et al., (1989) and almost exclusively consisted of tonalitic gray gneisses with Archean Nd model ages. Whole-rock Pb isotopic analyses produced a Transposed Palaeoisochron, implying that the rocks of the Western section were significantly affected by the Grenville event approximately 1.1 Ga ago. Major and trace element analyses indicate that the Western section represents an arc and may be the exhumed basement of the Abitibi Volcanic Belt to the north, consistent with previous work by Ciesielski (1992).

In contrast to the Western section, the Central section which is separated from the Western section by the Allochthon Boundary Thrust of Rivers et al., (1989) has a very wide range of Nd model ages from 1.65 Ga to 2.35 Ga. The temporal and spatial range of Nd model ages, coupled with major and trace element analyses, indicates that the Central section represents an Andean style ensialic continental margin arc. The diapirs that reworked these rocks contain varying amounts of Archean material implied by the Early-Proterozoic Nd model ages of some samples, particularly in regions close to the Allochthon Boundary Thrust. Whole-rock Pb isotopic analyses produce a Transposed Palaeoisochron indicating significant U depletion caused by the Grenville orogeny.

The Eastern section is composed almost exclusively of gneisses with Nd model ages of ca. 1.5 Ga. The boundary between the Central and Eastern sections is based solely on lithological differences and an isotopic age break form the variable Nd model ages of the Central section, to the consistent model ages of the Eastern section. A Sm-Nd isochron for all samples with ca. 1.5 Ga Nd model ages produces an age of 1.50 +/- 0.07 Ga, in close agreement with previous work (Dickin and Higgins, 1992). The consistency of model ages (> 100,000 Km^2 when combined with data from Dickin and Higgins, 1992) coupled with major and trace element analyses, indicates the presence of an island arc

which formed at ca. 1.5 Ga and was sutured on to the Laurentian craton within 100 Ma of its formation.

Whole-rock Pb isotope analyses indicate that the Eastern section was not affected by the Grenville event as much as the Central or Western sections were.

Pb-Pb zircon dating for samples from the Central and Eastern sections failed to place a tight constraint between crystallization ages and Nd model ages because of excessive Pb loss.

ACKNOWLEDGEMENTS

I wish to thank my supervisor, Dr. Alan P. Dickin for his advice and for suggesting this research project. I would also like to thank Catharina Jaeger and Karen Goodger for assistance in the clean lab, and Jim McAndrew for his XRF analyses.

Gratitude for help with the omnivorous VG Isolab is given to Tuong Nguyen, and graduate student Cherylyn Hiekoop. Thanks is also extended towards Anlin Guo for field assistance and intellectually stimulating conversations.

I would also like to thank Weeks Home Hardware (" your one-stop department hardware store ") for cardboard boxes.

A special thanks is given to Sophie Martin and Darlene Djumlin for support and typing respectively, throughout my university career.

TABLE OF CONTENTS

LIST OF FIGURES

FIGURE **PAGE**

APPENDIX

LIST OF TABLES

CHAPTER 1

INTRODUCTION

In order to understand the growth of the continental crust over geological time, it is necessary to reconstruct ancient orogenic belts. However, conventional methods such as stratigraphy, sedimentology, or paleontology cannot be applied to reconstruct ancient orogenic belts because this evidence is either absent or erased by metamorphism. However, isotopic studies, coupled with major and trace element geochemical analyses are capable of elucidating the history of these belts. In many cases, isotope geochemistry is the only method that can provide absolute age constraints on the history of crustal genesis and terrane amalgamation associated with ancient orogenies (e.g. Moorbath et al., 1969; Jacobsen and Wasserburg, 1978a; Nelson and DePaolo, 1985; Dickin and McNutt, 1989).

The Grenville Province in North America is an important example of an ancient orogeny. Isotopic studies of the Grenville Province, however, must contend with the intense metamorphism (amphibolite to granulite grade) associated with the ca. 1.0 Ga mountain-building event. While many

isotopic dating systems such as K-Ar or Rb-Sr are unable to remain closed at such high levels of metamorphism, other isotopic dating systems, such as Sm-Nd and U-Pb have proven quite useful for determining the pre-Grenvillian history of this orogenic belt.

Nd model age dating has been successfully used as a reconnaissance tool for mapping crustal formation ages and locating sutures between different aged terranes over large geographical regions in Ontario, Canada (e.g. Dickin and McNutt, 1989; Dickin et al., 1990). Similarly, Sm-Nd studies done in Quebec, Canada have also revealed large terranes with the same crustal formation age that were previously unrecognised (Dickin and Higgins, 1992).

U/Pb dating of zircons has also been used successfully in the Grenville Province (Easton, 1986; VanBreemen et al., 1986; Krogh et al., 1990; Ketchum et al., 1994). Zircons are ideal minerals for determining crystallization ages for high-grade metamorphic rocks because they are fairly resistent to isotopic resetting. However, metamorphic zircons frequently contain younger metamorphic rims surrounding older cores. Thus, to accurately date the time of igneous crystallization, the metamorphic rims should be removed. Methods developed such as air abrasion (Krogh, 1982b) are effective for removing younger metamorphic rims. However, this method is quite labor intensive and is not useful for recconaiscance

studies.

Pb-Pb dating of zircons by direct evaporation, on the other hand, is a good alternative to U/Pb dating because far less time and effort is required. Although Pb-Pb dating of zircons cannot differentiate between discordant and concordant samples, it can still yield fairly precise estimations of igneous crystallization dates (Mueller, 1991; Martin, 1992).

The purpose of the present study is to utilise Sm-Nd and Pb-Pb dating techniques as reconnaissance tools in the Central Grenville Province in the Lac St. Jean region of Quebec. This isotopic reconnaissance study will attempt to characterize the crustal formation ages in the Lac St. Jean region of Quebec, and correlate these results with other isotopic studies done east and west of this area (Martin, 1992; Guo and Dickin, 1992; Dickin and Higgins, 1992). The results will also be used to test established structural-tectonic models for this region of the Grenville Province (e.g. Rivers et al., 1989), and to develop a credible tectonic model for the rocks in the Lac St. Jean area of Quebec.

CHAPTER 2

GEOLOGICAL BACKGROUND

2.1 The Grenville Province

The Grenville geological province encompasses a large area of the North American craton. The 1,000,000 km^2 of exposed Grenville in Canada stretches nearly 2000 km from Labrador to South Central Ontario. Northwest of the Grenville province lies the Archean aged Superior province, while the southeast margin of the Grenville is bounded by the Appalachian orogeny, and is covered in part, by Palaeozoic cover. Figure 2.1 illustrates the location of the exposed Grenville province basement in North America.

The Grenville orogeny represents the youngest mountain building episode of the Canadian Shield (Moore, 1986) and was first distinguished from adjacent regions based on structural differences and changing degrees of deformation. Wynne-Edwards (1972) divided the Grenville into seven major sections: the Grenville Foreland Belt, the Grenville Front Tectonic Zone, the Central Gneiss Belt (subdivided geographically into the Ontario and Quebec Gneiss segments), the Central Metasedimentary Belt, the Central Granulite

Figure 2.1: The geographical location of the Grenville Province in Canada and the Northeastern U.S. (Figure 1 after Rivers et al., 1989)

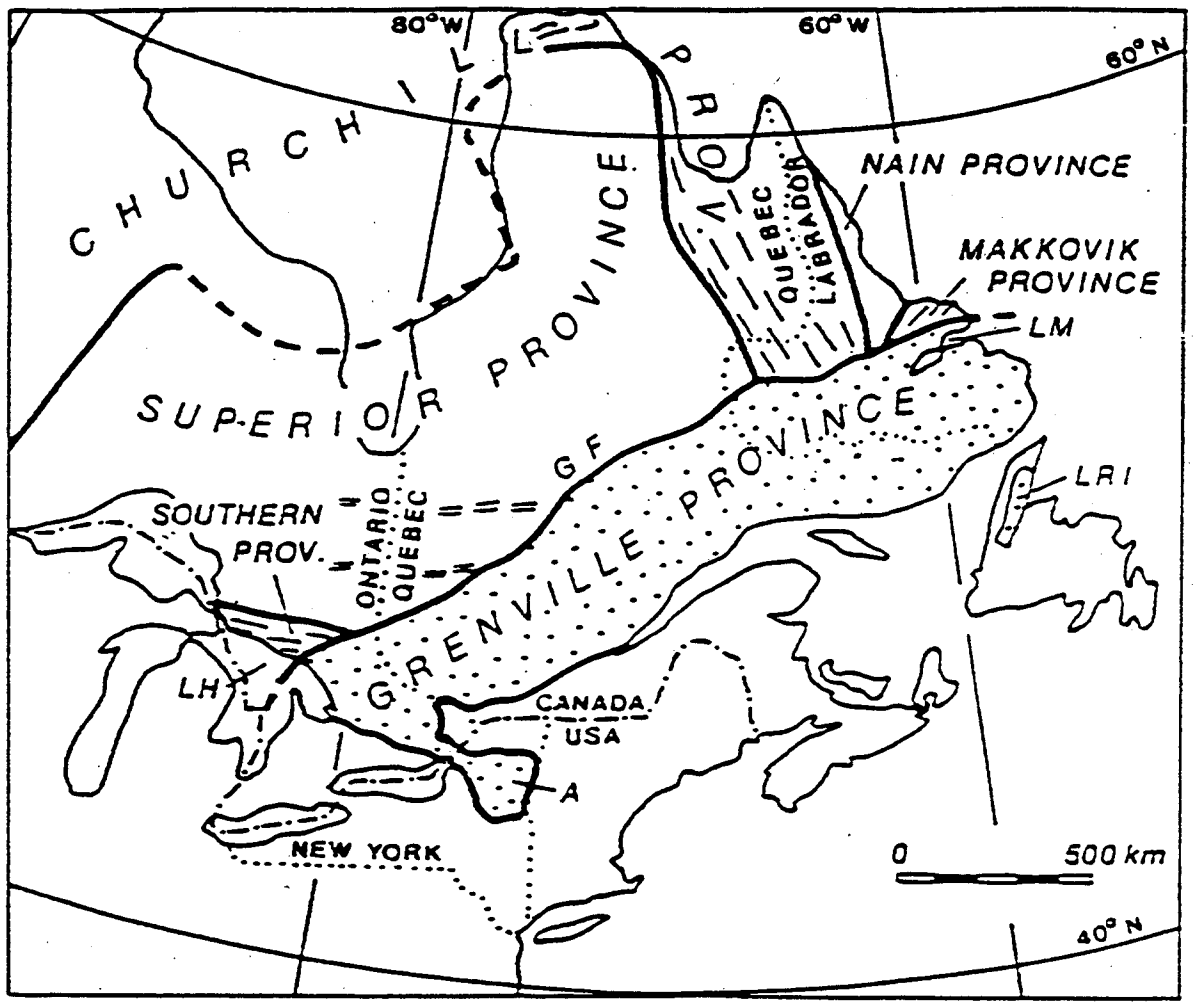
80°W
60°W
60°N
CHURCH
SUPERIOR PROVINCE
PROVINCE
QUEBEC
LABRADOR
NAIN PROVINCE
MAKKOVIK
PROVINCE
LM
GF
GRENVILLE PROVINCE
LRI
SOUTHERN
PROV.
ONTARIO
QUEBEC
LH
CANADA
USA
A
NEW YORK
0
500 km
40°N

Figure 2.2: The tectonic framework of the Grenville Province in Canada showing the initial divisions of Wynne-Edwards (1972)

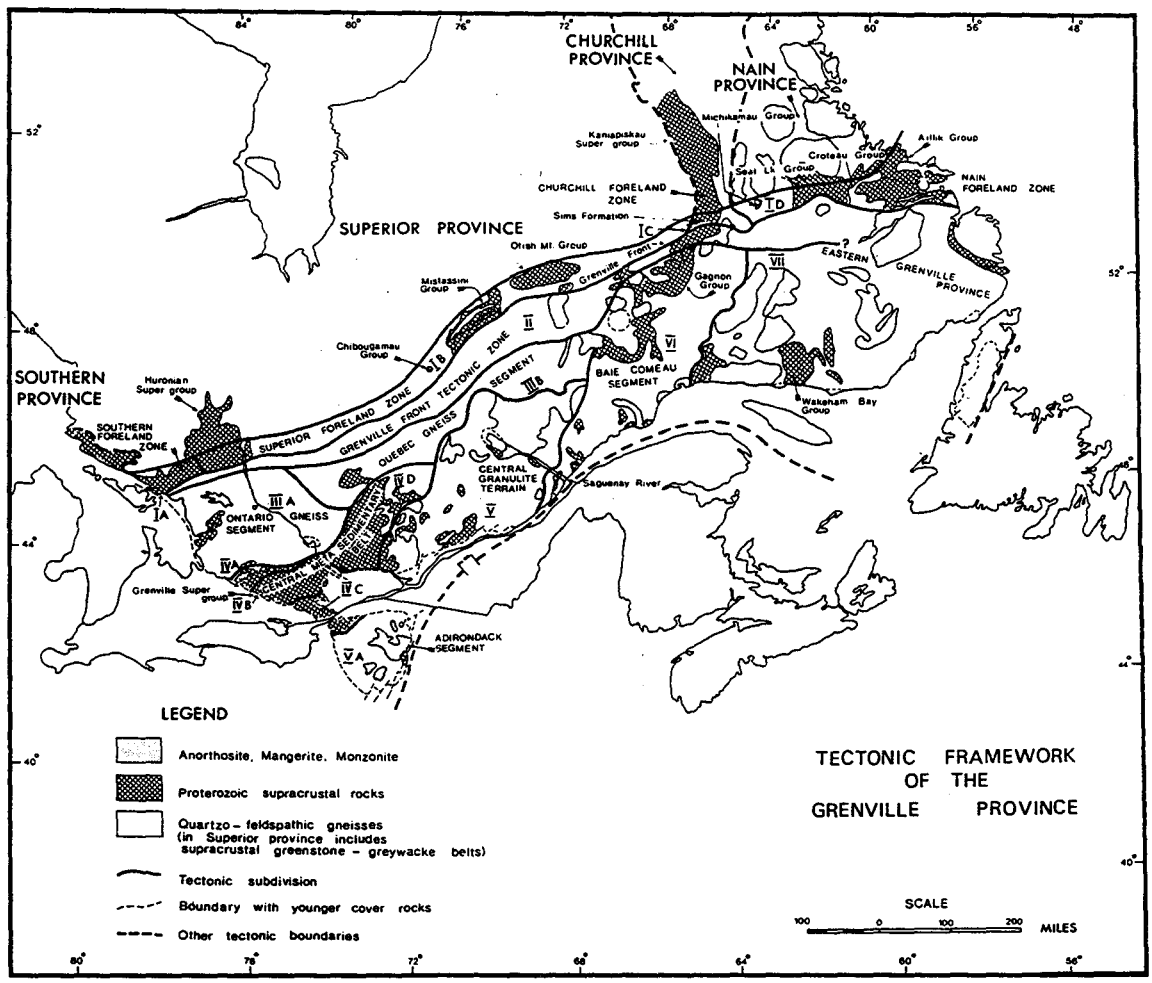
CHURCHILL PROVINCE
NAIN PROVINCE
SUPERIOR PROVINCE
SOUTHERN PROVINCE
CHURCHILL FORELAND ZONE
NAIN FORELAND ZONE
EASTERN GRENVILLE PROVINCE
SUPERIOR FORELAND ZONE
GRENVILLE FRONT TECTONIC ZONE
QUEBEC GNEISS SEGMENT
BAIE COMEAU SEGMENT
CENTRAL GRANULITE TERRAIN
ONTARIO GNEISS SEGMENT
CENTRAL METASEDIMENTARY BELT
ADIRONDACK SEGMENT
SOUTHERN FORELAND ZONE
Huronian Super group
Grenville Super group
Kamaplskau Super group
Michikamau Group
Seal La Group
Croteau Group
Attik Group
Sims Formation
Otish Mt. Group
Mistassini Group
Chibougamau Group
Gagnon Group
Wakeham Bay Group
Saguenay River
Grenville front
LEGEND
Anorthosite, Mangerite, Monzonite
Proterozoic supracrustal rocks
Quartzo-feldspathic gneisses (in Superior province includes supracrustal greenstone - greywacke belts)
Tectonic subdivision
Boundary with younger cover rocks
Other tectonic boundaries
TECTONIC FRAMEWORK OF THE GRENVILLE PROVINCE
SCALE
100 0 100 200 MILES

Terrain, the Baie Comeau Segment, and the Eastern Grenville province (Figure 2.2).

These Grenville sub-provinces were recognized by Grenvillian geologists for nearly 17 years. However, recent work has produced new tectonic subdivisions of the Grenville province. The new divisions developed by Rivers et al., (1989) differ from those of Wynne-Edwards (1972) and are based on structural, geophysical, and geochronological data. These new divisions define three first order tectonic boundaries separating three first order longitudinal belts. The new tectonic framework for the Grenville is shown in Figure 2.3. In the north, the Grenville Front marks the northwesterly limit of Grenvillian metamorphic and deformational effects. South of the Grenville Front lies the Parautochthonous Belt, within which lateral transport of crustal blocks is thought to be of limited extent. This belt is up to 150 km wide and contains a number of Archean and Proterozoic terranes that are separated by second order Grenville tectonic boundaries.

The Allochthon Boundary Thrust divides the Parautochthonous Belt to the north from the Allochthonous Polycyclic Belt to the south. The Allochthon Boundary Thrust is thought to represent a locus of major thrust displacements to the northwest. The Allochthonous Polycyclic Belt is composed of transported terranes and in part, tectonically

overlies the Parautochthonous Belt in the north.

Not only does the Allochthon Boundary Thrust represent a structural discontinuity, it also corresponds to a discontinuity in isotopic ages. In general, the Allochthon Boundary Thrust
divides Archean aged Superior Province rocks to the north from Proterozoic aged rocks in the Allochthonous Polycyclic Belt to the south. The terranes of the Allochthonous Polycyclic Belt represent pre-Grenvillian, high grade gneissic accretionary blocks, composed of ortho- and paragneisses that are interspersed with orogenic and anorogenic intrusions of granite, gabbro, and anorthosite. These rocks produce a range of ages from early to late Proterozoic, and were likely subjected to two and maybe even three metamorphic events.

The Monocyclic Belt Boundary zone separates the polycyclic rocks to the north from monocyclic rocks to the south. The Allochthonous Monocyclic Belt to the south of this boundary represents a series of terranes containing only Grenvillian-aged metamorphic signatures.

Although this new tectonic framework satisfactorily divides the Grenville Province on a regional scale, it does not address secondary boundaries that are contained within the first order belts, particularly in the Allochthonous Polycyclic Belt. For instance, within the Ontario segment of the Central Gneiss Belt, detailed structural mapping has

Figure 2.3: The new tectonic divisions of the Grenville Province. A = Parautochthonous Belt; B = Allochthonous belts (after Rivers et al., 1989)

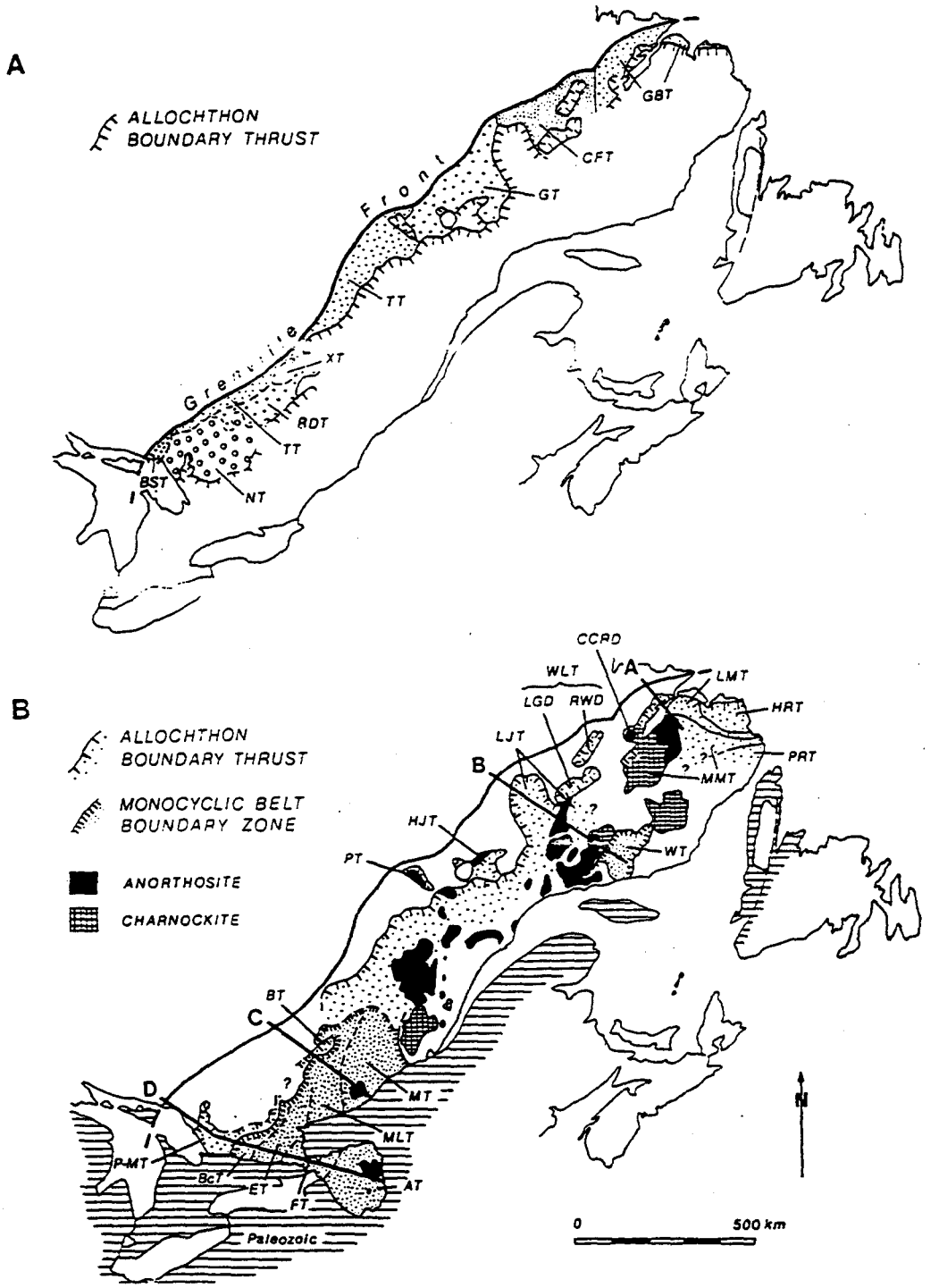
A
ALLOCHTHON
BOUNDARY THRUST
Grenville Front
GBT
CFT
GT
TT
XT
BDT
TT
BST
NT
B
ALLOCHTHON
BOUNDARY THRUST
MONOCYCLIC BELT
BOUNDARY ZONE
ANORTHOSITE
CHARNOCKITE
CCRD
WLT
A
LMT
LGD
RWD
HRT
LJT
PRT
B
MMT
HJT
WT
PT
BT
C
D
MT
MLT
P-MT
BcT
ET
FT
AT
Paleozoic
N
0
500 km

revealed a series of domains and subdomains (Davidson, 1986; Davidson and Grant, 1986; Hamner, 1988). These lithotectonic domains and subdomains result from the Grenville orogeny, which produced crustal shortening and thickening along inclined ductile shear zones. Figure 2.4 is a map representing the domains of Davidson and Grant (1986). The numbers, from 1 to 4, represent the stacking order resulting from Grenville thrusting approximately 1.0 Ga ago. However, Culshaw et al. (1990) revised the stacking order making the Grenville foreland the basal block, the Britt domain the second block, the Shawanaga domain the third block, and the Parry Sound domain the fourth block, and the Moon River, Rosseau, and Seguin domains the top of the thrust stack. These detailed structural studies reveal the complexity of the " geological jigsaw puzzle " that comprises the Grenville Province.

Not only is the Grenville Province structurally complex, it is also geochronologically complex. There has been a substantial volume of geochronological work done in the Grenville Province using a variety of methods. Easton (1986) documented much of the work done in the Grenville up until May, 1985. The data show a very wide range, from K/Ar cooling as oages of approximately 1.0 Ga, to igneous crystallization ages ld as 2.7 Ga. Archean ages are almost entirely contained in the Parautochthonous Belt (Frith and Doig, 1975; Krogh et

Figure 2.4: Lithotectonic domains and subdomains of Davidson and Grant (1986). Stacking order due to Grenville thrusting. Stack 1: B - Britt, K - Kiosk, R - Rosseau, G - Go Home, N - Novar, H - Huntsville, MC - McCraney, ML - McLintock, O - Opeongo. Stack 2: PS - Parry Sound. Stack 3: M - Muskoka, MR - Moon River, S - Seguin. Stack 4: CMBBZ - Central Metasedimentary Belt Boundary Zone. Shaded area indicates field area of Davidson and Grant.

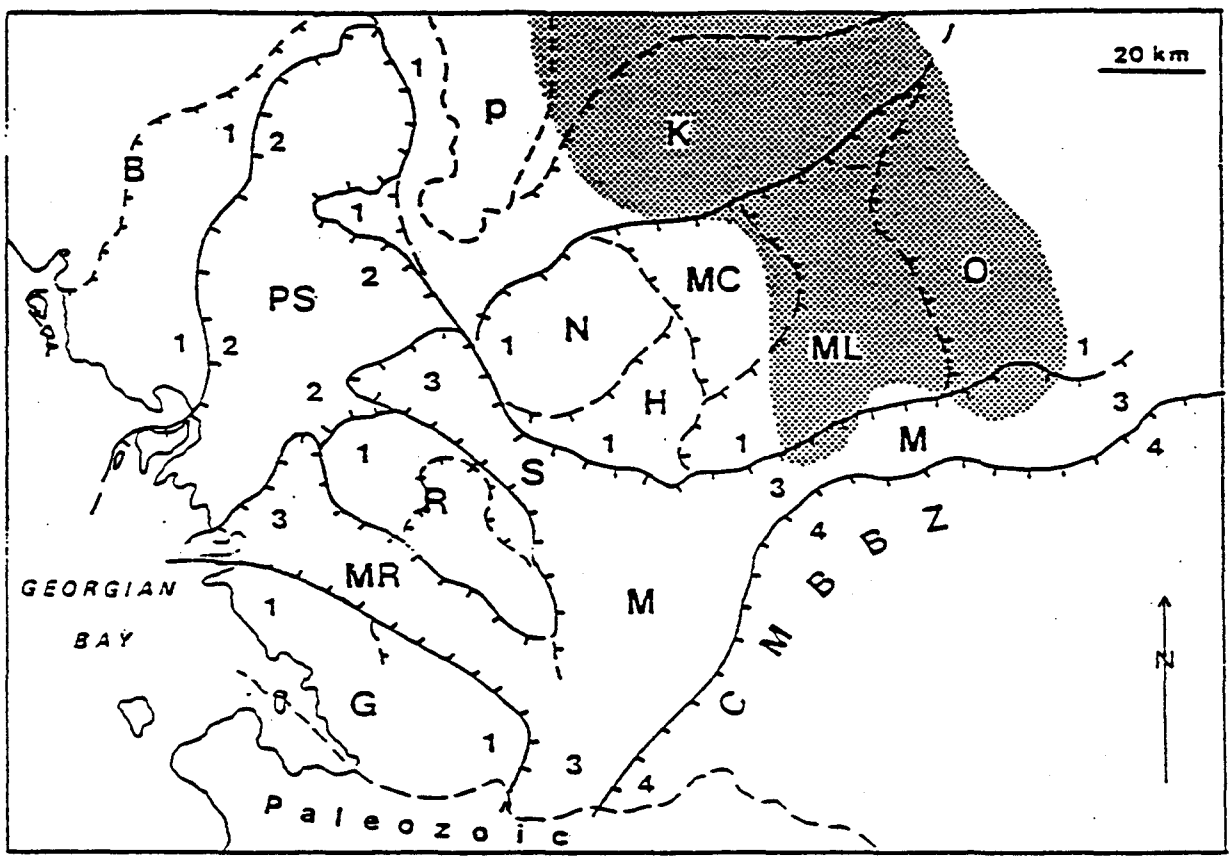
20 km
B
P
K
PS
MC
N
ML
O
H
M
S
R
MR
M
G
GEORGIAN
BAY
Paleozoic
CMBBZ
N

al., 1990; Ciesielski, 1992), consistent with the interpretation that the Parautochthonous Belt represents the uplifted basement of the Abitibi Greenstone Belts of the Superior Province to the north (Ciesielski, 1992).

The rocks of the Allochthonous Polycyclic Belt, on the other hand, represent a range of ages from early to late Proterozoic. For example, in the Eastern Grenville Province there is evidence of an orogeny that occurred approximately 1.65 Ga ago (Labrador Orogeny: Thomas and Nunn, 1986; Wardle et al., 1986). The high grade gneiss terranes that compose the Labrador orogeny stretch from Labrador to eastern Quebec, and have produced U-Pb zircon ages as old as 1720 Ma. Similarly, Van Breeman et al., (1986) obtained upper intercept U-Pb zircon ages of approximately 1.46 Ga for granulite grade rocks from the Algonquin domain in the western Grenville Province in Ontario. Recently, Ketchum et al., (1994) have reported U-Pb zircon ages as old as of 1.74 Ga from the Central Gneiss Belt in Ontario.

This wide chronological range exemplifies the fact that the Grenville Province, and in particular, the Allochthonous Polycyclic Belt, has suffered a polymetamorphic, polygenetic, history.

In contrast to the use of U-Pb to determine igneous crystallisation, the Sm-Nd dating system is best suited for dating crustal formation ages of high grade metamorphic rocks.

This is because Rare Earth Elements (REE) are far less mobile than other elements such as Rb, Sr, U, and Pb, during metamorphism (DePaolo, 1988). In fact, Sm and Nd undergo very little relative fractionation during erosional, sedimentary, and metamorphic processes (Dickin and McNutt, 1990). Thus, the initial Sm-Nd ratio inherited in the magma body when it separated from the mantle remains largely unchanged. Sm-Nd isotopic studies have also produced mid-Proterozoic ages from the Ontario segment of the Central Gneiss Belt (eg. Dickin and McNutt, 1989; Martin, 1992). In contrast, the Allochthonous Monocyclic Belt contains rocks no older than ca. 1300 Ma (Heaman et al., 1986; Easton, 1986; Rivers et al., 1989).

As an adjunct to the Sm-Nd isotopic dating system, Pb-Pb dating can also provide information regarding the history of pre-Grenville metamorphism through the use of zircon dating and common Pb-Pb dating. Although the Pb isotopic system may not be as resistant to resetting as the Sm-Nd system, Pb-Pb zircon dating can still provide lower age limits on crystallization ages of igneous rocks. Common Pb-Pb whole rock dating can be used not only to date the time of formation of the rocks, but can also indicate if any magma mixing of older and younger components has occurred.

Finally, the use of several isotopic dating systems for the same samples is essential for geochronological studies

because it allows for comparison of results from independent isotopic systems.

2.2 THE FIELD AREA:

Figure 2.5 represents the field area in relation to the tectonic divisions of Rivers et al.,(1989). The field area covered approximately 100,000 km^2, extending northwards from the southern edge of Lac St. Jean (48^0 15′ N) to Lac Peribonca (50^0 15′ N) and is bounded to the west by the Gouin Reservoir, (approximately 74^0 30′ W) and to the east by the Pipmuacan Reservoir (70^0 30′). Sampling could not be extended beyond the Gouin Reservoir or Pipmuacan Reservoir because of the lack of forestry access roads.

Frith and Doig (1975) recognized a distinct change in aeromagnetic signatures along Highway 167 approximately 150 km northwest of Roberval in the Lac St. Jean area of Quebec. Frith and Doig (1975) defined the " aeromagnetic discontinuity " which separates diffuse magnetic patterns to the north from intense swirling patterns to the south. Their initial geochronological work using Rb-Sr revealed Archean aged (ca 3.0 Ga) tonalitic gneisses north of this aeromagnetic discontinuity, and an early-Proterozoic signature (1750 Ma) in a granitic body (the Lorne granite) south of this discontinuity. This study was one of the first to observe an

Figure 2.5: The field area shown with the tectonic divisions of Rivers et al., (1989).
PB = Parautochthonous belt; ABT = Allochthon Boundary Thrust; APB = Allochthonous Polycyclic Belt
stippled area = Lac St. Jean Anorthosite
shaded area = Parent-Clova charnockite belt

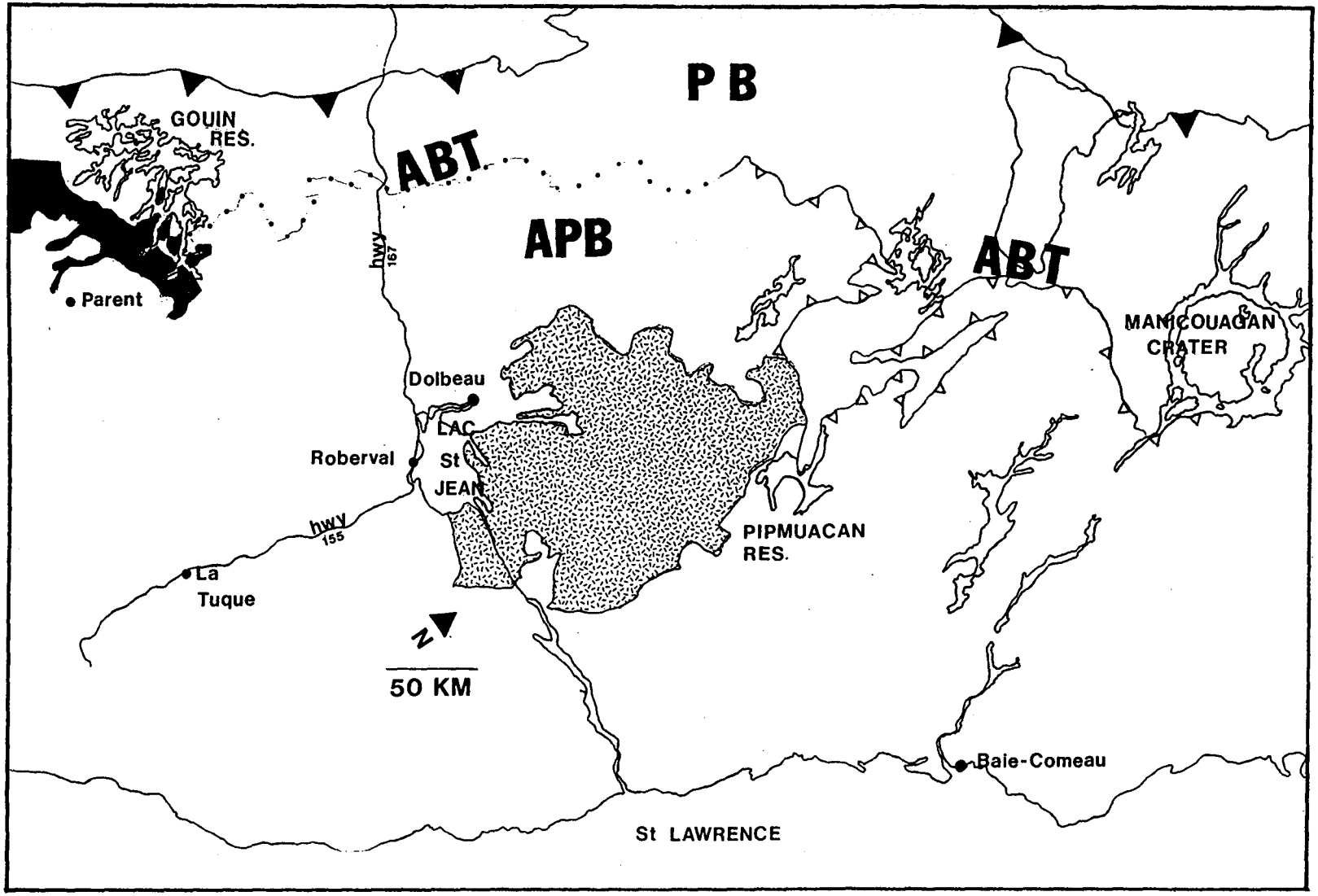
PB
ABT
APB
ABT
GOUIN
RES.
Parent
hwy
167
Dolbeau
LAC
St
JEAN
Roberval
hwy
155
La
Tuque
PIPMUACAN
RES.
MANICOUAGAN
CRATER
N
50 KM
Baie-Comeau
St LAWRENCE

isotopic age boundary which coincided with a magnetic discontinuity in the Central Grenville province in Quebec.

By 1985, aeromagnetic maps at 1:1 000 000 for the whole of the Grenville province allowed individual terranes to be recognized. Rivers et al., (1989) used the trace of the magnetic discontinuity recognized by Frith and Doig (1975), coupled with structural and geochronological data to infer the widely accepted tectonic divisions of the Grenville province recognized today (eg. PB, ABT, APB). The field area of the present study was chosen not only to provide age refinements on rocks studied by Frith and Doig (1975), but also to test the placement of the ABT by Rivers et al., (1989) in the Lac St. Jean region of Quebec. The results are presented in chapters 4, 5, and 6.

The field area represented by this study contains the southern portion of the PB, the ABT, and the APB in central Quebec. The field area has been divided up into three main sections based on Sm-Nd model age mapping performed in this study: Western, Central, and Eastern. The Western section is located in the PB, with a southern boundary coinciding with the ABT. The Central section is located in the APB, with a northern boundary coinciding with the ABT. The Eastern section is located in the APB. The boundaries between the Central and Eastern section have been defined using Sm-Nd model age mapping performed in this study, and Dickin and

Higgins (1992).

The lithologies of the field area are dominated by gneissic rocks. The geological maps produced by Ministere de l'Energie et des Ressources, Gouvernement du Quebec (MERQ) were used as an initial guideline for sampling. The field area covered portions of the following maps: 32A, 32B, 32H, 32I, 22E, and 22L. Original sampling strategies involved collection of rocks labelled as G1 (Archean gray gneiss complexes) and their migmatized equivalents (G20) on the MERQ maps. However, field observations soon indicated that areas mapped as G1 or G20 in the Allochthonous Polycyclic Belt were often incorrect because these areas contained many other lithologies. Similarly, in many circumstances, large " batholithic-proportioned " areas mapped as G19 (granitic pegmatites) seldom contained large volumes of granitic rocks, particularly the large " granitic pegmatite " on map 32 H.

However, in some circumstances, the MERQ maps were a reasonable representation of lithological distributions, particularly charnockitic rocks (G4) across the entire field area, and gray gneisses (G1) located north of the aeromagnetic discontinuity recognized by Frith and Doig (1975) (the PB of Rivers et al., (1989)).

In order to restrict analyses to older basement rocks, granitic and mafic intrusions were largely ignored. When possible, the samples were restricted to gray tonalitic

gneisses. However, some localities contained only charnockitic gneisses while other localities were dominated by migmatitic rocks. Charnockites which clearly showed evidence of melting such as large pyroxene crystals and lack of foliation were avoided. Similarly, heterogeneous migmatites which contained extensive feldspar augens were also avoided.

CHAPTER 3

ISOTOPE SYSTEMATICS

3.1 THE Nd ISOTOPIC SYSTEM:

The Sm-Nd model age system is based on the radiometric decay of ^{147}Sm to ^{143}Nd. Although the half-life of this decay is 106 Ga, it is still short enough to produce measurable differences in daughter isotope ratios. Of the seven naturally occurring Sm isotopes, two others, besides ^{147}Sm are radioactive: ^{148}Sm and ^{149}Sm. ^{148}Sm decays to ^{144}Nd while ^{149}Sm decays to ^{145}Nd (DePaolo, 1988). However, ^{148}Sm and ^{149}Sm have such long half-lives (approximately 1×10^{16} years) that their decay does not alter ^{144}Nd and ^{145}Nd abundances significantly.

Nd has seven naturally occurring isotopes as well: ^{142}Nd, ^{143}Nd, ^{144}Nd, ^{145}Nd, ^{146}Nd, ^{148}Nd, and ^{150}Nd. Of these isotopes, ^{144}Nd is the second most abundant and is considered to be stable and therefore used as a normalization isotope, even though ^{144}Nd is actually radioactive. However, ^{144}Nd decaying to ^{140}Ce has such a long half-life ($>10^{14}$ Ga) that during the 4.5 Ga history of the Earth, ^{144}Nd has only decreased by 0.00015% which is less than analytical precision (DePaolo,

1988).

The decay of ^{147}Sm to ^{143}Nd, normalized with ^{144}Nd, is the basis of Sm–Nd geochronology. By determining the Sm and Nd isotopic abundances, an equation can be written in the form y = mx + b :

$$\frac{^{143}Nd}{^{144}Nd_{present}} = \frac{^{143}Nd}{^{144}Nd_{initial}} + \frac{^{147}Sm}{^{144}Nd}\left(e^{\lambda t} - 1\right)$$

Thus, by measuring the present day $^{143}Nd/^{144}Nd$ and $^{147}Sm/^{144}Nd$ ratios of the rock in question, it is possible to determine the initial $^{143}Nd/^{144}Nd$ by extrapolation, as well as the isochron age of the rock, t. However, isochrons require large numbers of samples for each age determination. But, if the isotopic evolution of the rock forming reservoir could be modelled, then it would be possible to determine the age of a single rock sample.

3.2 Nd MODEL AGES:

The Earth's crust has evolved through time by selective removal of low density elements from the Earths mantle. Although some low density continental material may get subducted at convergent plate boundaries (White and Dupre,

1986), most lighter (sialic) material remains on the Earths surface. The net result is the generation of a mantle that has been depleted in large ion lithophiles. Large ion lithophiles such as Nd and Sm represent incompatible elements that are easily melted off and the last elements to solidify during the evolution and cooling of a magma body. Thus, over time, Sm and Nd have changed their isotopic composition in the Earth's mantle.

Early models (eg. DePaolo and Wasserburg, 1976b) for the Nd isotope evolution of the Earths interior were based on the isotopic ratios measured in chondritic meteorites. Chondrites contain both refractory elements as well as volatiles. The presence of both high and low temperature elements suggests that chondrites had not undergone substantial fractionation. Therefore, the isotopic ratios observed in chondrites should represent the Uniform Reservoir from which all planets in the solar system had formed. This has led to the **CHUR** (**CH**ondritic **U**niform **R**eservoir) model for the isotopic evolution of Sm and Nd. The CHUR model assumes that the Earth's interior has not undergone substantial differentiation and that continental material formed directly from the uniform reservoir. The reservoir has only changed its isotopic composition due to the decay of ^{147}Sm to ^{143}Nd ($t_{1/2}$ = 106 Ga). Thus, by measuring Sm and Nd isotope ratios in a sample, a model age could be determined for that sample,

provided that during the crustal extraction event, there was sufficient fractionation between Nd and Sm. The model age calculated for the sample corresponds to the time in the past when the Nd isotopic ratio of the sample equalled that of the Chondritic Reservoir. This model age equation is shown below:

$$t = \frac{1}{\lambda} \ln \left| \frac{(^{143}/_{144})^{present}_{sample} - (^{143}/_{144})^{present}_{CHUR}}{(^{147}/_{144})^{present}_{sample} - (^{147}/_{144})^{present}_{CHUR}} \right| + 1$$

This equation can be used to calculate the model age of the sample provided that the Sm/Nd ratio of the sample did not change since the time of separation from the chondritic reservoir.

However, unlike the chondrites, the Earth has differentiated through time. Thus, the Sm-Nd evolution in the fractionated mantle differs from the Sm-Nd evolution in the unfractionated chondritic reservoir. The Sm-Nd fractionation has occurred because Sm and Nd behave slightly differently during melting events. While both elements tend to increase in concentration in the liquid fraction with increasing amounts of melting, the Sm/Nd ratio tends to decrease. This occurs because partial melting of a magma will tend to increase Nd with respect to Sm. This Nd enrichment results because Nd^{3+} has a larger ionic radius than Sm^{3+}. The larger ionic radius produces a lower ionic potential. Thus, Nd^{3+}

forms weaker bonds then Sm^{3+} and therefore Nd^{3+} bonds are easier to break than Sm^{3+} bonds. The net result is that Nd gets enriched in the liquid phase relative to Sm. On the other hand, the residual solids left over will tend to have a higher Sm/Nd ratio. These residual solids are known as depleted regions, and are depleted in the light Rare Earth Elements (Nd). The Earth's mantle is a good example of a depleted region because, through time, the partial melts that formed from the mantle to produce continental material has preferentially removed Nd and left a mantle enriched in Sm relative to Nd. However, Sm and Nd are very similar chemically and only produce slight relative fractionations. Thus, the differences in the Nd isotope ratios due to ^{147}Sm decay are quite small. Therefore, in 1976 DePaolo and Wasserburg introduced the epsilon parameter. The epsilon parameter is essentially a magnified difference between the $^{143}Nd/^{144}Nd$ ratio of the sample and CHUR at some time in the past:

$$\text{Epsilon-Nd (T)} = 10^4 \frac{\left({}^{143}Nd/{}^{144}Nd_{sample} - {}^{143}Nd/{}^{144}Nd_{CHUR(T)} \right)}{\left({}^{143}Nd/{}^{144}Nd_{CHUR(T)} \right)}$$

* The initial value of $^{143}Nd/^{144}Nd$ (at time T) for the sample can be determined from a whole rock isochron.

If the sample was formed from a chondritic reservoir, then it should have had an Epsilon-Nd = 0 when it first separated. However, if the Epsilon-Nd value at time of formation t is positive, then this indicates that the sample in question was formed from a region of the Earth depleted in Nd/Sm, whereas a negative Epsilon-Nd value implies that the sample was formed from an enriched source having a lower Sm/Nd ratio than CHUR.

DePaolo and Wasserburg (1976b) analyzed rocks produced from several different types of tectonic environments. They found that Archean rocks worked quite well with the CHUR model. However, DePaolo and Wasserburg also found that young mid-ocean-ridge basalt differed considerably from the CHUR evolution line as shown in Figure 3.1 (DePaolo and Wasserburg, 1976b). However, there was no data from the Proterozoic rocks. It was not until 1981 when DePaolo analyzed Proterozoic rocks from the Colorado Front Range, that this gap was filled. These mid-Proterozoic rocks clearly had positive Epsilon-Nd values. Thus, DePaolo developed the Depleted Mantle Model (T_{dm}). This model is based on the Epsilon-Nd values of present day island arc rocks, from the basement of the Colorado Front Range, and chondritic Nd 4.6 Ga ago. DePaolo fitted a curve to these three points which represented the evolution of Nd ratios in the depleted mantle through time. Island arc rocks and calc-alkali series

Figure 3.1: Epsilon-Nd versus time illustrating that some younger samples have positive Epsilon-Nd values, indicating that these samples were formed from magma depleted in Nd (after DePaolo and Wasserburg, 1976b).

MORB = Mid Ocean Ridge Basalt.

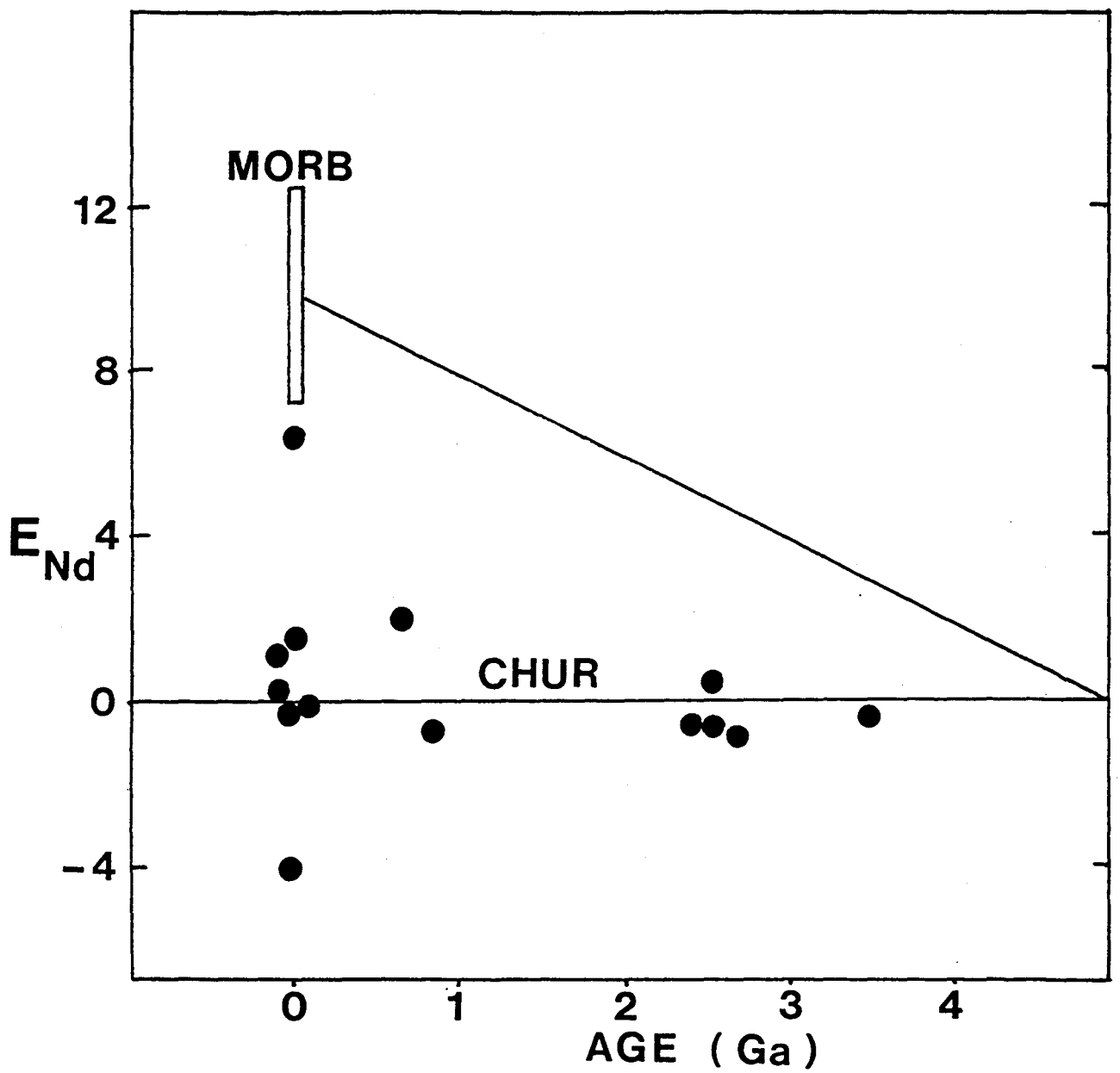
MORB
12
8
4
0
-4
E_{Nd}
CHUR
0
1
2
3
4
AGE (Ga)

volcanics were used because they are thought to directly sample the island arc magma suite, which is thought to be produced by melting of the mantle wedge overlying an oceanic subduction zone. The curvi-linear trend determined by DePaolo as compared to the CHUR at time T is given as (DePaolo, 1981c):

$$\text{Epsilon-Nd}_{(T)} = 0.25T^2 - 3T + 8.5$$

This equation represents the Nd isotopic evolution in the Earth's depleted mantle. Through time, extraction of crustal material has increased Sm/Nd ratios in the mantle, which in turn has increased the $^{143}Nd/^{144}Nd$ ratios of the mantle. Hence, material formed from a depleted region will have higher Nd ratios than material formed from CHUR. This difference corresponds to T_{dm} model ages several hundred million years older than T_{CHUR} model ages. Figure 3.2 is an illustration exemplifying the differences between the CHUR and Depleted Mantle Model.

One of the most important factors that makes the Sm and Nd geochronological system useful in multiply metamorphosed terranes such as in the Grenville Province, is that Sm and Nd experience very little relative fractionation during intra-crustal events such as erosion, sedimentation, and metamorphism.

Figure 3.2: Illustration showing the isotopic evolution of Nd for the CHUR model as well as the Depleted Mantle Model. The diagram shows the large difference in model ages calculated using the Depleted Mantle model and the CHUR model for a hypothetical sample (after DePaolo, 1981c)

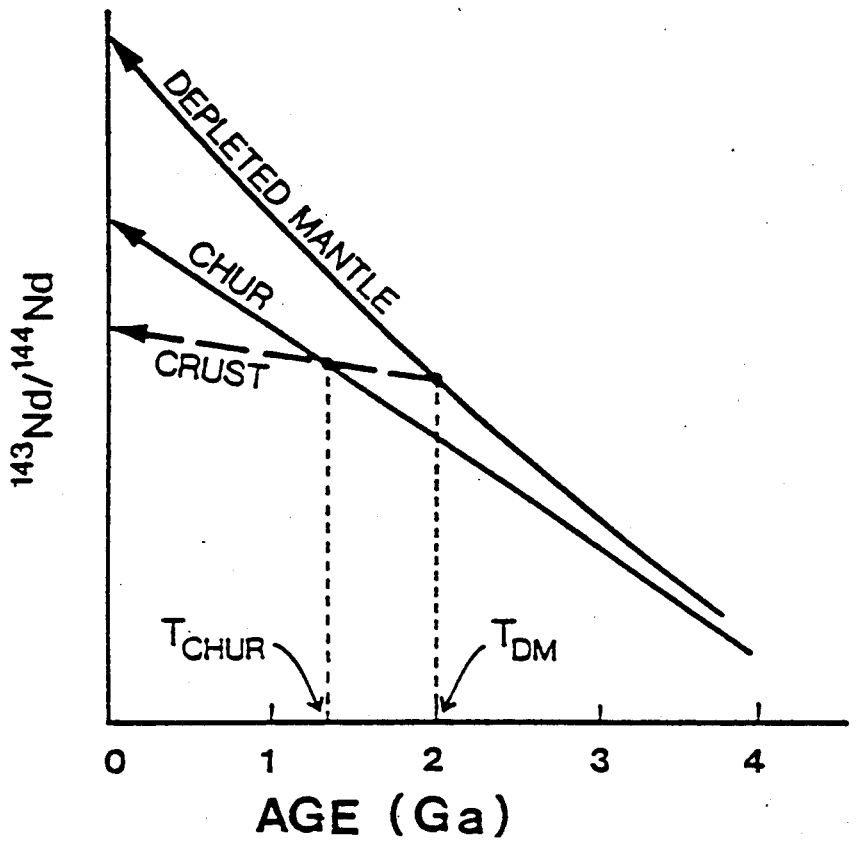
DEPLETED MANTLE
CHUR
CRUST
$^{143}Nd/^{144}Nd$
T_{CHUR}
T_{DM}
0
1
2
3
4
AGE (Ga)

For example, an isotopic study on a mylonitized granite from the Harquahala Mountains in western Arizona indicates that while Rb-Sr isotopic data produce a wide scatter on isochron diagrams, the Nd isotopic system produces good quality isochrons (Barovich and Patchett, 1991). The Sm-Nd system remains undisturbed throughout the shear zone (deformation ranging from unaltered to ultramylonite) implying that even at high grades of deformation, the Sm-Nd system remains closed. Figure 3.3 is a hypothetical example illustrating that the Nd evolution line is unaffected by metamorphism or sedimentation.

However, Arndt and Goldstein (1987) list several assumptions that must be taken into account when interpreting Nd model ages. Firstly, the isotopic evolution of the mantle source of the continents must be known. Secondly, the time of mantle extraction, crustal emplacement and crystallization is short so as not to produce significant changes to the Sm-Nd ratios. Thirdly, the Sm/Nd ratio of the rock-forming magma has not been modified by later intra-crustal events.

Ardnt's and Goldstein's third assumption is perhaps the most common reason for the misinterpretation of Nd model ages. There are several intra-crustal and crustal events that could alter the Nd isotope ratios. For instance, anatexis and assimilation of older or younger crust; sediment subduction at convergent plate boundaries in an orogenic setting;

Figure 3.3: Schematic diagram illustrating that Nd isotopic ratios are unaffected by metamorphism or sedimentation.

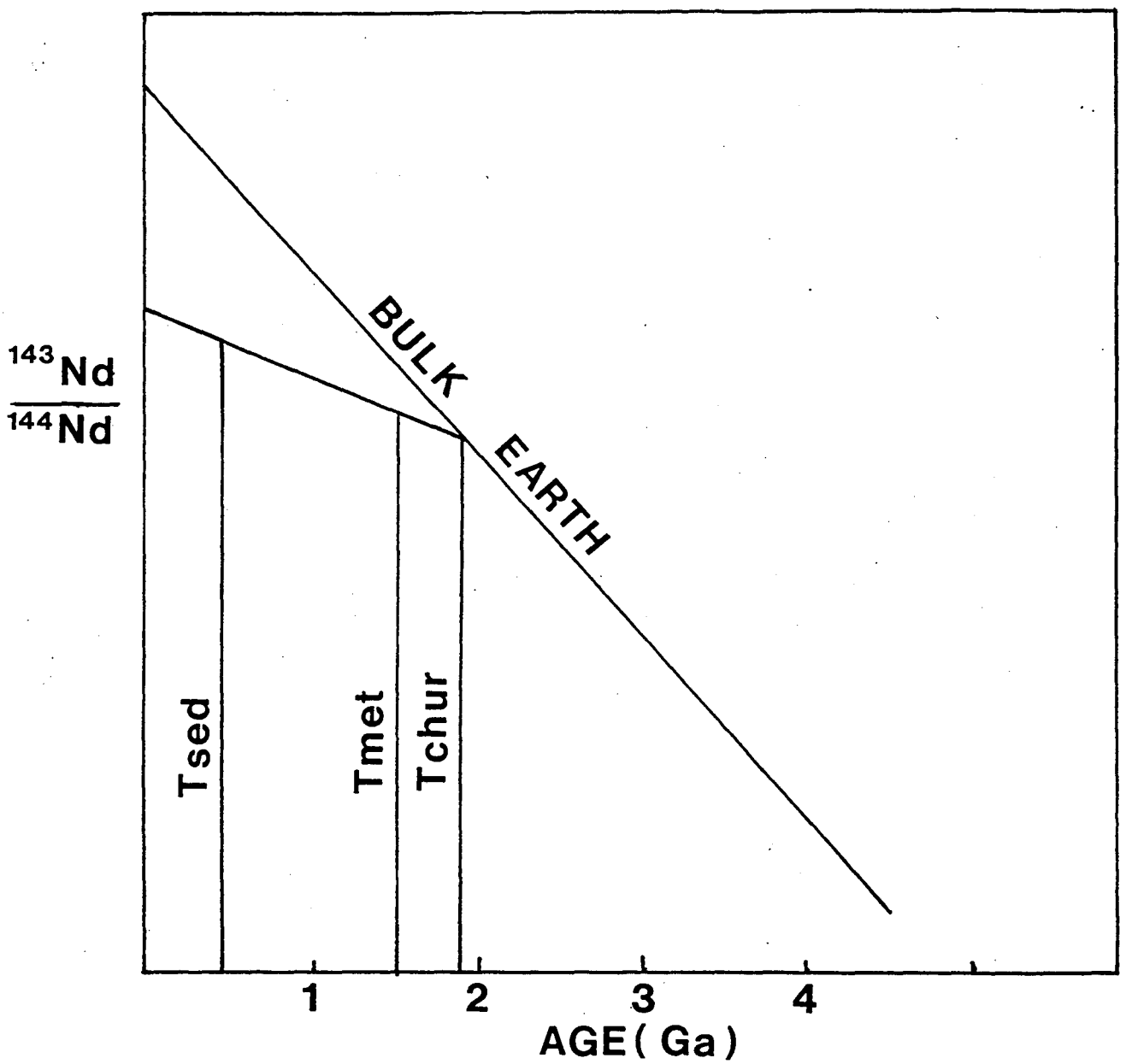
$^{143}Nd/^{144}Nd$
BULK EARTH
Tsed
Tmet
Tchur
1
2
3
4
AGE(Ga)

paragneisses with mixed provenances composed of older and younger components, and mixing of juvenile mantle-derived material with older crust, are several possibilities that may produce mixed model ages.

Figure 3.4 is an example of what may happen if a partial melt of existing continental crust mixes with a mantle derived component. Mixing at T_M produces a new Nd isotopic evolution line corresponding to a lower Epsilon-Nd value than the juvenile mantle value because the crust is Nd enriched, and therefore has negative Epsilon-Nd values. Incorporation of the older crustal material produces an older model age. Although such a result does not produce a true crustal formation age, it can be used to trace out the extent of older material at depth. For example, rocks with considerably older model ages than crystallization ages imply the partial assimilation of older crust at depth. Conversely, such a sample could also be produced by melting of older material followed by assimilation of younger material. Such possibilities underscore the need of multi-isotopic dating techniques.

Several other Depleted Mantle Models have been developed besides DePaolo's Depleted Mantle Model. One of the most significant deviations from DePaolo's model was developed by Goldstein et al., (1984). Goldstein's model is based upon a linear depletion of the upper mantle from Epsilon-Nd = 0 at

Figure 3.4: Diagram illustrating possible reasons for anomalous model ages produced from partial melting with subsequent mixing of a mantle derived component: A magma body separates from the mantle at T_{CF} and follows the " crustal source of granites " line. Then, mixing occurs at T_M and a new Nd evolution line is produced. The same type of Nd evolution line would occur if older and younger sediments mixed together. (after Nelson and DePaolo, 1985)

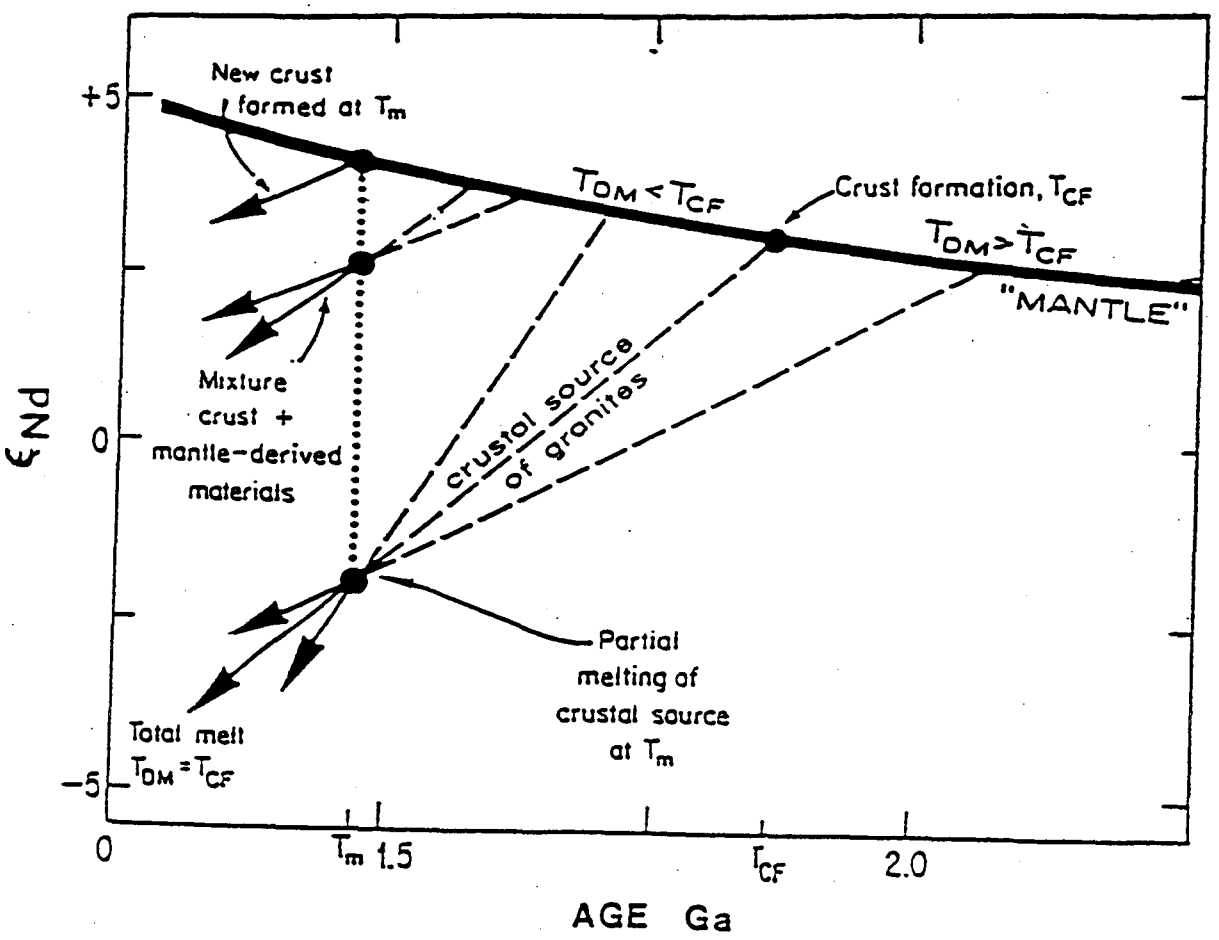
New crust
formed at T_m
+5
$T_{DM} < T_{CF}$
Crust formation, T_{CF}
$T_{DM} > T_{CF}$
"MANTLE"
Mixture
crust +
mantle-derived
materials
crustal source
of granites
ε_{Nd}
0
Partial
melting of
crustal source
at T_m
Total melt
$T_{DM} = T_{CF}$
−5
0
T_m 1.5
T_{CF}
2.0
AGE Ga

4.5 Ga ago, to Epsilon-Nd = +10 at 0 Ga. The present day Epsilon-Nd calculation was determined from MORB. However, subduction-related magmas have a lower present-day Epsilon-Nd value than MORB, and MORB are not a likely candidate for large scale continental growth because they represent spreading centres rather than collisional environments. Collisional environments are better candidates for continental growth because continental growth is based on the production and suturing of island arcs onto continental margins. Thus, DePaolo's Depleted Mantle Model is better suited for dating crust-forming events than Goldstein et al's., model.

Although other Depleted Mantle Models have been introduced, DePaolo's model has been used successfully for other Nd model age mapping in the Grenville province (Dickin and McNutt, 1989; Martin, 1992; Dickin and Higgins, 1992; Holmden and Dickin, 1995). Several of these studies contain Sm-Nd isochron ages and zircon crystallization ages that are within error of T_{dm} model ages. Thus, Depaolo's model is deemed the most useful for the present study.

3.3 THE U/Pb ISOTOPIC SYSTEM:

There are four natural isotopes of Pb: ^{204}Pb, ^{206}Pb, ^{207}Pb, and ^{208}Pb. Of these four isotopes, only ^{204}Pb is non-radiogenic. The others are the daughter products of ^{238}U, ^{235}U,

and ^{232}Th respectively. Although there are many intermediate daughter products, most have relatively short half-lives when compared to ^{235}U, ^{238}U and ^{232}Th ($t_{1/2}$ = approximately 0.7 Ga, 4.5 Ga, and 14 Ga respectively). The decay schemes of greatest interest are the $^{238}U/^{206}Pb$ and $^{235}U/^{207}Pb$ schemes.

From the radioactive decay law, an age can be determined by:

$$t\,(^{207}Pb/^{235}U) = 1/\lambda_{235} \ln ({}^{207}Pb/^{235}U + 1)$$

and

$$t\,(^{206}Pb/^{238}U) = 1/\lambda_{238} \ln ({}^{206}Pb/^{238}U + 1)$$

where λ_{235} and λ_{238} are the decay constants of ^{235}U and ^{238}U respectively ($\lambda_{235} = 9.8485 \times 10^{-10}\ a^{-1}$; $\lambda_{238} = 1.55125 \times 10^{-10}\ a^{-1}$). When $^{207}Pb/^{235}U$ and $^{206}Pb/^{238}U$ are plotted together for various ages (t), they form a curve known as the concordia line (Figure 3.5). At the time of crystallization, the U-bearing rock or mineral will plot at the origin because they will not contain any radiogenic Pb. Any rocks or minerals that represent closed systems since their original formation will follow the concordia line because their $t^{207}Pb/^{235}U$ and $t^{206}Pb/^{238}U$ ages are equal. The age of the rock or mineral at any time after its formation is given by the location on the concordia. However, samples that have been subjected to

Figure 3.5: Concordia diagram for U-Pb dating. Concordia line shown as a solid curve. Discordia shown as long-dashed line. Tu = upper intercept age Tl = lower intercept age. Short-dashed line = $^{207}Pb/^{206}Pb$ isochron.

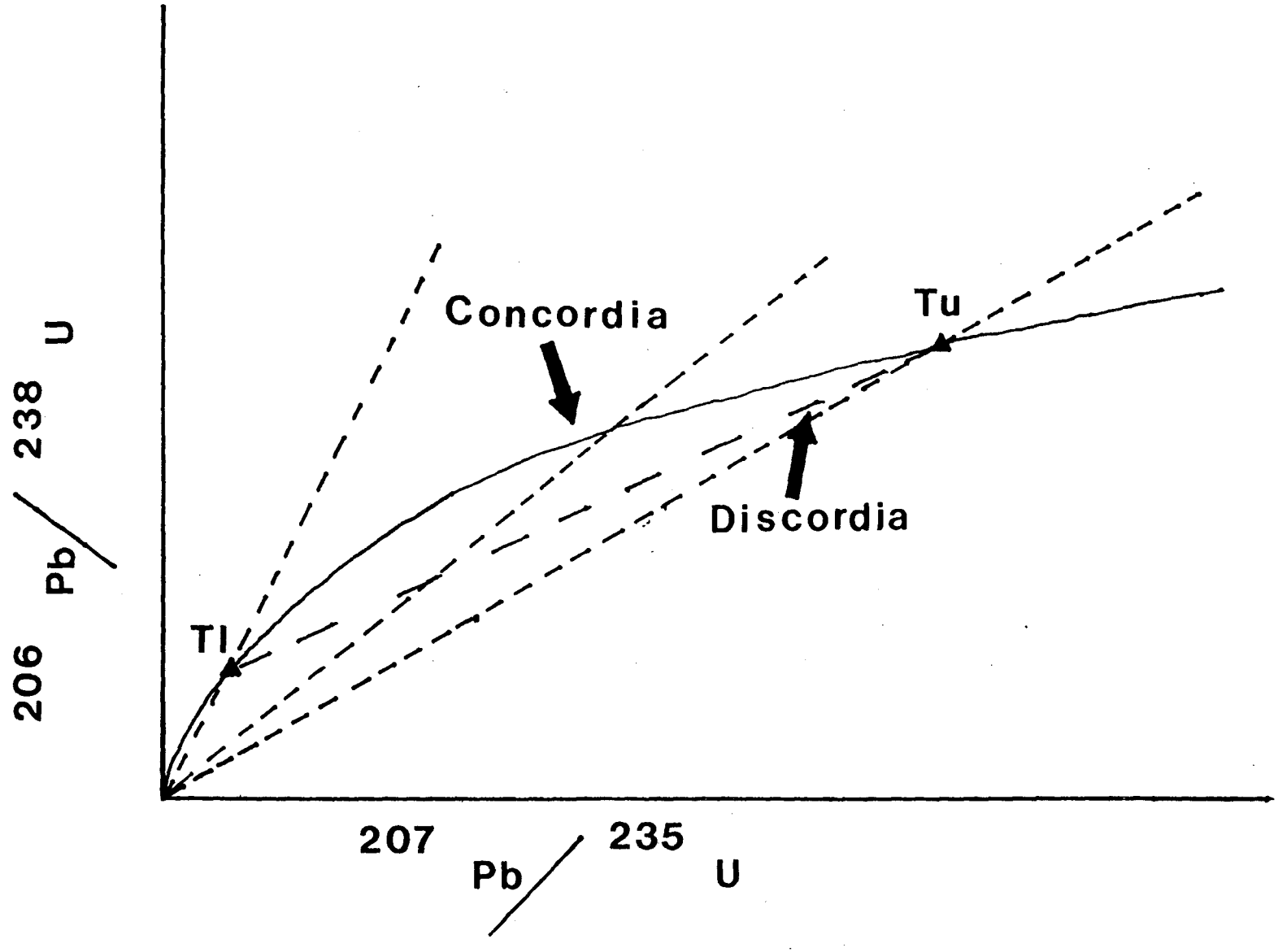
Concordia
Tu
Discordia
Tl
206 Pb / 238 U
207 Pb / 235 U

metamorphism or weathering, for example, will not plot on concordia. Instead, the U/Pb ratios for these open systems will lie somewhere below the concordia, and define a line known as a discordia.

There are several possibilities for open system U/Pb behaviour. For example, the rock or mineral may have experienced an episode of Pb loss produced by a metamorphic event. These rocks or minerals will thus be discordant.If a series of minerals such as zircons are analyzed from the same sample that has experienced episodic Pb loss, then they will plot as a series of points on a discordia line. The discordia line can be extrapolated in both directions and the upper and lower intercepts (T_U and T_L on Figure 3.5) with the concordia represents the time elapsed since original crystallization of the zircons (T_U) and the time elapsed since the zircons were closed after the episode of Pb loss (T_L) respectively.

Another possibility for open system U/Pb behaviour could be caused by continuous Pb loss where the rate of Pb diffusion is controlled by the diffusion coefficient and radius of the mineral in question. When plotted on a concordia diagram, such samples would also produce a discordia similar to episodic Pb loss, but the lower intercept age (T_L) would be meaningless. However, if independent evidence confirms that a metamorphic event did occur, then the samples have suffered

episodic Pb loss, and T_L does date the time elapsed since the samples were a closed system.

U-Pb dating however, is very labour intensive, particularly for samples that have been subjected to multi-metamorphic events. For example, zircons separated from metamorphic rocks can produce a wide range of U/Pb ages because some zircons can have larger metamorphic rims than others. Thus, accurate U/Pb ages require chemical preparation or air abrasion to remove the younger metamorphic rims. However, Pb/Pb analysis by direct evaporation requires less work and can still yield fairly precise ages. Dates determined by Pb-Pb dating are known as 207/206 ages. Analyses of Pb isotopes produces an isochron (short dashed line on Figure 3.5) on the concordia diagram that originates at the origin. The point of intersection of the isochron with concordia defines the Pb-Pb " apparent age ".

3.4 Pb-Pb ZIRCON DATING:

Zircon geochronology by direct evaporation is a very useful reconnaissance tool. The method requires very little chemical preparation. Zircons are fairly common minerals and therefore are readily available. The procedure used in the present study is similar to Kober's (1987) method. The complete procedure is listed in the Appendix.

The direct evaporation technique for zircons yields $^{207}Pb/^{206}Pb$ ratios for which ages can be derived from the equation:

$$\frac{^{207}Pb}{^{206}Pb} = \frac{(\,^{235}U\,)}{(\,^{238}U\,)t_o} \cdot \frac{(\,e^{\lambda 235 t} - 1\,)}{(\,e^{\lambda 238 t} - 1\,)}$$

where $^{235}U/^{238}U_{to}$ = 1/137.88 (a constant value observed throughout the solar system); λ_{238} and λ_{235} are the decay constants of ^{238}U ($1.55125 \times 10^{-10}\ y^{-1}$) and ^{235}U ($9.8485 \times 10^{-10}\ y^{-1}$).

There are two different ways that the Pb data can be plotted. The Pb ratios could be plotted on co-ordinates of $^{207}Pb/^{204}Pb$ vs. $^{206}Pb/^{204}Pb$ (slope method: Figure 3.6) or $^{207}Pb/^{206}Pb$ vs. $^{204}Pb/^{206}Pb$ (intercept method: Figure 3.7). In the slope method, several analyses are required so that a " best-fit " line can be used to determine the slope. The slope ($^{207}Pb/^{206}Pb$) is then used to calculate the age of crystallization of the zircon.

Alternatively, a plot of $^{207}Pb/^{206}Pb$ vs. $^{204}Pb/^{206}Pb$ (intercept method) can also be used as a graphical method for determining zircon crystallization ages. In this method, the intercept on the Y axis ($^{207}Pb/^{206}Pb$) is used to determine the age from the above equation. The $^{207}Pb/^{206}Pb$ ratios are determined during zircon analysis. As in the slope method, a best-fit line is plotted through the data points, allowing the

y-intercept to be determined.

When zircons crystallize from a melt, they do not readily incorporate Pb into their lattices. The only Pb that is usually present in the zircon crystals is Pb that may have been present in inclusions and Pb produced from the U and Th decay chains.

^{204}Pb is used as an indicator of how much " common " Pb had been included during crystallization of the zircon. Determination of common Pb concentrations is critical for Pb-Pb dating of zircons. Firstly, to correct for initial radiogenic Pb and secondly as an indicator that Pb may have subsequently entered the zircon grain after crystallization. The Pb may have entered through fractures and crystal-lattice damage caused by U decay.

Since zircons contain common Pb, even if only in minute quantities, it is still necessary to correct for this. The value of common Pb is derived from Stacey and Kramers (1975) two stage Pb evolution curve. The common Pb point for the age of the rock is included in the zircon data sets. Kober et al., (1989) consider a $^{206}Pb/^{204}Pb$ value of 10000 to be high enough so that any common Pb correction is not needed. However, zircons with $^{206}Pb/^{204}Pb$ ratios down to 100 may still be used for determining crystallization ages. If there are high concentrations of radiogenic Pb compared to common Pb ($\geq$ 10000 : 1), then the age of the zircon corresponds to the

Figure 3.6: Illustration of the slope method for determining $^{207}Pb/^{206}Pb$ ages for zircons.

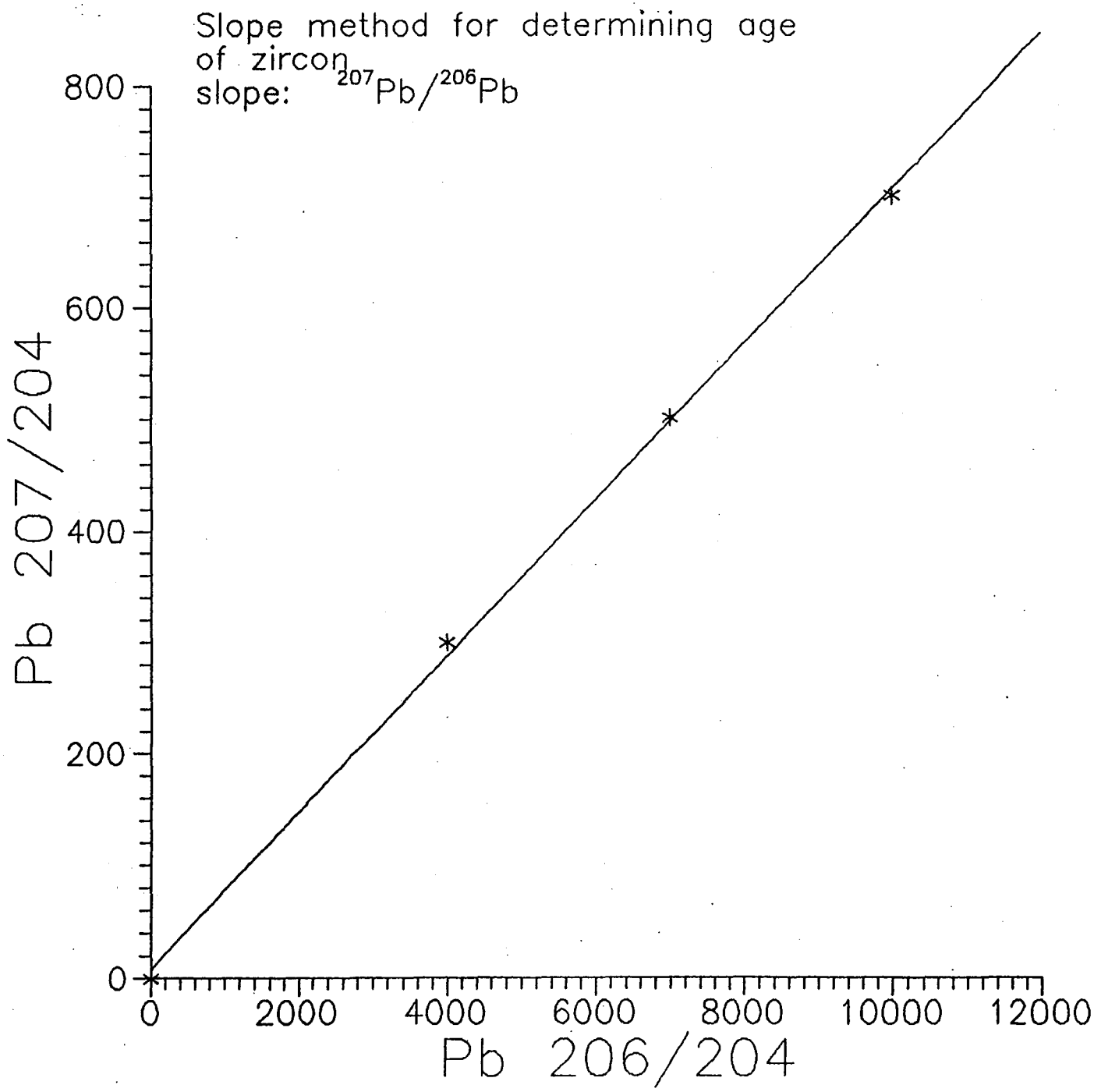
Slope method for determining age of zircon
slope: $^{207}Pb/^{206}Pb$
800
600
400
200
0
Pb 207/204
0
2000
4000
6000
8000
10000
12000
Pb 206/204

Figure 3.7: Illustration of the intercept method for determining $^{207}Pb/^{206}Pb$ ages for zircons.

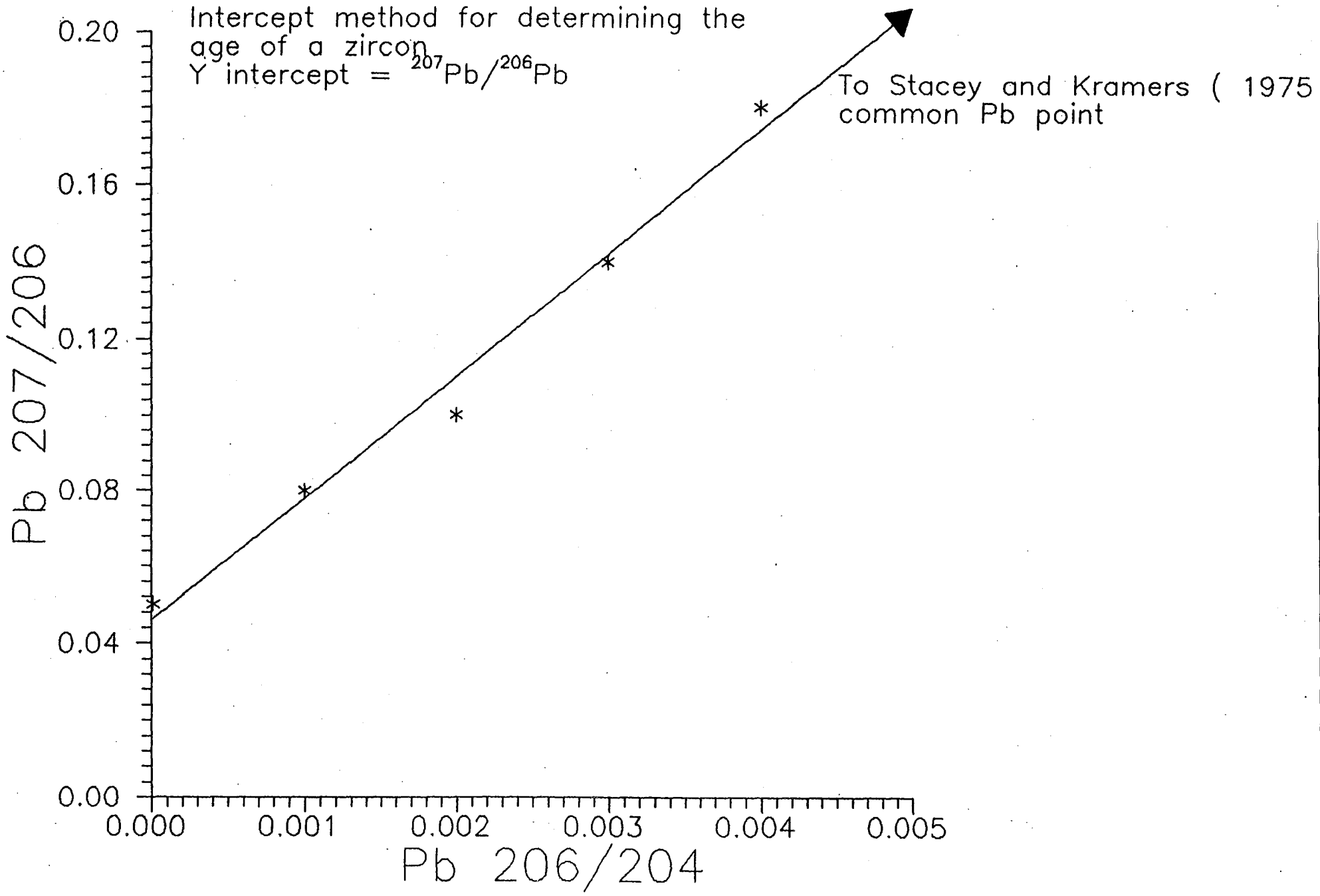
Intercept method for determining the age of a zircon
Y intercept = 207Pb/206Pb
To Stacey and Kramers (1975 common Pb point
Pb 207/206
0.20
0.16
0.12
0.08
0.04
0.00
0.000
0.001
0.002
0.003
0.004
0.005
Pb 206/204

$^{207}Pb/^{206}Pb$ ratio alone, without any common Pb correction.

Although the Pb-Pb direct evaporation technique requires very little chemical preparation, it is impossible to determine which zircons are concordant, and which are discordant. In general, zircons that are highly fractured are excluded from the analyses. Zircons with many inclusions are also excluded. Any zircons that might be discordant are recognized by their spread in ages. No magnetic zircons should be analyzed because discordant grains tend to be magnetic due to alteration which introduces hematite into the zircon fractures. Discordant zircons could be caused by Pb loss due to metamorphism, metamorphic overgrowths, or Pb loss due to metamictization of the grains.

3.5 COMMON Pb-Pb WHOLE ROCK DATING:

The whole-rock Pb isotope system, like U-Pb isotopes, can be used to determine the ages of rocks provided that the rocks have remained closed systems. However, the whole-rock Pb-Pb dating system has one advantage over the whole-rock U-Pb system: recent events such as weathering, will not disrupt the Pb-Pb system because Pb is not as mobile as U. Thus, Pb isotope ratios measured in a sample that has recently suffered alteration, will still reflect the pre-weathering U concentrations.

Combining and rearranging the U decay equations so that the Pb terms are all on one side produces the Pb-Pb isochron equation:

$$\frac{(^{207}Pb/^{204}Pb)_{present} - (^{207}Pb/^{204}Pb)_{initial}}{(^{206}Pb/^{204}Pb)_{present} - (^{206}Pb/^{204}Pb)_{initial}} = \frac{1/137.88\,(e^{\lambda 235T} - e^{\lambda 235t})}{(e^{\lambda 238T} - e^{\lambda 238t})}$$

where 1/137.88 represents the $^{235}U/^{238}U$ ratio that is a constant in the solar system.

One of the main problems of the common Pb-Pb whole-rock dating method is its dependence on U/Pb ratios. U/Pb ratios can easily be disrupted by metamorphic events. Because of the relatively high mobility of U as compared to Pb, metamorphic events can deplete the rocks of U, producing low U/Pb ratios. The depletion of U will affect subsequent Pb/Pb isotope ratios, resulting in spurious Pb-Pb ages. However, in the above equation there are two terms for time: T and t. T is the time of formation and t is the last U depletion event that caused complete U resetting to uniformly low U/Pb ratios. If the rocks to be dated have only experienced U/Pb ratio resetting in recent times then t will correspond to the present day. However, if there has been an event that resets the U/Pb ratios to uniform values for all samples and it occurred at an intermediate time between T and the present,

then t will correspond to the time of the event, and not the present. The slope of the array at t will not change from t to the present provided that the rocks were depleted in U to uniform levels at t. Further U decay will shift the array towards the right. This array is known as a transposed palaeoisochron (Moorbath and Taylor, 1985; Whitehouse, 1990)(Figure 3.8). Regression of this array will produce an anomalously old age if t is set to zero.

Transposed palaeoisochrons are fairly common in studies of ancient rocks that have been subjected to high grade metamorphism after their original formation (Moorbath and Taylor, 1985). High-grade Grenville metamorphism is liable to produce transposed palaeoisochrons and thus, common Pb-Pb whole rock dating in the Lac St. Jean region of Quebec must take this into account.

There have been many models developed to describe the Pb isotopic evolution of the mantle. The models can be used to date whole-rock samples as well as individual minerals by comparison of measured Pb-Pb isotopes with Pb ratios suggested by these models. These models also allow estimations of the amount of common Pb (^{204}Pb) which is important for Pb-Pb dating of zircons. Original models developed independently by Holmes (1946) and Houtermanns (1946) were based on a single stage Pb evolution of the Earth using conformable galena deposits. While the single stage model could date some

Figure 3.8: Example of a transposed palaeoisochron

TPI = transposed palaeoisochron

True isochron represented by dashed line

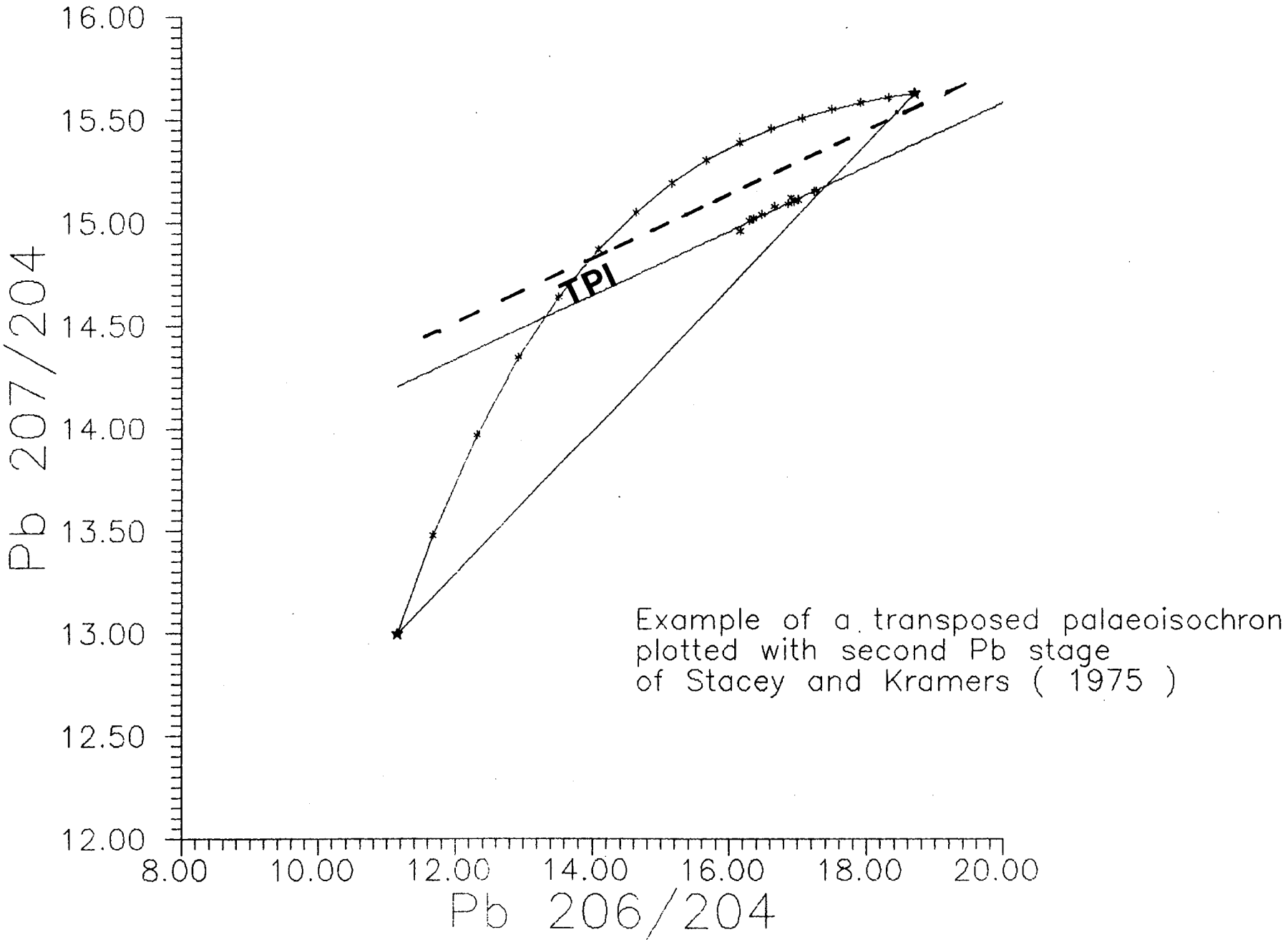

Example of a transposed palaeoisochron plotted with second Pb stage of Stacey and Kramers (1975)

galena deposits, it failed with others, producing anomalous model Pb ages. Some galenas produced common Pb-Pb ages far too old for the rocks they were contained in, while others produced a future age. These problems gave rise to a revised Pb evolution of the Earth developed by Stacey and Kramers (1975). Stacey and Kramers (1975) developed a two stage Pb evolution model with different u values (Figure 3.9). The first stage was a closed system (upper mantle) with a u value of 7.2. The second stage closed system (lower crust), starting at 3.7 Ga ago, had a u value of 9.7. Stacey and Kramers based their model on meteoritic Pb isotopes and an average of modern Pb isotopes from ocean sediments and island arc rocks. This model is used in this study for both common Pb-Pb whole-rock dating as well as Pb-Pb dating of zircons because a two-stage model for the evolution of Pb in the Earth is more realistic than a single-stage model. A single-stage model consists of only one differentiation event that changes the U/Pb ratios of the Earth. However, the Earth has differentiated more than once, and thus a two-stage model seems more plausible.

Figure 3.9: Illustration of Stacey and Kramers 2 stage Pb evolution of the Earth. Stage 1 = 4.57 Ga to 3.7 Ga (Q); u_1 = 7.192. Stage 2 = 3.7 Ga (Q) to present (P); u_2 = 9.735. Slopes of isochrons can be used to determine the time elapsed since the Pb isotopes separated from the mantle reservoir (after Faure, 1986).

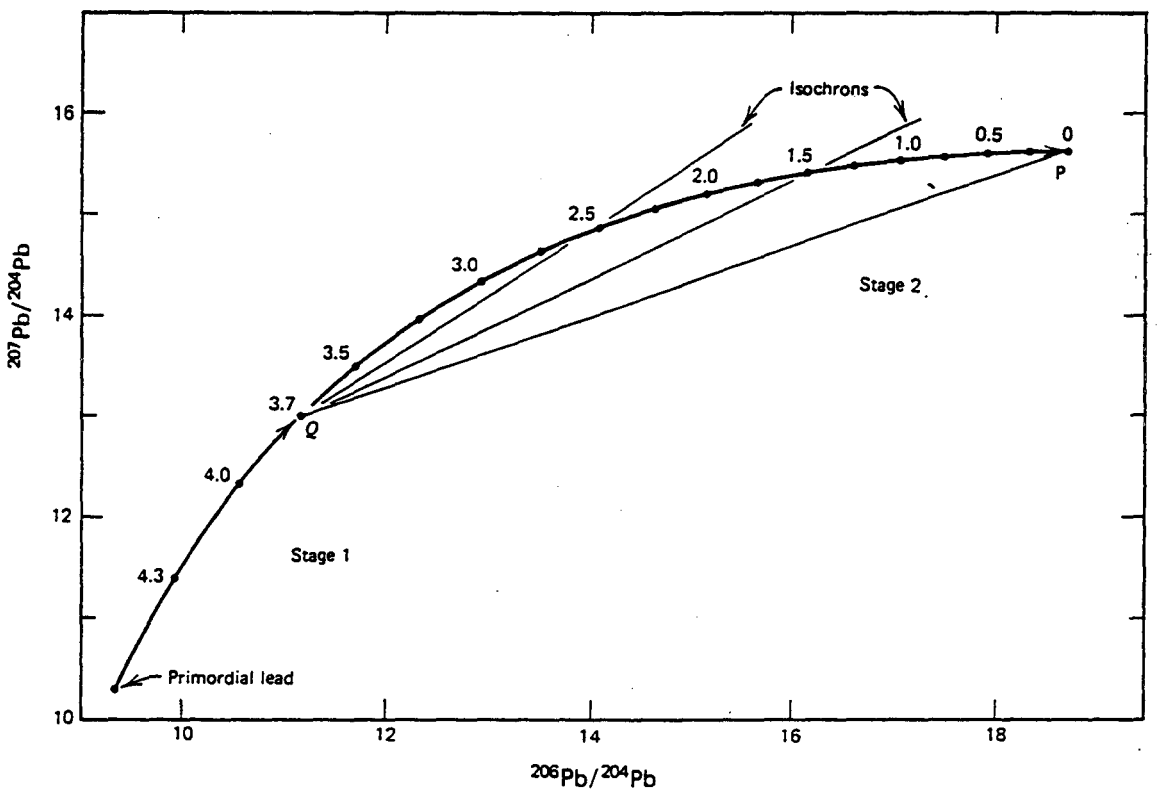
Isochrons
0
0.5
1.0
1.5
2.0
2.5
3.0
3.5
3.7
4.0
4.3
P
Q
Stage 1
Stage 2
Primordial lead
16
14
12
10
10
12
14
16
18
$^{207}Pb/^{204}Pb$
$^{206}Pb/^{204}Pb$

CHAPTER 4

RESULTS:

WESTERN SECTION

The Western section covers approximately 6000 Km^2 and runs parallel to the Allochthon Boundary Thrust of Rivers et al., (1989). Frith and Doig (1975) analyzed several gray gneisses along Highway 167, which travels through the Western section in a northwest direction. Their Rb-Sr whole rock analyses yielded an isochron age of approximately 3.0 Ga. South of the aeromagnetic discontinuity recognized by Frith and Doig (1975), Rb-Sr analyses produced Proterozoic ages of 1750 and 1100 Ma. This discontinuity represents the Allochthon Boundary Thrust of Rivers et al., (1989). Thus, the southern limit of the Western section was chosen as the Allochthon Boundary Thrust because this appears to mark the boundary between Archean and Proterozoic aged rocks. The area is bounded to the west by the Gouin Reservoir (approximately 74° 30′ W) and to the east by Lac Rivard (73° 8′ W) (Figure 4.1). Sampling on the eastern side was restricted beyond Lac Du Principal because of the lack of forestry access roads. On the western side, the Gouin Reservoir prevented further

Figure 4.1: Map of the Western section.

Symbols: closed circle = Nd model ages > 2.60 Ga

open circle = Nd model ages < 2.60 Ga.

P.B. = Parautochthonous Belt

A.P.B. = Allochthonous Polycyclic Belt

large filled triangles = Grenville Front

A.B.T. shown as dotted line.

large stipple = Lac St. Jean Anorthosite

small stipple = " granitic pegmatite " (G19) from MERQ maps

no pattern = gray gneisses and migmatized equivalents

dark shading = Amphibolite (G2 on MERQ maps)

light shading = all other units

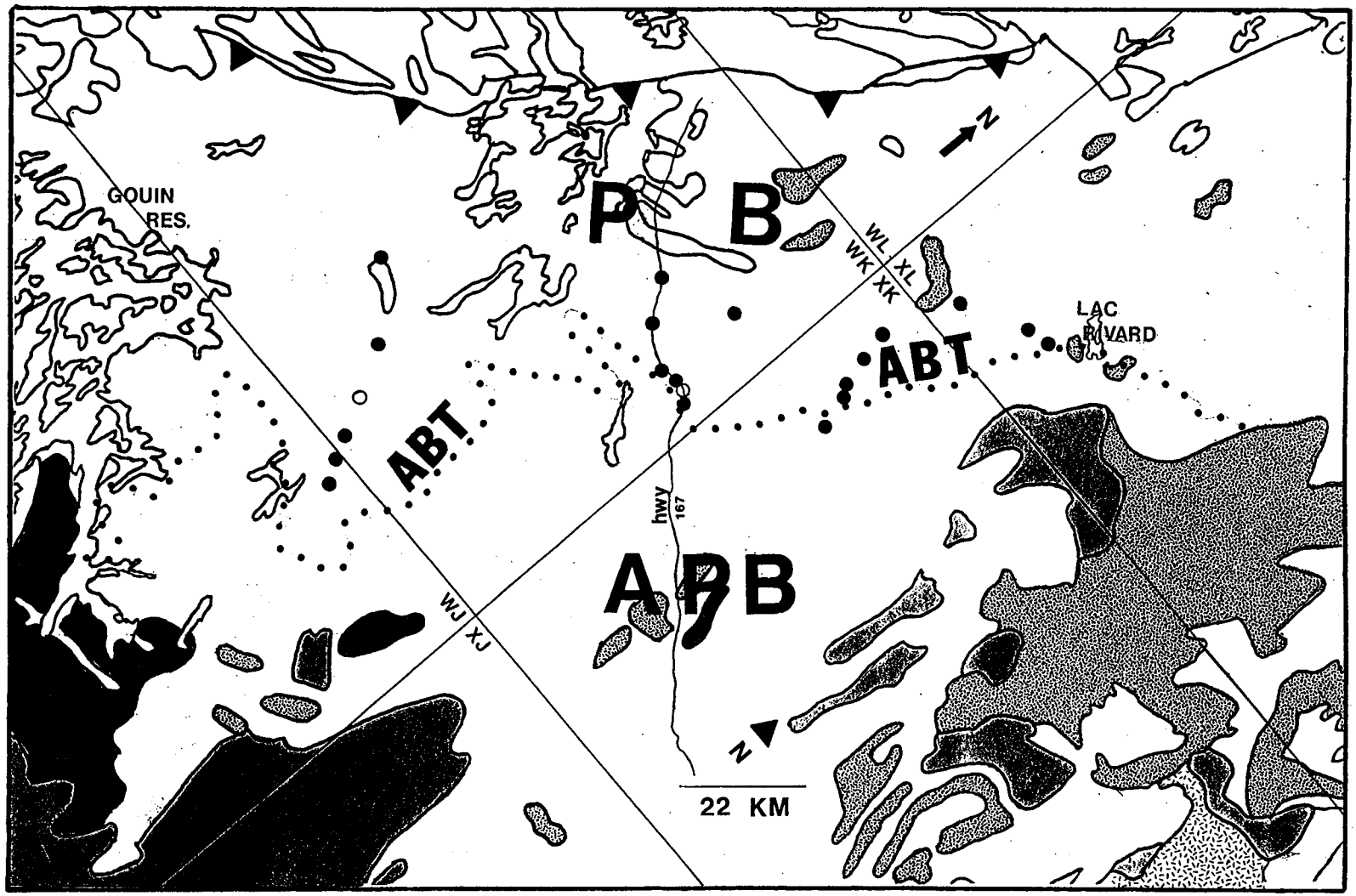
GOUIN
RES.
P
B
WL
XL
WK
XK
LAC
RIVARD
ABT
ABT
hwy
167
WJ
XJ
22 KM

passage.

The lithologies of the Western section were fairly consistent, composed almost exclusively of tonalitic gneisses with minor granitic intrusions (G1 and G19 respectively on the MERQ geological maps 32 H and 32 B). In this part of the field area, the lithologies indicated on the MERQ maps were consistent with field observations. However, in certain areas in the northwestern part of the Western section, the geological maps differentiated between tonalitic gray gneisses (G1) and granitic gneisses (G2). This was not consistent with field observations because samples taken from both rock types failed to reveal any differences. Hence, this distinction is not made in Figure 4.1.

In the Western section, 22 samples were analyzed for Sm-Nd dating. The sample locations and Sm-Nd isotopic data are listed in Table 4.1 and are shown in Figure 4.1. Of these 22 samples analyzed for Nd model age dating, 12 representative samples were analyzed for Pb isotope concentrations and 13 representative samples were analyzed for major and trace element concentrations. The Pb isotope data are shown in Table 4.2 while the major and trace element data are in the appendix.

A histogram of all of the Sm-Nd data for the Western section is shown in Figure 4.2. The histogram illustrates that in this part of the field area, which lies north of the

TABLE 4.1: Sm/Nd data for the Western section

Sample	Grid Ref.		Cor	Qz	*	Nd ppm	Sm ppm	$^{147}Sm/^{144}Nd$	$^{143}Nd/^{144}Nd$	TDM GA
DOLBEAU										
DO12	WJ	683007			nd	24.21	3.55	.0887	.510828	2.72
DO13	WK	673037	-0.7	21.9	TN	14.88	3.02	.1226	.511418	2.74
DO14	WK	664056	0.5	23.4	TN	1.41	0.23	.0984	.511011	2.71
DO16	WK	500171	-1.3	12.1	QD	23.23	4.09	.1065	.511325	2.45
DO17	WK	495175	-1.8	21.9	TN	18.10	3.56	.1189	.511286	2.85
DO18	WK	433268	-4.1	21.1	TN	15.54	2.89	.1124	.511197	2.80
SAINT-THOMAS-DIDYME										
TD15	XK	103883			nd	23.97	4.00	.1009	.510980	2.81
TD16	XK	085915	0.4	25.5	TN	9.18	1.66	.1095	.511186	2.74
TD18	XL	105015	0.5	22.3	TN	10.42	1.93	.1122	.511255	2.71
TD19	XK	113849	0.6	26.2	TN	6.61	0.89	.0803	.510653	2.75
TD21	XK	119772			nd	5.59	0.63	.0676	.510661	2.50
PB3	XK	115723			nd	6.41	1.05	.0989	.511149	2.53
PB7	WK	905752			nd	11.39	1.92	.1016	.511062	2.71
ND4	XL	241108			nd	3.66	0.55	.0948	.510859	2.72
ND6	XL	219108			nd	5.44	0.96	.1098	.511177	2.76
LAC-ST-JEAN										
LSJ15	WK	946549	-0.3	11.7	QD	14.41	2.19	.0920	.511039	2.52
LSJ16	WK	943564			nd	12.89	1.98	.0929	.510940	2.67
LSJ17	WK	918582	2.0	23.3	TN	19.22	3.20	.1006	.511010	2.76
LSJ19	WK	846601	2.0	25.8	TN	31.14	5.12	.0993	.511037	2.69
LSJ24	WK	700730	-2.3	13.9	QD	27.55	4.75	.1043	.511101	2.73
CC02			1.8	29.6	TN	4.73	1.16	.1477	.511956	2.53
CC05	WK	950560	1.5	30.5	TN	7.04	.74	.0637	.510799	2.29

Note:
Negative corundum = diopside
nd = not determined
Gneissic type: TN = tonalite; QD = quartz diorite
Normative mioneralogy: Cor = corundum; Qz = quartz

Table 4.2: Pb data for samples from the Western section

Sample Name	Grid Refer.	$^{206}Pb/^{204}Pb$	$^{207}Pb/^{204}Pb$	$^{208}Pb/^{204}Pb$	Lithology
TD 16	XK 085915	13.863	14.592	33.628	TN
TD 15	XK 103883	17.475	15.463	37.260	nd
TD 19	XK 113849	14.112	14.671	34.149	TN
DO 12	WJ 683007	16.688	15.447	36.007	nd
DO 13	WK 673037	17.423	15.484	36.629	TN
DO 14	WK 664056	15.329	15.007	35.405	TN
DO 17	WK 495175	15.029	15.019	34.967	TN
DO 18	WK 433268	14.644	14.814	39.472	TN
ND 4	XL 241108	16.015	15.143	34.269	nd
ND 6	XL 219108	14.071	14.635	34.483	nd
PB 7	WK 905752	15.528	15.009	34.789	nd

Notes: nd = not determined
Lithology determined from Q-P plot
TN = tonalite; QD = quartz diorite

Figure 4.2: Histogram of Nd model ages for all samples from the Western section.

Histogram of samples from the Western section

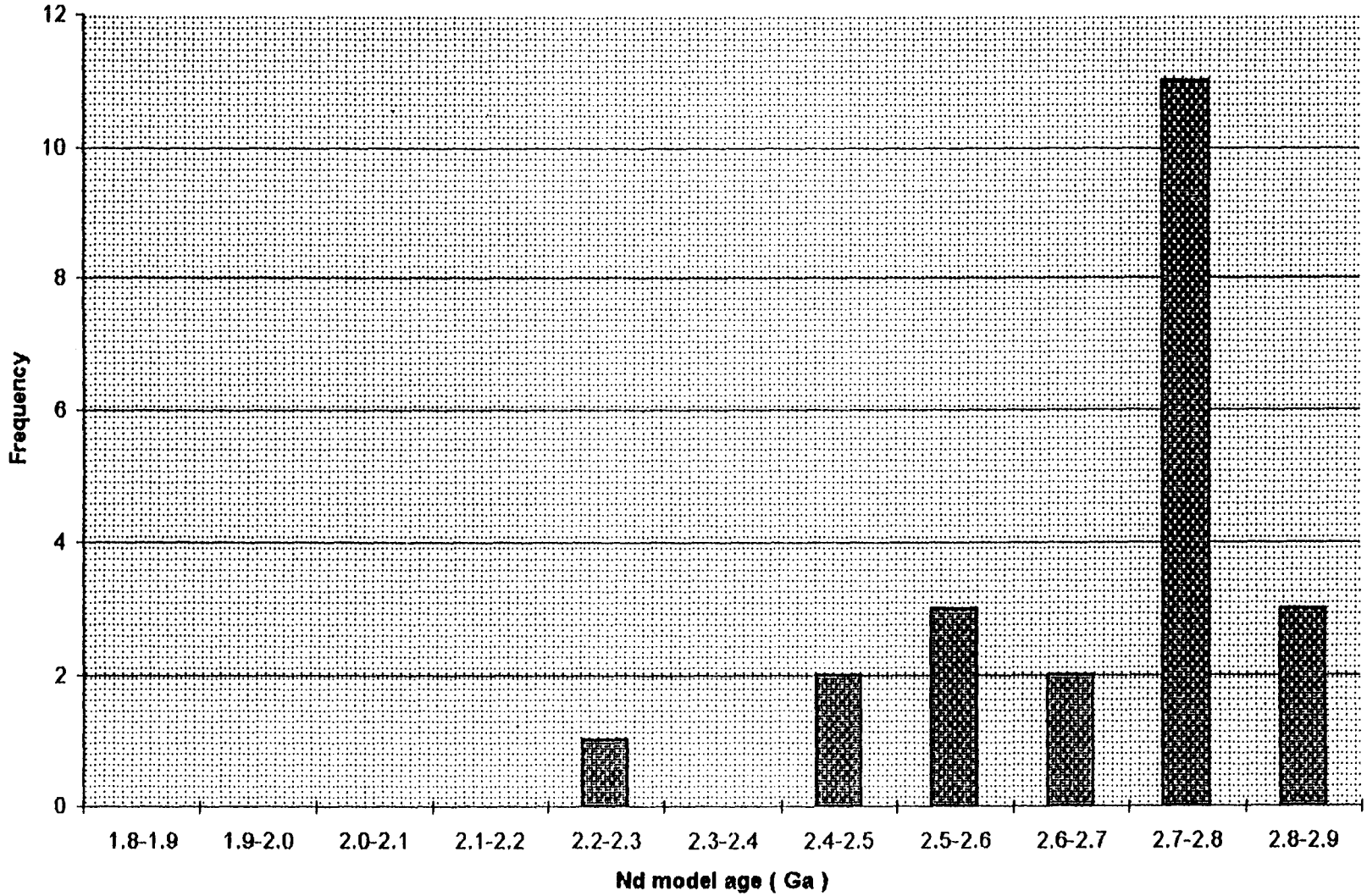

ABT, the rocks represent variably re-worked Archean rocks.

In an effort to understand the geology of the Western field section, three different tectonic discrimination diagrams were used: 1) AFM (Irvine and Barager, 1971), 2) Q-P (Debon and LeFort, 1983), and 3) Y vs. Nb (Pearce et al., 1984). Figure 4.3 represents the AFM plot for the Western section. The diagram indicates that the rocks represent a calc-alkaline trend. The trend observed is very similar to the Blanco Batholith of Peru; a subduction related ensialic arc (outlined on Figure 4.3).

The Q-P diagram (Figure 4.4) illustrates that the Western section is composed almost exclusively of tonalitic rocks. Virtually all of the samples with Nd model ages greater than 2.6 Ga plot in the tonalite field (one exception; LSJ24). Two of the three samples that fall in the quartz diorite field have Nd model ages less than 2.6 Ga: DO16 and LSJ15. This suggests that these samples represent younger plutonism. For comparison, the field outlined across the top of the diagram represents Mid-Proterozoic gray gneisses thought to exemplify island arc rocks analyzed by Dickin and Higgins (1992) while the field outlined down the right represent anorogenic plutons analyzed by Dickin et al., (1990). Such a consistent lithology, excluding the three previously mentioned samples, would not be expected in an ensialic arc such as the Blanco Batholith.

Figure 4.3: AFM diagram for samples from the Western section.

closed circle = Nd model age > 2.60 Ga

open circle = Nd model age < 2.60 Ga

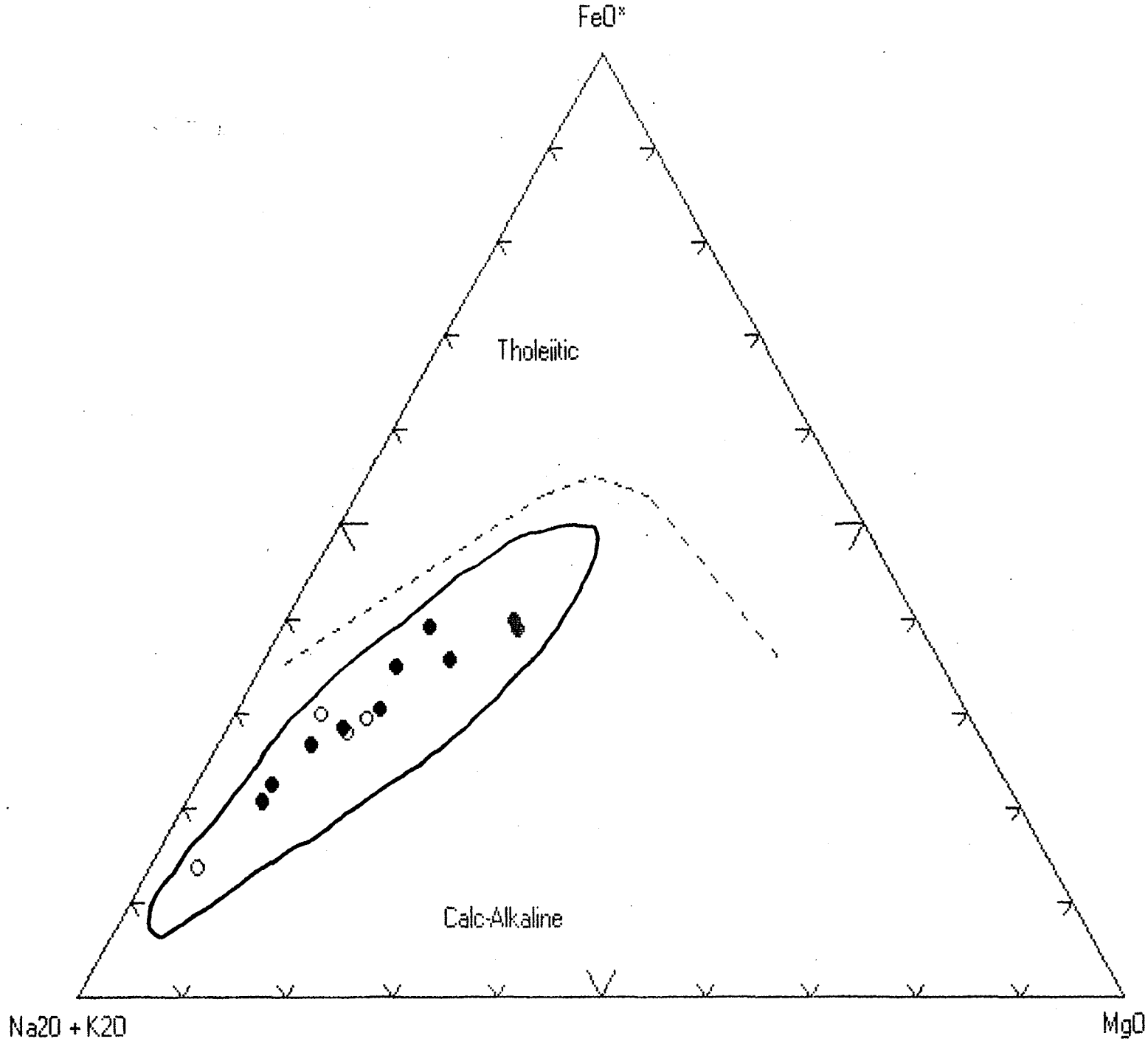
FeO*
Tholeiitic
Calc-Alkaline
Na2O + K2O
MgO

Figure 4.4: Q vs. P plot for samples from the Western section. Symbols as in Figure 4.3. 1 = granite; 2 = adamellite; 3 = granodiorite; 4 = tonalite; 5 = quartzsyenite; 6 = quartzmonzonite; 7 = quartzmonzodiorite; 8 = quartzdiorite; 9 = syenite ; 10 = monzonite; 11 = monzogabbro; 12 = gabbro.

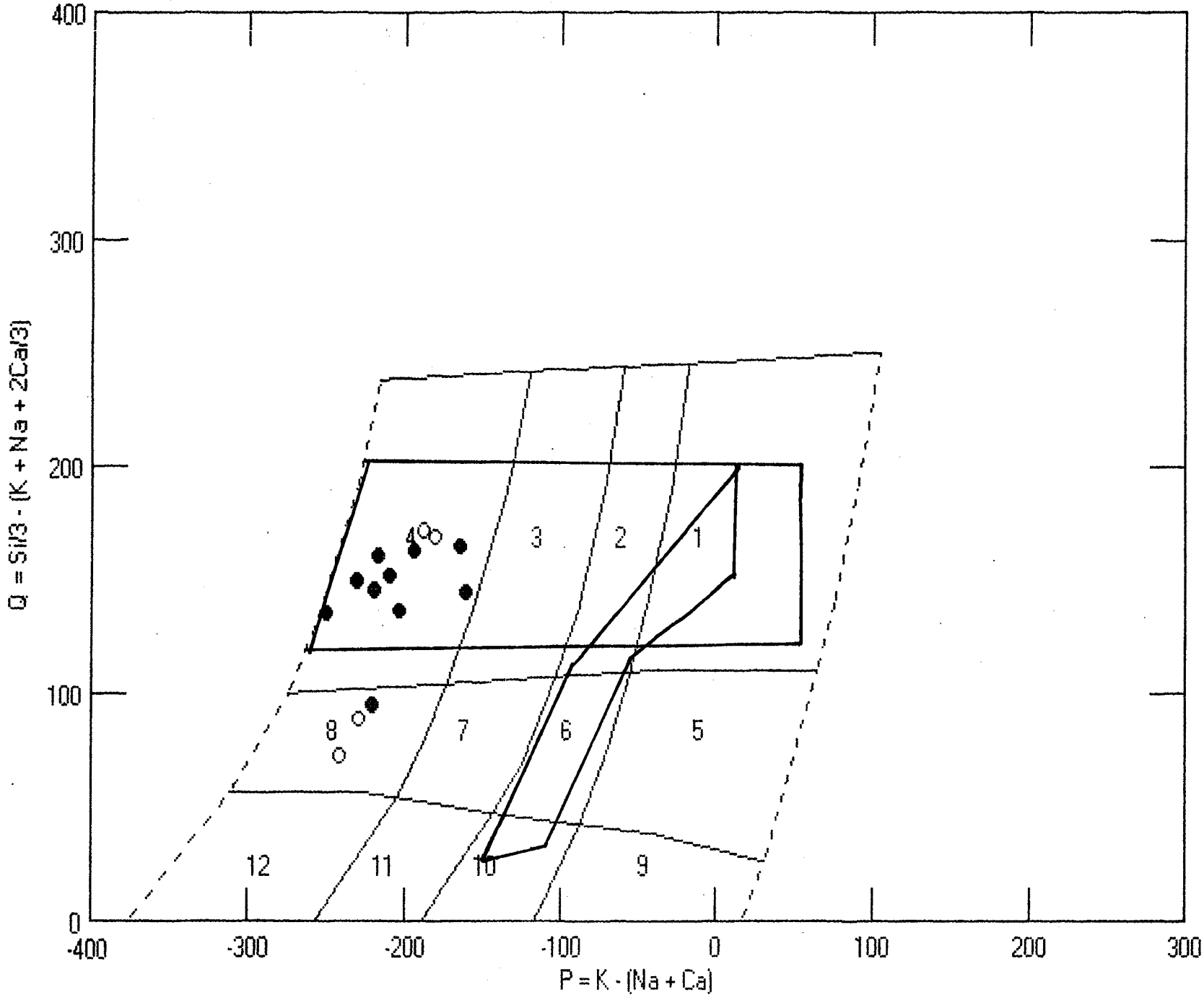
400
300
200
100
0
-400
-300
-200
-100
0
100
200
300
Q = Si/3 - (K + Na + 2Ca/3)
P = K - (Na + Ca)
1
2
3
4
5
6
7
8
9
10
11
12

Figure 4.5: Y vs. Nb plot for samples from the Western section. Symbols as in Figure 4.3. WPG = within plate granitoids; ORG = ocean ridge granitoids; VAG = volcanic arc granitoids

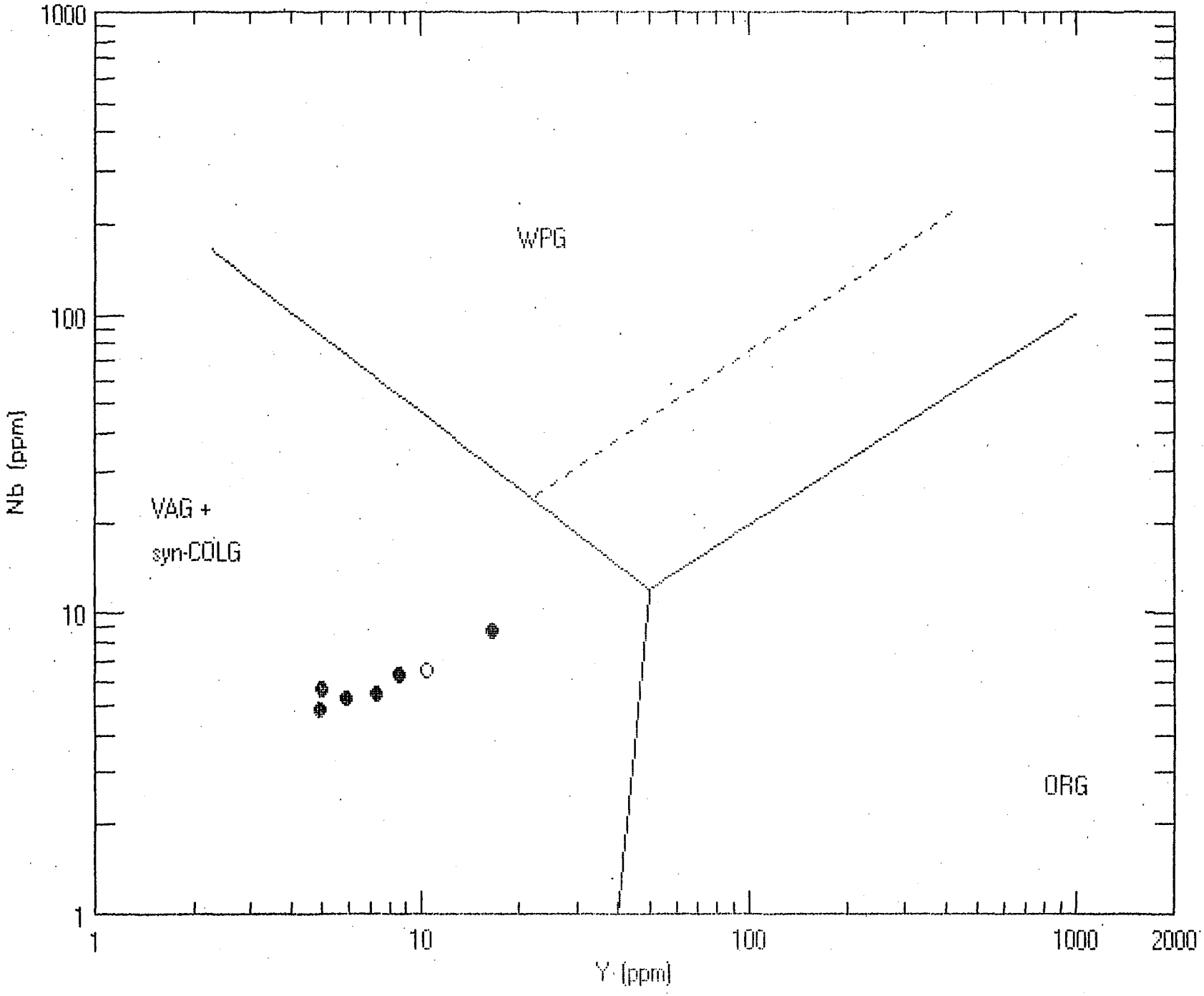
1000
100
10
1
Nb (ppm)
WPG
VAG +
syn-COLG
ORG
1
10
100
1000
2000
Y (ppm)

Figure 4.6: Pb isochron diagram for samples from the Western section.

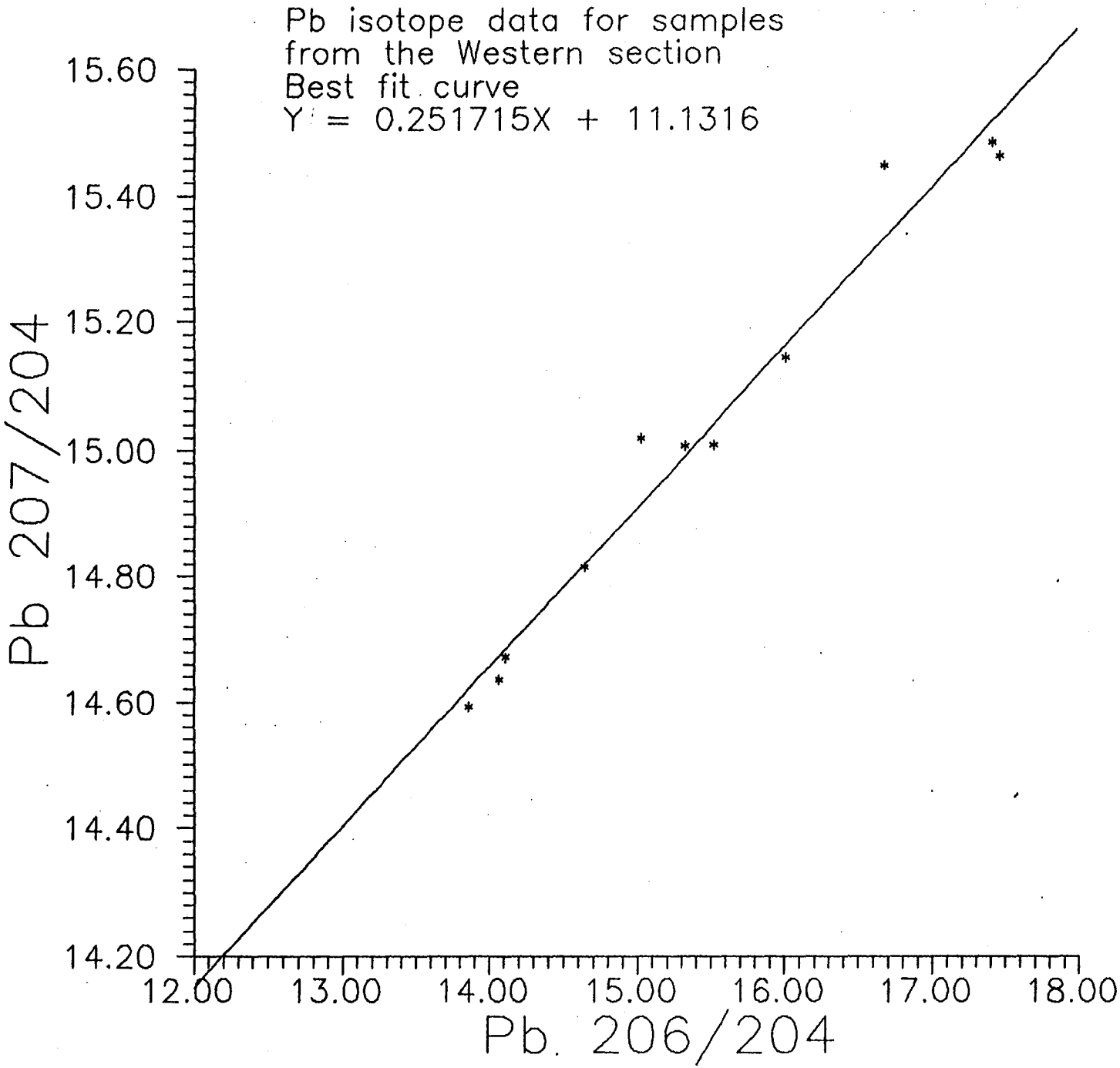
Pb isotope data for samples
from the Western section
Best fit curve
Y = 0.251715X + 11.1316
15.60
15.40
15.20
15.00
14.80
14.60
14.40
14.20
Pb 207/204
12.00
13.00
14.00
15.00
16.00
17.00
18.00
Pb. 206/204

The Y-Nb diagram is shown in Figure 4.5. All samples plot in the VAG and SYN-COLG (Volcanic Arc Granitoids and Syn-Collisional Granitoids, Pearce et al., 1984), confirming that the rocks are representative of an arc-related orogeny.

Pb isotopic data, given in Table 4.2, is shown graphically in Figure 4.6. The linear best-fit line produces a slope of 0.2517 +/- 0.012. The slope of this array corresponds to a single stage $^{207}Pb/^{206}Pb$ apparent age of 3.19 Ga +/-0.08. This age is considerably older than ages determined from other techniques such as U-Pb zircon dating or Sm-Nd model age dating. This date is likely a result of metamorphism that occurred after the initial formation of these rocks at ca. 2.7 Ga. The metamorphic event was probably strong enough to reset the U/Pb ratios for the rocks to a uniform ratio. Subsequent radioactive decay caused the array to shift to the right, producing a transposed palaeoisochron. The metamorphic event also occurred sufficiently long after crustal formation to disrupt the Pb-Pb dating system.

In an attempt to produce conformable Pb-Pb and Nd model ages, the Pb data was re-calculated assuming that the metamorphic event that reset the U/Pb ratios coincided with the Grenville event (1100 Ma). The age produced from the slope of this isochron is 2737 Ma (+ 206 Ma, - 239 Ma). The slope age for the array corresponds to the time period ending at t_2 (1100 Ma). This is shown graphically in Figure 4.7

Figure 4.7: Pb data from Western section plotted with, Pb evolution curve of Stacey and Kramers (1975), starting at 3.7 Ga ago (2nd stage). Illustrates possible transposed palaeoisochron that originates at 2.7 Ga and passes through 1.1 Ga on Pb evolution curve.

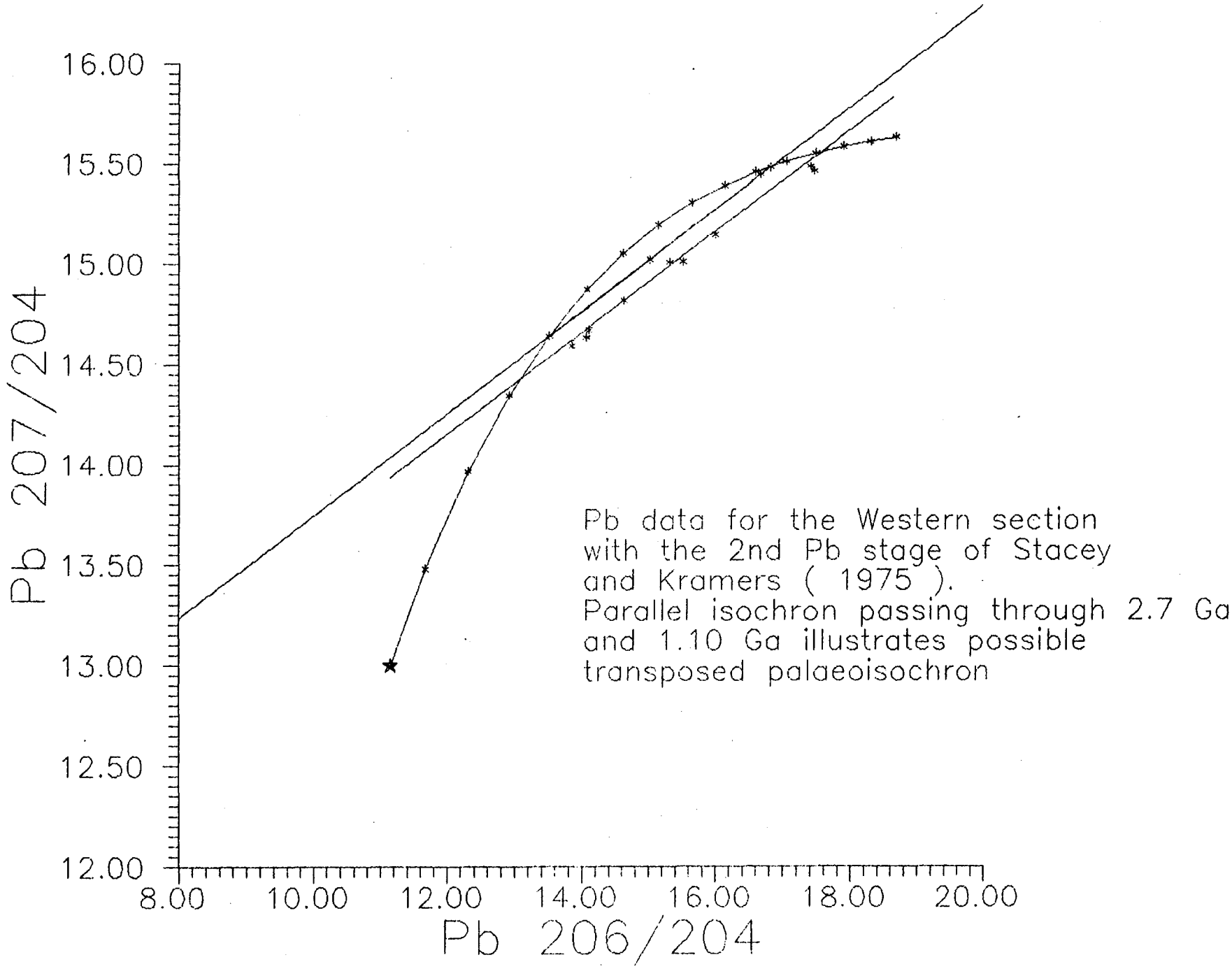
16.00
15.50
15.00
14.50
14.00
13.50
13.00
12.50
12.00
Pb 207/204
8.00
10.00
12.00
14.00
16.00
18.00
20.00
Pb 206/204
Pb data for the Western section with the 2nd Pb stage of Stacey and Kramers (1975).
Parallel isochron passing through 2.7 Ga and 1.10 Ga illustrates possible transposed palaeoisochron

along with the Pb evolution curve of Stacey and Kramers (1975). The diagram shows only the second stage starting at 3.7 Ga.

The age produced by the Pb data after recalculating the slope to include the Grenville metamorphic event is similar to Sm-Nd model ages for these samples, implying that the Pb data do represent a transposed palaeoisochron. This suggests that the rocks of the Western section actually represent a four-stage Pb evolution. The first stage occurred from the formation of the Earth to 3.7 Ga ago. The second stage ran from 3.7 Ga to 2.7 Ga. The third stage began at 2.7 Ga and ended at 1.1 Ga, at which time the U/Pb ratios were completely reset. The fourth and final stage corresponds to the time period between 1.1 Ga and the present.

CHAPTER 5

RESULTS:

CENTRAL SECTION

The Central section covers over 18,000 Km^2 and is shown in Figure 5.1. The northern limit of the Central section is defined by the Allochthon Boundary Thrust of Rivers et al., (1989). The location of the southern limit of the Central section was chosen because it represents a jump in isotopic ages from early to mid-Proterozoic. It follows a line approximately parallel to the Allochthon Boundary Thrust but 75 Km further south, stretching from just west of the Mistassibi river (72° 30′ W) to Lac Brochu (part of the Gouin Reservoir, approximately 74° 30′W).

The Central section lies in portions of the MERQ maps 32 H, 32 B, and 32 I. There were a wide range of lithologies in the Central section. Charnockitic gneiss was present throughout the area, but was dominant in the northern half. Similarly, there were many areas consisting of granitic and tonalitic gneisses and their migmatized equivalents. However, the geology observed in the field was not always what was indicated on the MERQ maps. For instance, large areas mapped as " granitic pegmatite " (G19) contained much less granitic

Figure 5.1: Map of the Central section.

Symbols: diamonds = Nd model age < 1.80 Ga

inverted triangles = Nd model age between 1.80 Ga and 1.90 Ga

circles = Nd model age between 1.90 Ga and 2.00 Ga

squares = Nd model age between 2.00 Ga and 2.10 Ga

small triangles = Nd model age between 2.10 Ga and 2.50 Ga.

southern boundary shown as thin line

large triangles = Grenville Front

A.B.T. = dotted line

stipple patterns as in Figure 4.1

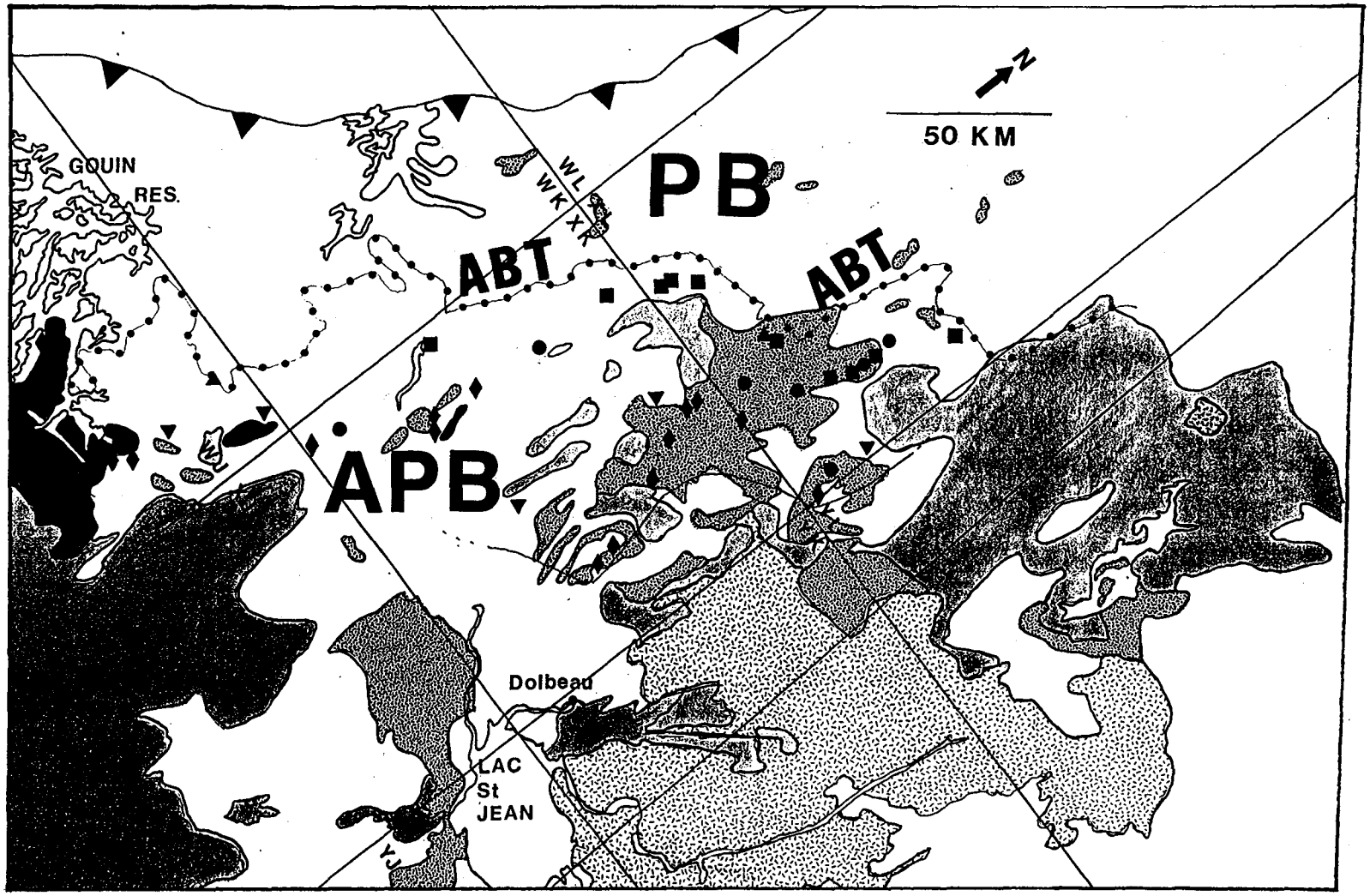
N
50 KM
GOUIN
RES.
WL
WK
XR
PB
ABT
ABT
APB
Dolbeau
LAC
St
JEAN
YJ

rocks than implied by the MERQ maps. Similarly, portions of the map labelled as migmatites (G20) often contained many outcrops that were not migmatized. This distinction was not made in Figure 5.1. However, areas that were classified as charnockites (G4) were often consistent with field observations.

Forty-six samples were analyzed for Sm-Nd model age mapping. The data are shown in Table 5.1. Of the forty-four samples, eleven were analyzed for Pb isotopic compositions (Table 5.2).

A histogram of Sm-Nd model ages is shown in Figure 5.2. The Nd model ages are quite variable, ranging from 1.61 Ga to 2.34 Ga. One sample had a Nd model age of 1.32 but is likely a product of younger plutonism than the rest of the terrane. The variation in Nd model age is not limited to the east or west, but instead, occurs across the entire section.

Major and trace element analyses were performed on twenty-two representative samples from the Central section and are listed in the appendix. Once again, to determine the geological history of the area, three different lithotectonic discrimination diagrams were used. An AFM diagram is shown in Figure 5.3. As in the Western section, samples from the Central section lie in the calc-alkaline field, and are similar to the field defined by the Blanco Batholith of Peru (shown on Figure 5.3).

TABLE 5.1: Sm/Nd data for the Central section

Sample	Grid Ref.	Cor	Qz	*	Nd ppm	Sm ppm	$^{147}Sm/^{144}Nd$	$^{143}Nd/^{144}Nd$	TDM GA
GIRARDVILLE									
GA4	XL 723155	<0.1	15.3	GR	31.17	4.98	.0965	.511563	1.92
GA5	XL 764217	-2.6	3.8	GO	44.65	7.75	.1049	.511605	2.02
GA6	XL 782252	-2.4	17.4	GR	34.52	5.95	.1041	.511591	2.02
GA7	XL 792304	-5.6	3.5	GO	46.61	8.08	.1048	.511670	1.92
GA8	XL 788410	-3.1	14.7	GR	39.65	6.77	.1032	.511596	2.00
GA9	XL 840600	-5.2	7.8	QMD	34.56	6.02	.1053	.511627	1.99
GV4	XL 070637	-0.6	10.5	QMD	58.92	9.87	.1012	.511595	1.96
GV5	XL 59?19?	-0.7	18.7	GR	31.54	5.84	.1118	.511586	2.18
GV6	XL 57?19?	-0.1	15.1	GR	35.26	6.37	.1092	.511620	2.08
GL2	XK 769499			nd	36.65	7.57	.1249	.512079	1.65
GL3	XK 739531			nd	31.82	6.73	.1280	.512141	1.60
GL4	XK 682735			nd	57.54	11.97	.1257	.512030	1.75
GL5	XK 641828			nd	11.42	2.09	.1105	.512151	1.32
GL7	XK 598908			nd	60.63	11.88	.1185	.511933	1.77
GL8	XK 603933			nd	42.48	8.09	.1151	.511914	1.74
GL12	XL 688039			nd	37.33	5.57	.0902	.511706	1.65
GL16	XL 877596			nd	44.51	8.53	.1158	.511694	2.10
LAC-AUX-RATS									
RT1	XL 965057	0.4	21.7	GR	65.36	12.84	.1187	.511971	1.72
RT2	XL 978107	0.7	20.1	GR	13.16	2.79	.1283	.511942	1.96
RT3	XL 994208	1.3	28.3	GR	44.06	8.37	.1148	.511850	1.84
SAINT-THOMAS-DIDYME									
TD3	XK 524315			nd	25.82	5.43	.1270	.511967	1.89
TD10	XK 208657	-1.3	6.2	QMD	46.61	8.08	.1048	.511667	1.93
TD11	XK 212886	-5.6	5.5	QMD	40.61	7.45	.1107	.511668	2.03
ND8	XL 284047			nd	33.03	5.72	.1046	.511569	2.06
ND9	XL 287056			nd	32.76	5.52	.1018	.511535	2.06
PB2	XK 193505			nd	54.09	7.79	.0870	.511614	1.72
ND10	XL 329104			nd	38.07	6.25	.0992	.511473	2.09
LAC-ST-JEAN									
LSJ 6	XK 476174	0.9	28.4	AD	33.40	5.53	.1001	.511776	1.70
LSJ 7	XK 421174	-0.6	11.9	QD	39.60	9.05	.1381	.512087	1.93
LSJ 8	XK 367180			nd	71.82	13.43	.1130	.511973	1.62
LSJ 9	XK 227311	0.0	18.5	GD	53.02	10.16	.1158	.511920	1.75
LSJ10	XK 202325	-3.1	11.8	QMD	58.34	10.58	.1096	.511876	1.71
LSJ13	WK 972482	0.8	33.3	G	50.86	8.70	.1034	.511579	2.02
LSJ26	XK 523826			nd	27.29	4.55	.1008	.511661	1.86

DOLBEAU

DO5	XK	073081	-1.2	10.6	QMD	52.32	8.70	.1005	.511592	1.95
DO6	XJ	054994	0.5	15.2	TN	32.34	5.30	.0990	.511695	1.79
DO9	WJ	900976	-2.8	2.7	MO	48.50	9.05	.1128	.511788	1.89
DO11	WJ	752918			nd	2.77	0.36	.0785	.510972	2.34

GOUIN RESERVOIR

BG3	WJ	773774			nd	20.77	2.36	.0687	.511291	1.84
BG4B	WJ	753651			nd	40.53	8.21	.1225	.512078	1.61
BG6	WJ	708579			nd	57.02	9.52	.1009	.511715	1.79
BG7	WJ	712497			nd	52.71	7.71	.0884	.511554	1.81
BG13	WJ	387613			nd	32.14	3.70	.0695	.511464	1.67

Notes: nd = not determined
Negative corundum = diopside
Gneissic type: TN = tonalite; MO = monzonite; QMD = quartz-monzodiorite; G = granite; GD = granodiorite; AD = adamellite; QD = quartz diorite
Normative mineralogy: Cor = corundum; Qz = quartz

Table 5.2: Pb data for samples from the Central section

Sample Name	Grid Refer.	$^{206}Pb/^{204}Pb$	$^{207}Pb/^{204}Pb$	$^{208}Pb/^{204}Pb$	Lithology
ND 10	XL 329104	16.870	15.394	36.395	nd
GL 16	XL 877596	16.157	15.259	35.958	nd
GA 4	XL 723155	16.291	15.308	36.186	GR
GA 5	XL 764217	16.327	15.319	36.003	GO
GA 6	XL 782252	16.900	15.418	36.540	GR
GA 8	XL 788410	17.246	15.453	36.757	GR
GA 9	XL 840600	16.666	15.381	36.251	QMD
GV 4	XL 070637	16.480	15.339	36.160	QMD
GV 5	XL 595195	17.012	15.408	nd	GR
GV 6	XL 575195	16.948	15.402	36.192	GR
TD 11	XK 212886	17.270	15.455	36.623	QMD

Notes: nd = not determined
Lithology determined from Q-P plot
GR = granodiorite; GO = gabbro; QMD = quartz-monzo-diorite

Figure 5.2: Histogram of Nd model ages for all samples from the Central section.

Histogram of samples from the Central section

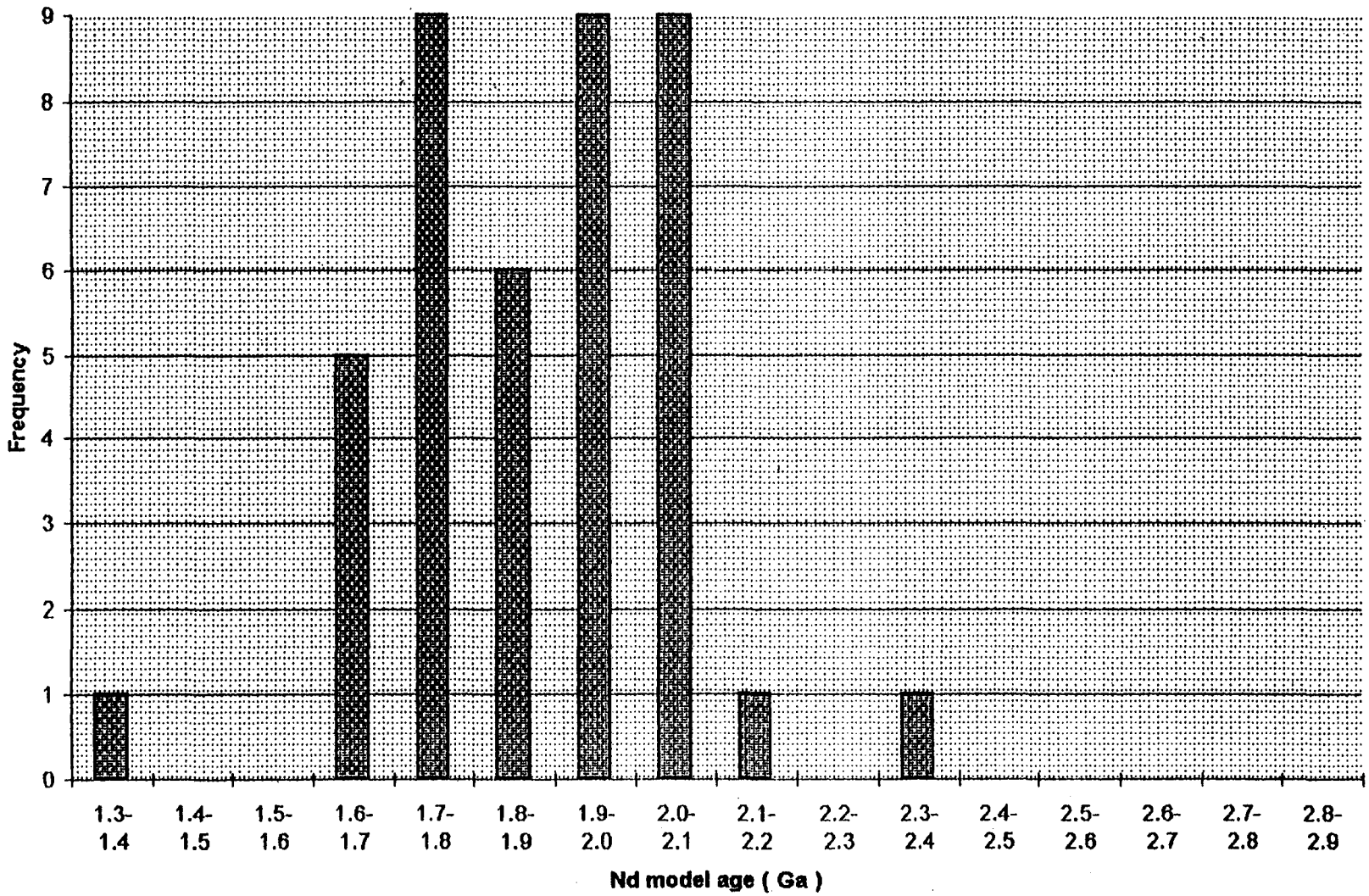

Figure 5.3: AFM diagram for samples from the Central section.

Symbols: diamonds = Nd model age < 1.80 Ga

inverted triangles = Nd model age between 1.80 Ga and 1.90 Ga

circles = Nd model age between 1.90 Ga and 2.00 Ga

squares = Nd model age between 2.00 Ga and 2.10 Ga

triangles pointing up= Nd model age > 2.10 Ga

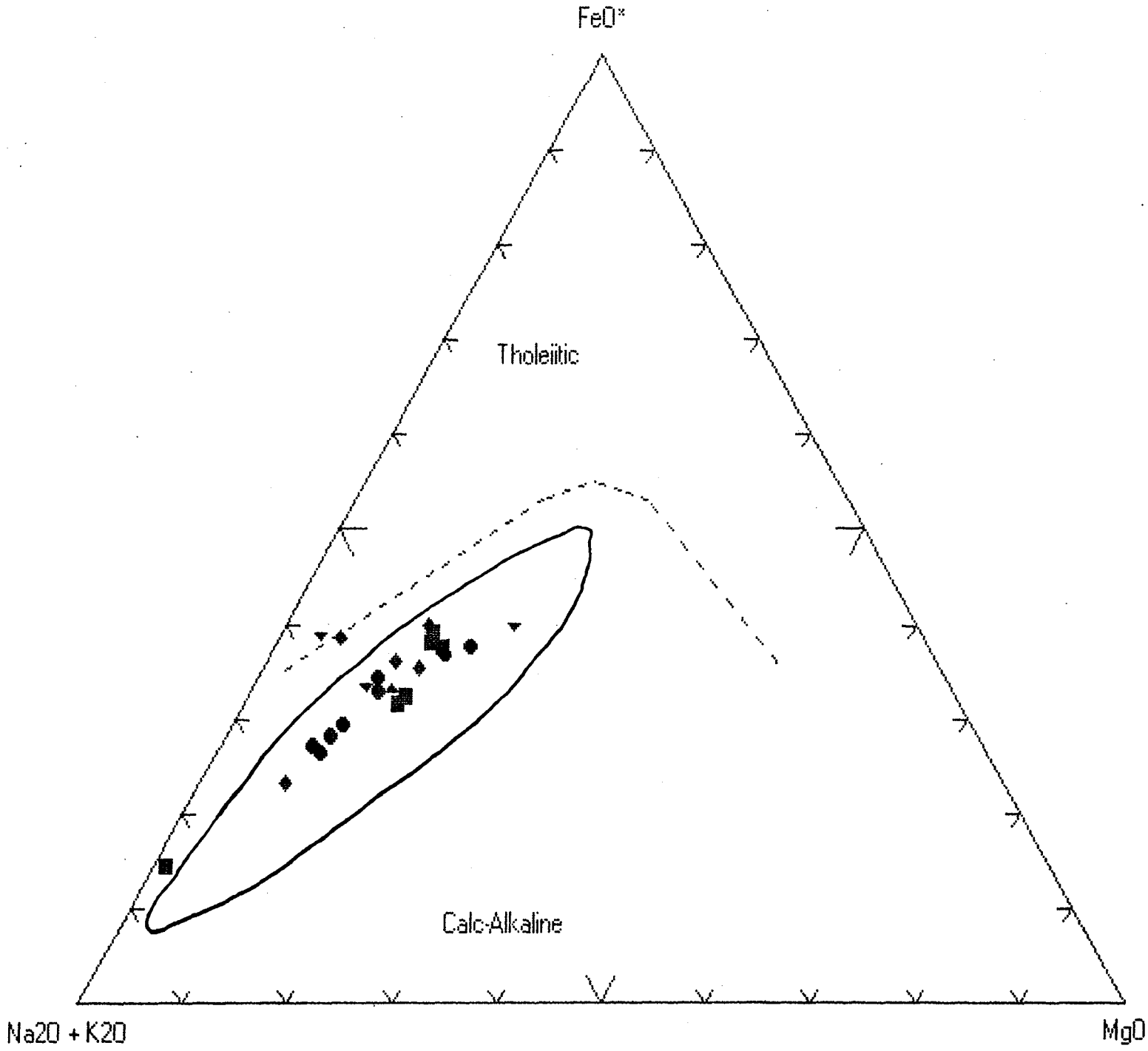
FeO*
Tholeiitic
Calc-Alkaline
Na2O + K2O
MgO

Figure 5.4: Q vs. P plot for samples from the Central section. Numbers as in Figure 4.4. Symbols as in Figure 5.3.

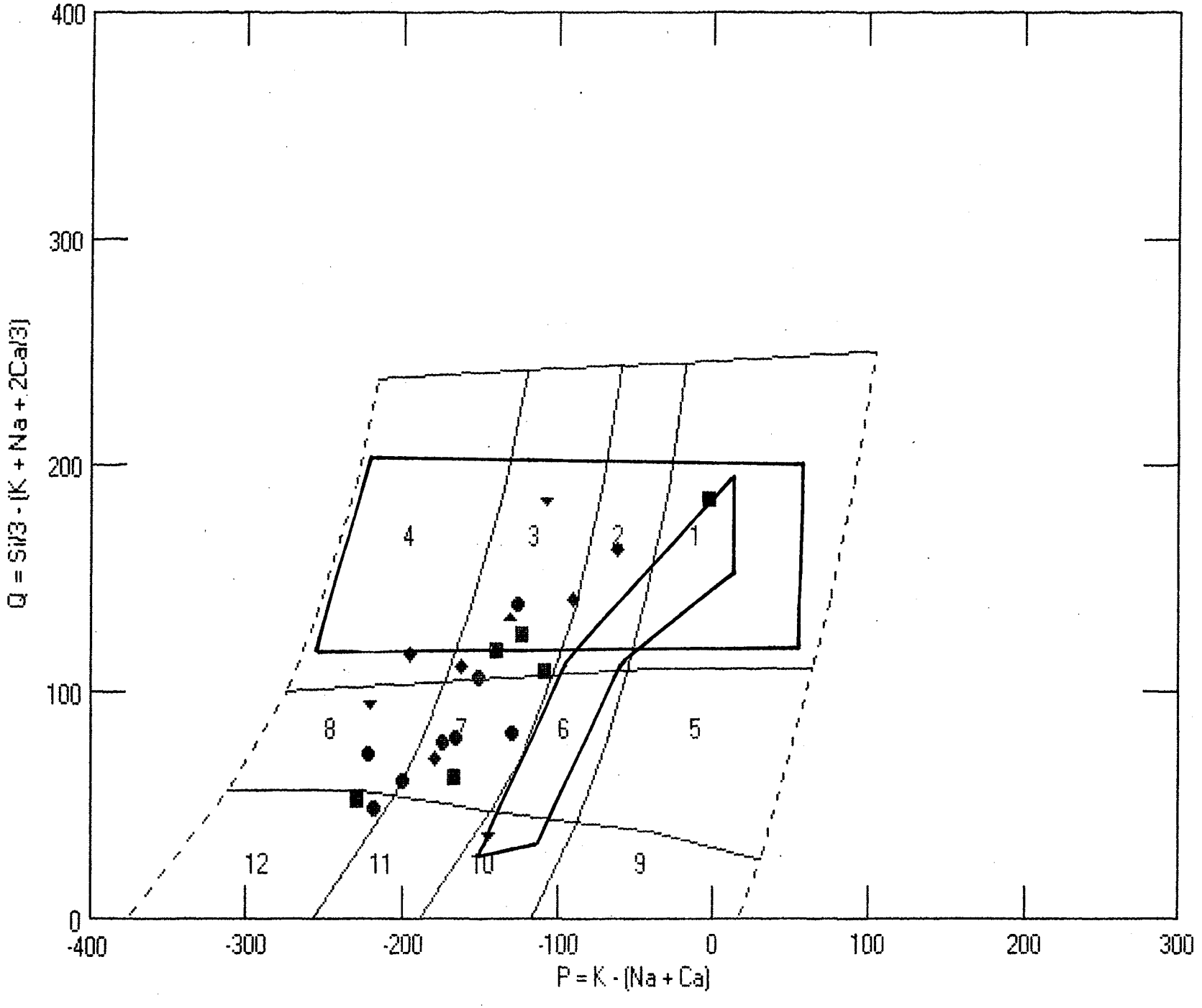
400
300
200
100
0
-400
-300
-200
-100
0
100
200
300
Q = Si/3 - (K + Na + 2Ca/3)
P = K - (Na + Ca)
1
2
3
4
5
6
7
8
9
10
11
12

Figure 5.4 is a Q-P plot of samples from the Central section. The field outlined to the right represent anorogenic plutons analyzed by Dickin et al., (1990), while the field across the top represents gray gneisses that are thought to exemplify an oceanic arc analyzed by Dickin and Higgins (1992). The samples of the Central section fall between these two fields, implying that these rocks represent intermediate conditions. Such a distribution is consistent with an ensialic arc. Diapirs formed above a subduction zone dipping beneath a continental margin can assimilate varying amounts of country rock. The diapirs are also rising through a thickened crust, which may alter their chemistry from the tonalite-granite suite towards monzonite and quartzmonzonite. For comparison, a QAP diagram for Peru is shown in Figure 5.5. The diagram illustrates that Peru contains similar lithologies as those of the Central section.

Figure 5.6 is a Y-Nb diagram of representative samples from the Central section. Most samples plot in the VAG and SYN-COLG field while some plot in the WPG field. Such a distribution would be expected in an ensialic arc because some of the rising diapirs are forced through a thickened crust, which could alter their trace element concentrations because of assimilation of larger amounts of country rock. A thicker crust allows a greater potential for higher degrees of differentiation, which would also increase trace element

Figure 5.5: QAP diagram for the Lima (closed circles) and Arequipa (open circles) segments of the Peruvian Coastal Batholith. (after Atherton et al., 1979)

Numbers: 1 = Quartzolite; 2 = Tonalite; 3 = Quartz diorite/Quartz gabbro/Quartz anorthosite 4 = Diorite/Gabbro/Anorthosite; 5 = Granodiorite 6 = Quartz monzodiorite/Quartz monzogabbro; 7 = Monzodiorite/monzogabbro; 8 = Adamellite; 9 = Quartz monzonite; 10 = Monzonite; 11 = Granite 12 = Quartz syenite; 13 = Syenite; 14 = Alkali feldspar granite; 15 = Alkali feldspar quartz syenite; 16 = Alkali feldspar syenite

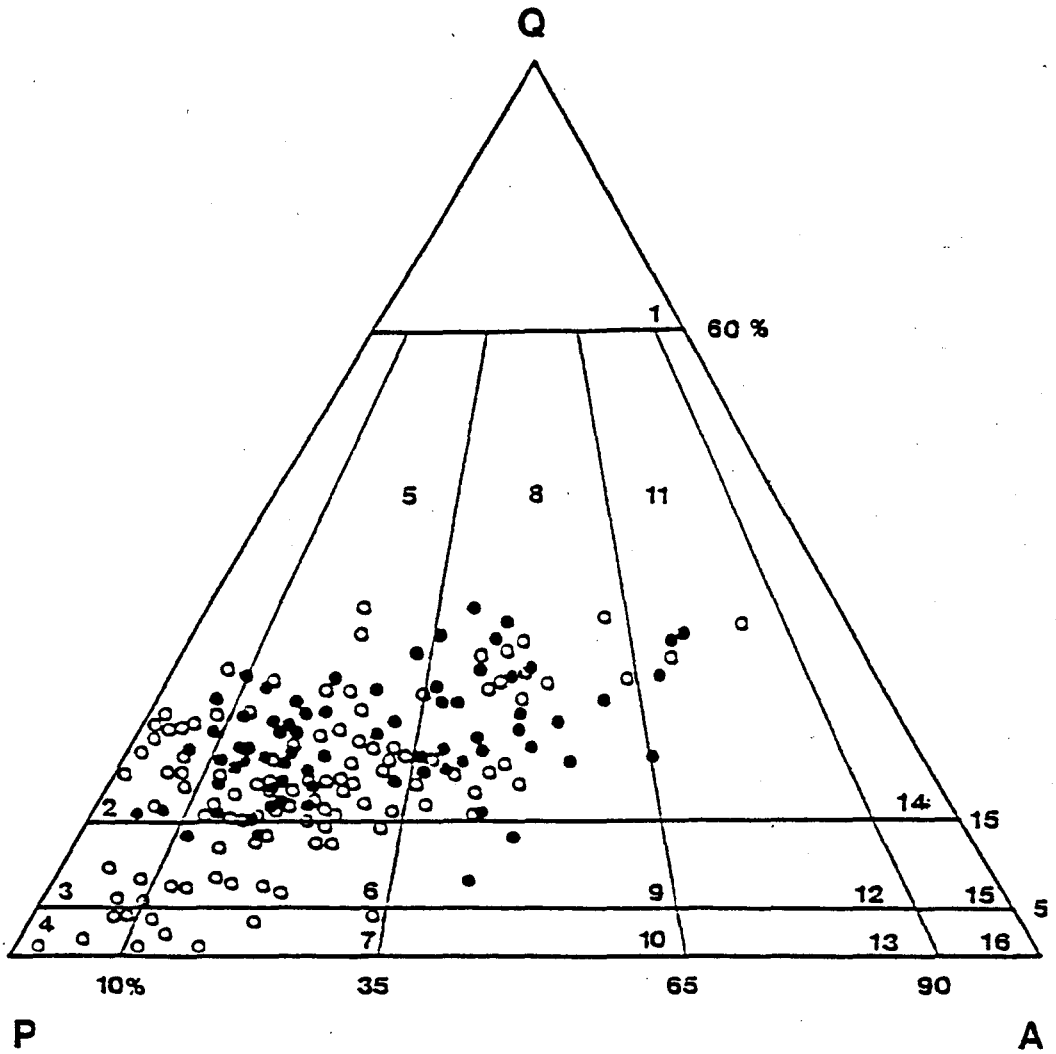
Q
1
60 %
5
8
11
2
14
15
3
6
9
12
15
5
4
7
10
13
16
10%
35
65
90
P
A

Figure 5.6: Y vs Nb for samples from the Central section. Symbols as in Figure 5.3. WPG = within plate granitoid; ORG = ocean ridge granitoid; VAG = volcanic arc granitoid.

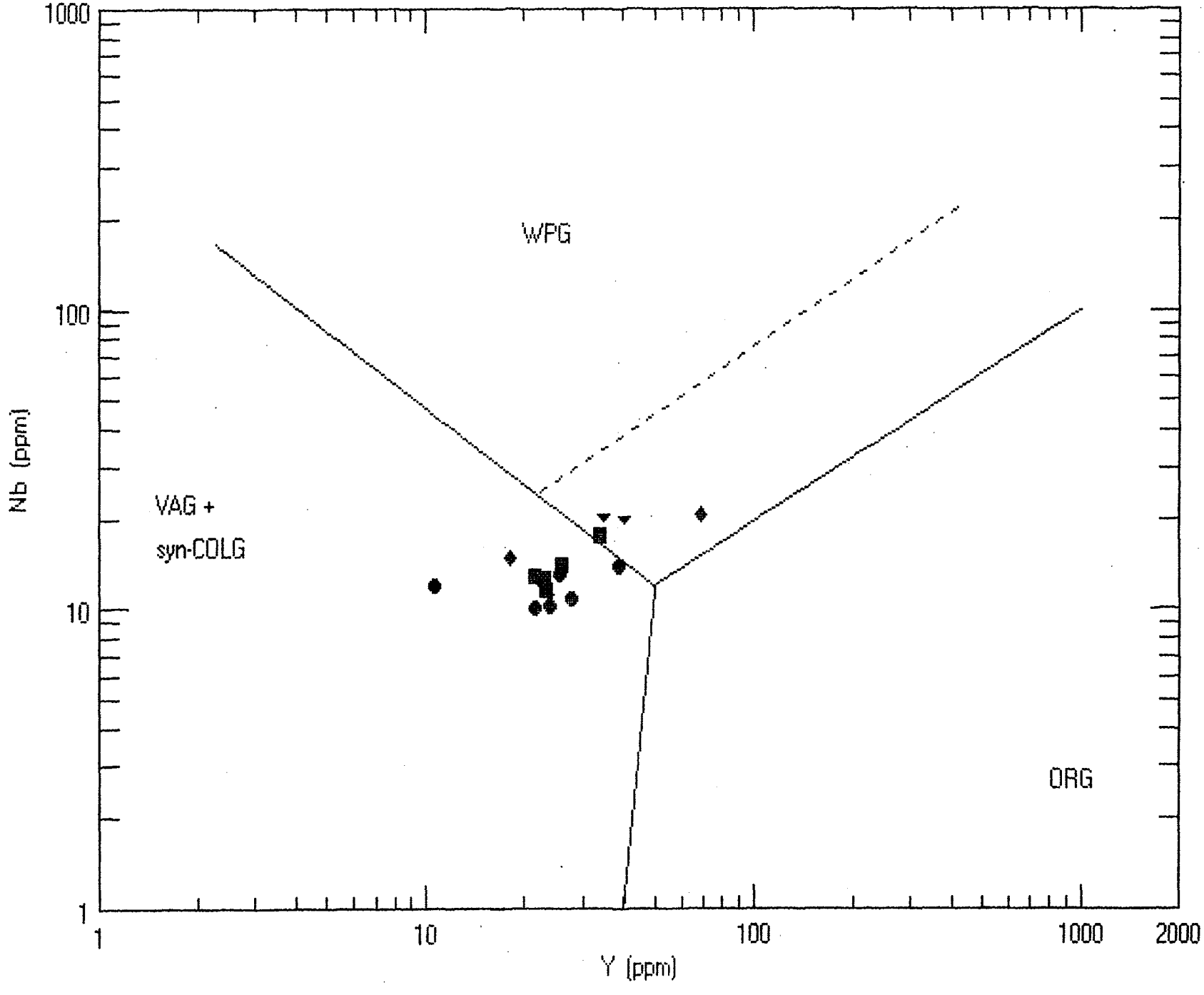
1000
100
10
1
Nb (ppm)
WPG
VAG +
syn-COLG
ORG
1
10
100
1000
2000
Y (ppm)

concentrations. Many of the samples cluster in one place within the VAG and SYN-COLG field. The cluster implies that these samples represent the same intrusion termed " granitic pegmatite " (G19) by the Government du Quebec geological map 32H (note however that only one sample plots in the granite field in Figure 5.4). While some of the outliers may have the same Nd model age, their positions on Figure 5.6 suggest a different melting event which involved different source rocks.

Figure 5.7 represents a Pb isochron diagram for representative samples from the Central section. The slope of this isochron corresponds to a single-stage $^{207}Pb/^{206}Pb$ apparent age of 2.46 Ga. This age is several hundred million years older than the Nd model ages for the Central section. In an attempt to test whether rocks of this section suffered the same Grenvillian metamorphism as the Western section, the Pb data was recalculated to include a metamorphic event that altered U ratios to a depleted, uniform level at 1.1 Ga. This age for metamorphism corresponds to the Grenville orogeny. The slope age of the new array (Figure 5.8) is 1832 Ma (+ 259 Ma, - 310 Ma). This age is typical of Nd model ages for the same rocks. Thus, the array of Pb isotopes for rocks from the Central section may represent a transposed palaeoisochron that has had near-uniform U/Pb ratios imposed during the Grenville orogeny. However, the Pb data may be the result of

Figure 5.7: Pb isochron diagram for samples from the Central section.

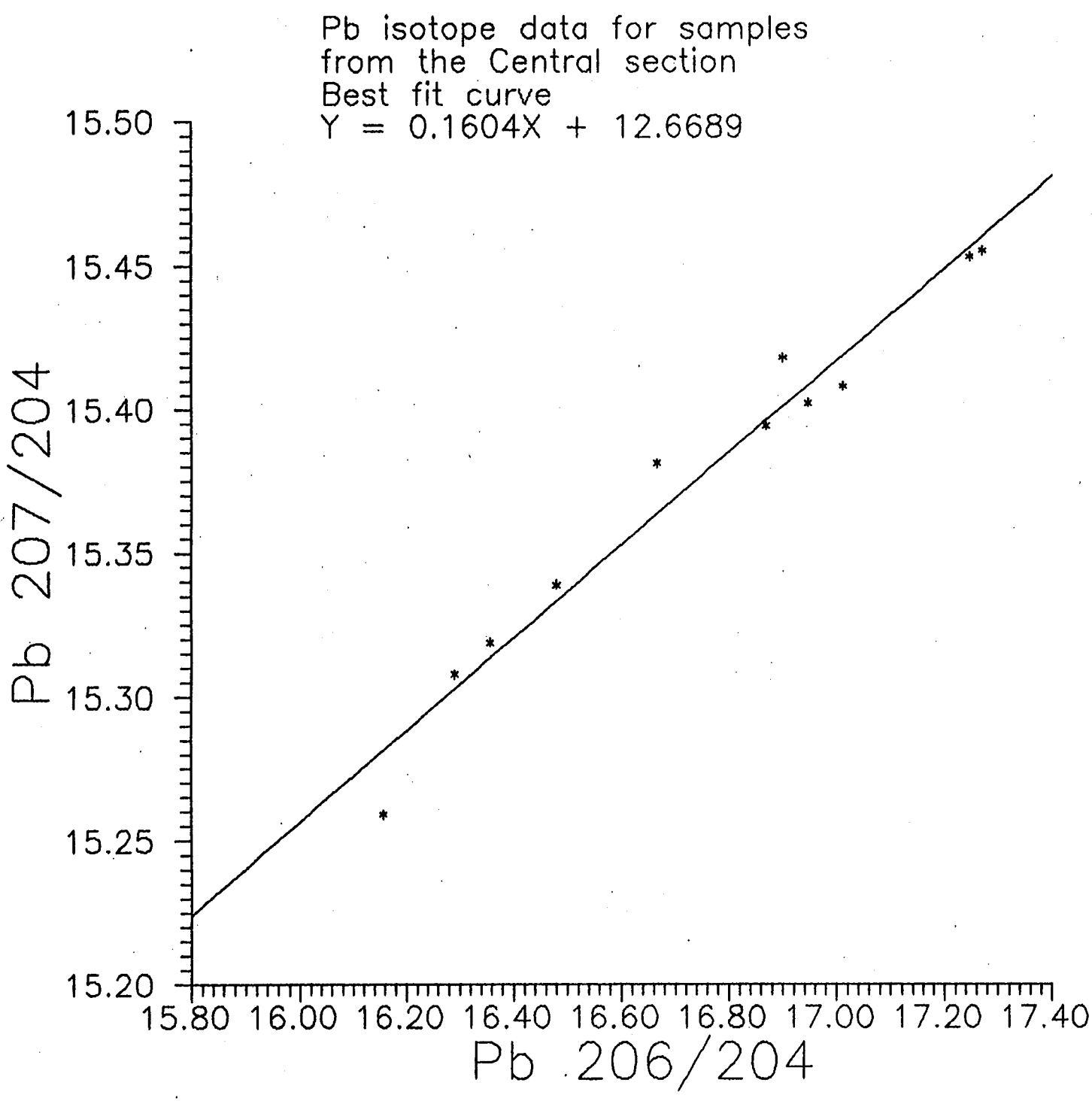
Pb isotope data for samples
from the Central section
Best fit curve
Y = 0.1604X + 12.6689
15.50
15.45
15.40
15.35
15.30
15.25
15.20
Pb 207/204
15.80 16.00 16.20 16.40 16.60 16.80 17.00 17.20 17.40
Pb 206/204

Figure 5.8: Pb data from Central section plotted with Pb evolution curve of Stacey and Kramers (1975), starting at 3.7 Ga ago (2nd stage). Illustrates possible transposed palaeoisochron that originates at 2.0 Ga and passes through 1.0 Ga on Pb evolution curve.

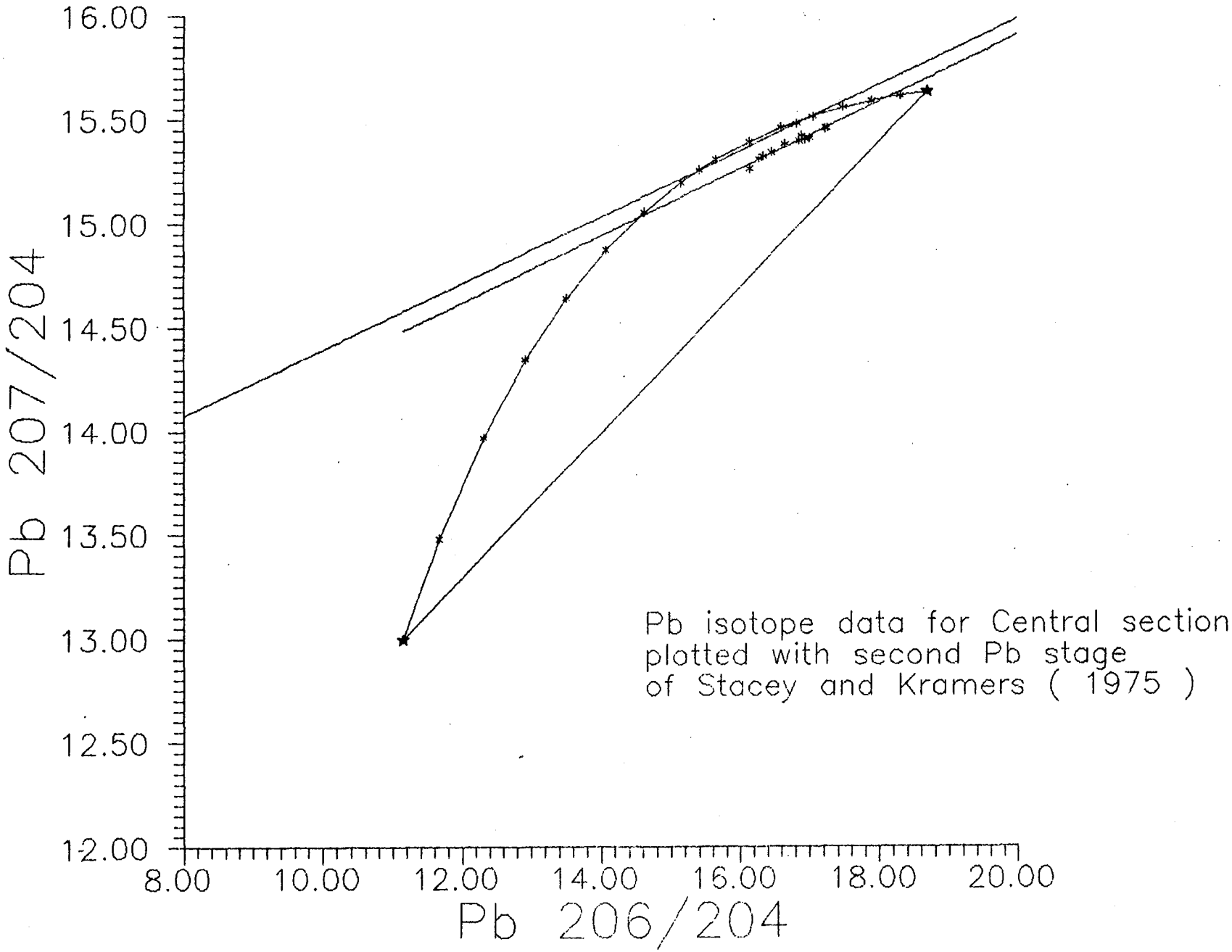
16.00
15.50
15.00
14.50
14.00
13.50
13.00
12.50
12.00
Pb 207/204
8.00
10.00
12.00
14.00
16.00
18.00
20.00
Pb 206/204
Pb isotope data for Central section
plotted with second Pb stage
of Stacey and Kramers (1975)

a combination of U/Pb resetting caused by the Grenville event, and Archean-Proterozoic mixing during the formation of this proposed ensialic arc. The implications of Archean-Proterozoic mixing are discussed in chapter 7.

5.1 ZIRCON DATING:

Zircon analyses were performed on two samples representing the Central section: GA 4 (T_{DM} = 1.92 Ga) and LSJ13 (T_{DM} = 2.02 Ga). Major element analyses for GA4 and LSJ13 indicated that these samples represent a granodiorite and a granite respectively. LSJ13 was taken from the Lorne Granite which was analyzed by Frithand Doig (1975) for Rb-Sr isotopes. The apparent Rb-Sr isochron age determined by these authors was 1745 +/- 23 Ma whereas the Sm-Nd model age for LSJ13 determined in this study was 2.02 Ga.

Nine zircons were extracted from GA4. These zircons were consistently subhedral and varied in length from less than 0.2 mm to 0.5 mm. Some contained dark inclusions and were transparent while others were stained brownish-orange, probably due to hematite along fractures. Zircons from GA4 generally had one end showing good crystal termination.

Zircons analyzed from LSJ13 were subhedral and quite large, some close to 1mm long. The zircons also tended to be a cloudy orange colour.

The purpose for analyzing zircons from GA4 was to determine the crystallization age of the large " granitic pegmatite " (G19: Government du Quebec map 32H7, 32H10, 32H15). Unfortunately, none of the zircons from GA4 contained enough Pb for any accurate Pb ratios to be determined.

However, LSJ13 did contain zircons with ample Pb for analysis. The data is shown graphically in Figure 5.9. Each zircon is represented by a different symbol. Concentrations of common Pb were estimated using Stacey and Kramers (1975) approximation of terrestrial Pb. The common Pb points were then combined with the Pb ratios from the zircons to make " two point isochrons " on a $^{207}Pb/^{206}Pb$ vs. $^{204}Pb/^{206}Pb$ plot. The intercept was then used to determine the ages of crystallization of the zircons.

The two zircons analyzed from LSJ13 contained enough Pb to produce several data points each. The oldest age was ca. 1430 Ma, which is about 590 Ma younger than the Sm-Nd model age, and 315 Ma younger than the result obtained from Rb-Sr dating by Frith and Doig (1975). The difference between Rb-Sr age and crystallization age is likely due to the Grenville event which reset the Rb-Sr system. The 265 Ma difference between the zircons suggests that the zircons have suffered Pb loss resulting from Grenville metamorphism. The large difference between Nd model age and crystallization age could

Figure 5.9: Zircon data from LSJ13.

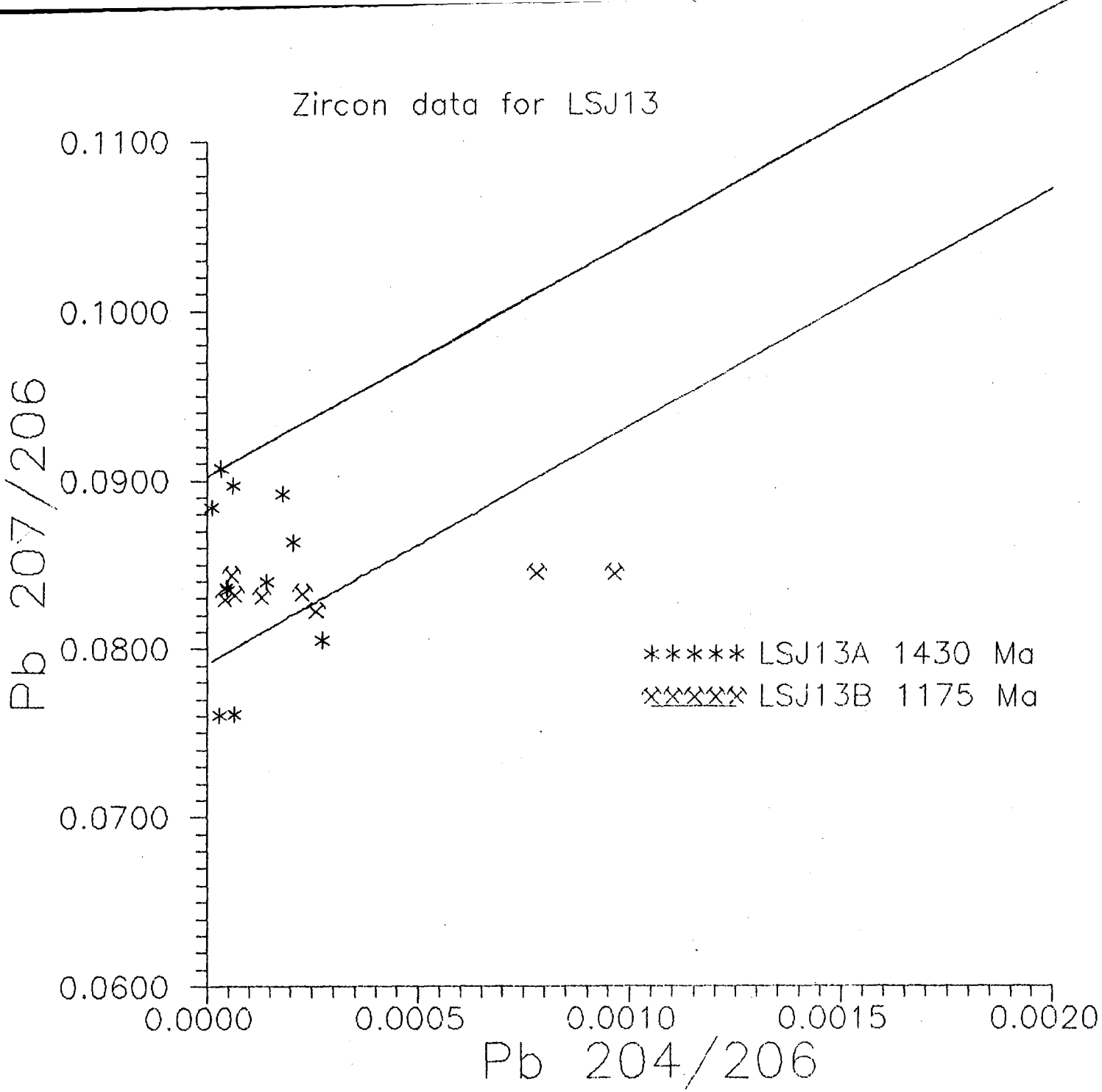
Zircon data for LSJ13
0.1100
0.1000
0.0900
0.0800
0.0700
0.0600
Pb 207/206
0.0000
0.0005
0.0010
0.0015
0.0020
Pb 204/206
***** LSJ13A 1430 Ma
xxxxx LSJ13B 1175 Ma

be caused by an Archean magma contribution that made the Nd model age older than the crystallization age. However, further zircon analyses for LSJ13 are required to determine if there are any inherited Archean zircons present.

CHAPTER 6

RESULTS:

EASTERN SECTION

The Eastern section covers approximately 30,000 Km^2 of the APB of Rivers et al., (1989), stretching northwards from Lac St. Jean to Lac Peribonca, and westwards from the Pipmuacan Reservoir to the Central section (Figure 6.1). Sampling east of Lac Rouvray could not be done because of the lack of access roads. Previous Sm-Nd work has been done further south and east of the Eastern section (Dickin and Higgins, 1992), revealing the possible existence of an accreted island arc approximately 1.5 Ga old.

Twenty-seven new samples were analyzed for Sm-Nd model age mapping. When combined with previously published data (Dickin and Higgins, 1992), the total number of samples analyzed is forty-seven. The data is shown in Table 6.1. Of the twenty-seven new samples, thirteen were analyzed for Pb isotopes.

A histogram of Sm-Nd model ages is shown in Figure 6.2 The model ages are fairly consistent over the Eastern field section, and are considerably younger than the neighbouring Central section. The strong consistency of model ages

Figure 6.1: Map of Eastern section.

Symbols: open circle = Nd model age > 1.50 Ga

open square = Nd model age < 1.50 Ga

small closed triangles = Nd model age between 1.50 Ga and 1.59 Ga

large triangles = Grenville Front

small open triangles = ABT of Rivers and Chown (1986)

closed triangle with circle = samples from Dickin and Higgins (1992)

box around closed triangle with circle = unpublished samples from the area studied by Dickin and Higgins (1992)

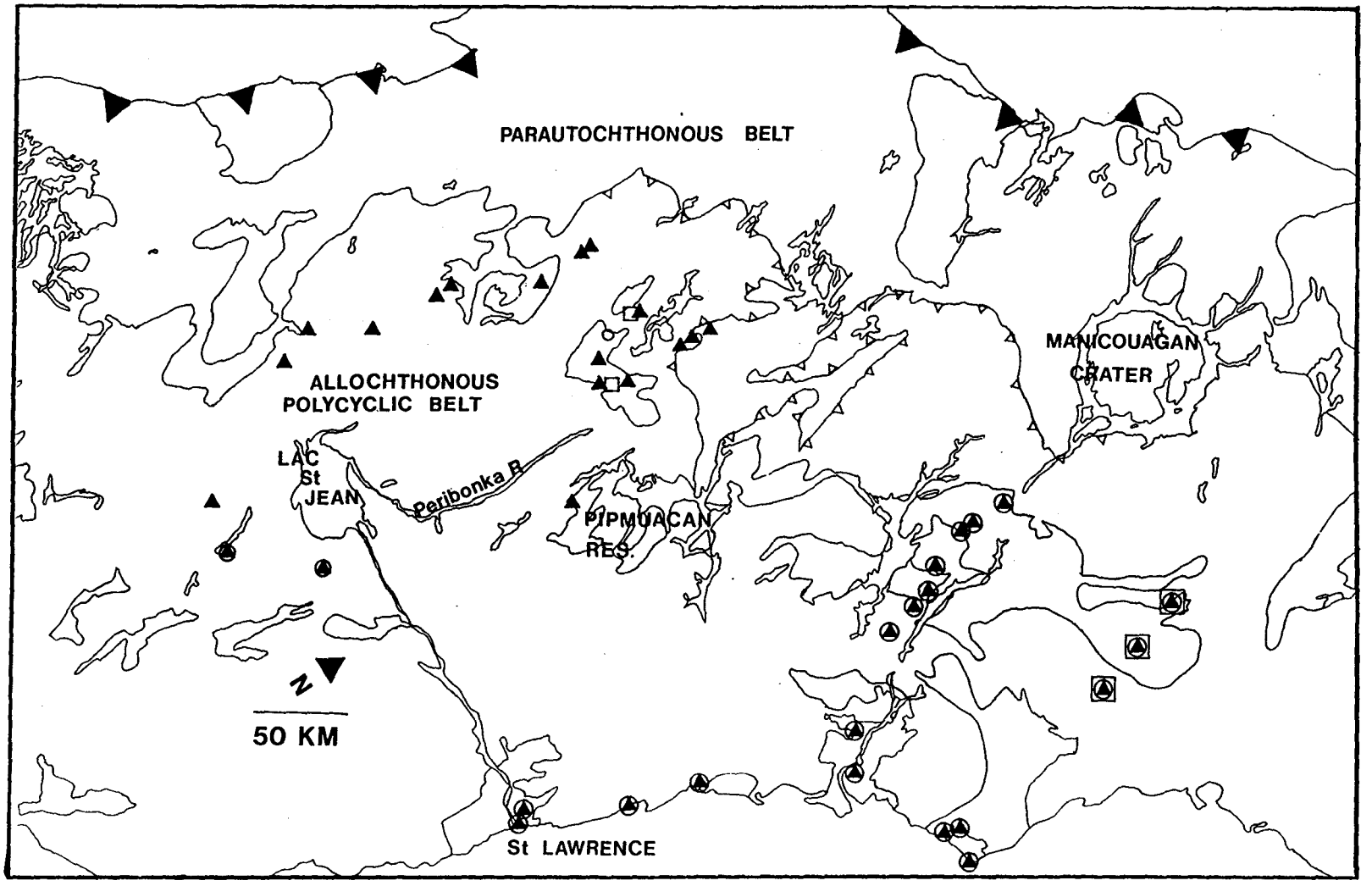
PARAUTOCHTHONOUS BELT
ALLOCHTHONOUS
POLYCYCLIC BELT
MANICOUAGAN
CRATER
LAC
St
JEAN
Peribonka R.
PIPMUACAN
RES.
N
50 KM
St LAWRENCE

TABLE 6.1: Sm/Nd data for Eastern section

Sample	Grid Ref.	Cor	Qz	*	Nd ppm	Sm ppm	$^{147}Sm/^{144}Nd$	$^{143}Nd/^{144}Nd$	TDM GA
MISTASSINI									
MS6	YL 860320	0.9	4.7	QM	124.90	17.42	.0843	.511762	1.51
MS8	YL 865540			nd	28.14	6.17	.1325	.512211	1.56
MS9	YL 150230			nd	40.16	7.42	.1117	.511991	1.57
FARLADEAU									
FA7	CE 635590	<-0.1	25.35	AD	50.75	10.13	.1206	.512107	1.53
GIRARDVILLE									
GL1	XK 754433			nd	41.48	8.60	.1253	.512132	1.57
LAC-AUX-RATS									
RA1	XK 939752			nd	20.35	3.87	.1150	.512008	1.59
RA4	XK 908854			nd	26.53	5.13	.1168	.512045	1.57
SAINT-LUDGE-DE-MILOT									
LU3	CF 358102	0.2	25.4	GR	41.76	8.60	.1246	.512135	1.55
LU5	CF 425129			nd	30.34	4.45	.0886	.511894	1.40
LU6	CF 448215	-0.8	20.2	GR	45.51	9.34	.1240	.512146	1.52
LU11	CF 279420	0.6	20.9	TN	16.31	2.60	.0962	.511863	1.53
LU12	CF 528575	-3.8	2.5	GO	41.73	9.11	.1320	.512199	1.57
LU14	CF 542608	0.2	16.3	TN	22.97	4.14	.1090	.511969	1.56
CDP1	CF 279185			nd	13.21	2.11	.0966	.511868	1.53
CDP2	CF 240312			nd	38.42	7.83	.1231	.512072	1.63
CDP4	CF 265453			nd	54.71	10.09	.1115	.512130	1.36
CDP5	CF 265475			nd	15.30	2.72	.1073	.511946	1.57
SAINT-THOMAS-DIDYME									
TD1	XK 645263			nd	24.36	5.11	.1269	.512139	1.58
SAINT-HEDWIDGE									
SH9	XJ 835565			nd	21.95	4.15	.1144	.512033	1.55

LAC-ST-JEAN									
LSJ 1	*XK	476174	3.2	24.8	TN	34.16	8.13	.1438	.512335 1.54
LSJ 2	*YJ	055320	1.3	27.0	AD	53.47	10.84	.1226	.512093 1.59
LSJ 4	*CD	022593	0.2	24.2	TN	23.38	4.25	.1099	.511985 1.55
NORTH SHORE OF ST. LAWRENCE RIVER									
NS 9	*DD	456393	2.0	24.1	TN	nd	nd	.0993	.511875 1.55
NS 11	*DD	498324	2.1	30.4	TN	nd	nd	.1044	.511939 1.54
NS 18A	*DD	814761	3.3	19.2	AD	34.45	6.85	.1202	.512072 1.58
NS 20	*DD	984062	2.2	28.0	GR	12.28	2.31	.1143	.512014 1.57
NS 29	*EE	996666	1.5	18.4	TN	13.43	2.60	.1171	.512081 1.51
NS 31	*FE	054734	3.9	16.9	GR	nd	nd	.1208	.512091 1.56
NS 32A	*FE	178638	4.2	33.2	GR	42.79	7.78	.1099	.511981 1.56
NS 32B	*FE	178638	3.2	33.1	G	32.07	6.29	.1186	.512059 1.57
MB 1	*EE	589512	2.1	33.1	GR	6.70	1.38	.1240	.511957 1.84
NS 27	*EE	718592	2.5	29.3	TN	14.12	2.44	.1045	.511808 1.71
MANICOUAGAN RIVER									
MA12.5	*EE	523607	1.8	30.7	TN	4.38	0.85	.1167	.512045 1.57
MA40	*EE	383743	1.9	16.5	GR	27.18	5.46	.1214	.512097 1.56
MA103	*EF	179205	0.5	25.6	GR	45.43	9.32	.1241	.512116 1.57
MA121	*EF	177364	2.0	26.3	TN	16.07	3.01	.1131	.512016 1.55
MA132.5	*EF	180464	1.4	30.9	AD	39.52	8.60	.1315	.512197 1.56
MA153.2	*EF	132573	2.5	33.8	GR	4.12	0.71	.1048	.511930 1.56
MA178.4	*EF	122812	1.0	28.2	GR	28.62	5.20	.1100	.511981 1.56
MA182.3	*EF	131859	3.1	32.0	AD	41.32	7.45	.1089	.511964 1.57
MA199.8	*EG	173022	1.8	24.9	TN	16.94	3.41	.1217	.512097 1.56
MA25.8	*EE	431643	3.0	25.0	AD	26.90	5.40	.1212	.511911 1.86
MA42.7	*EE	363753	1.6	31.9	GR	14.94	3.11	.1257	.511960 1.87
MA58.1	*EE	326867	0.5	27.7	G	49.16	9.50	.1168	.511791 1.97
MA67	*EE	297937	0.2	27.9	G	42.21	8.56	.1226	.511925 1.87
MA114.3	*EF	183304	1.5	26.5	GR	20.36	2.78	.0826	.511850 1.39

Notes; nd = not determined
Gneissic type: TN = tonalite; AD = adamellite; GR = granodiorite; G = granite; QM = quartz monzonite; GO = gabbro
Normative mineralogy; Cor = corundum; Qz = quartz
* = Dickin and Higgins, 1992
Negative corundum = diopside

Figure 6.2: Histogram of Nd model ages for all samples from the Eastern section.

Histogram of samples from the Eastern section

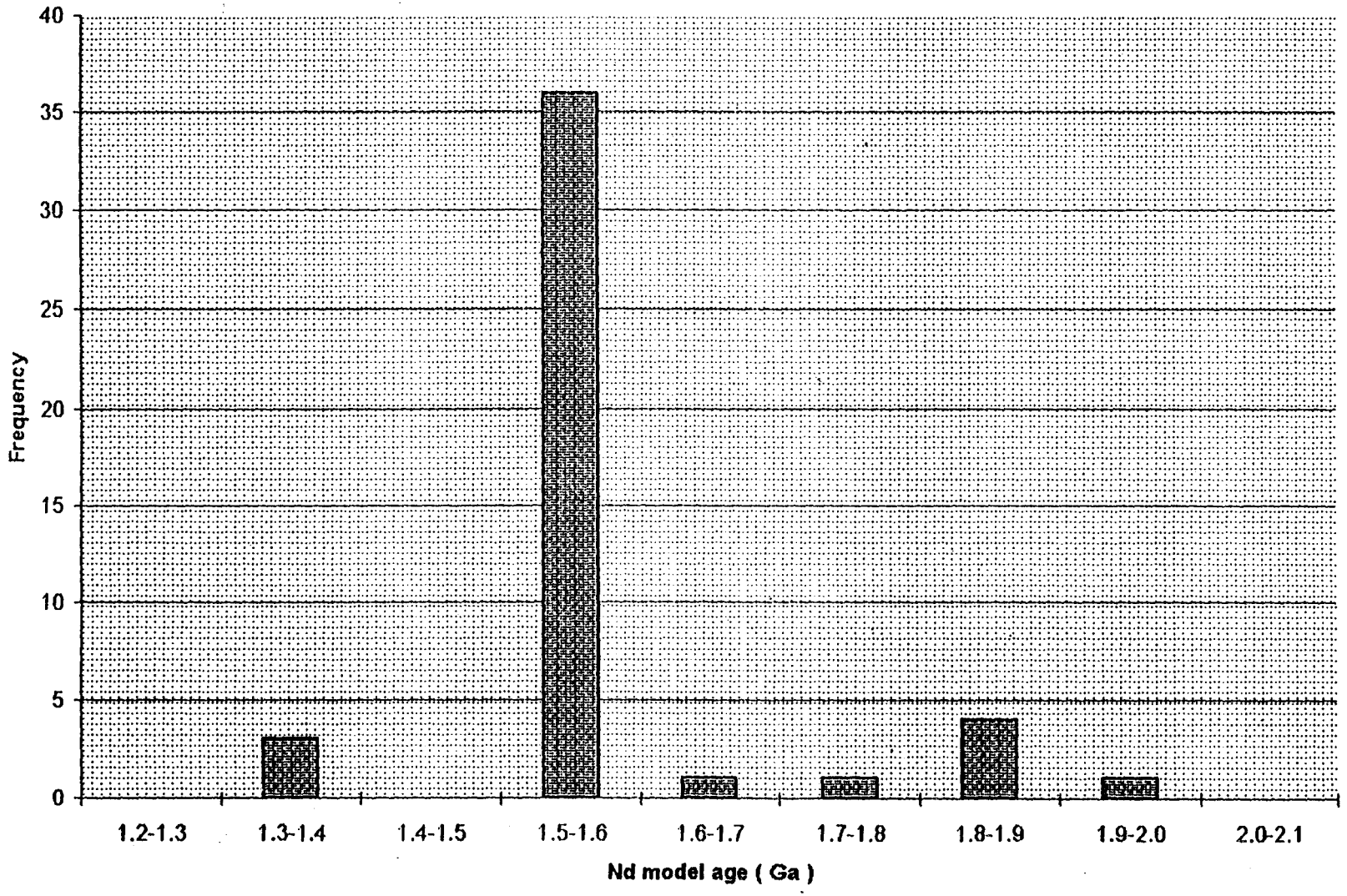

suggests that the rocks in the Eastern section all belong to the same rock association. A few samples, however, produced younger or older Nd model ages. The younger model ages are probably a product of later plutonism (CDP4, LU5).

The older Nd model ages (most of which are from Dickin and Higgins, 1992) may represent sedimentary rocks whose protoliths were early-Proterozoic granitoid rocks (Dickin and Higgins, 1992). These will not be considered further.

Geochemical analyses were performed on the samples to determine their tectonic affinities. Figure 6.3 is an AFM diagram. All but one sample (LU12) follows the calc-alkaline trend, implying an oceanic-continental subduction-related event. Figure 6.4 is the tectonic discrimination diagram of Debon and LeFort (1983). The gray gneisses form a distinct trend from tonalites to granites. This tonalitic rock suite is a prime candidate for orogenic, subduction-related island arc precursors that are associated with deep erosional levels of arc-related rocks (Windley and Tarney, 1986).

Figure 6.5 is a Y-Nb trace element diagram of all gray gneisses with ca. 1.5 Ga model ages. A large number of gray gneisses lie in the VAG and SYN-COLG, again implying an oceanic-continental subduction-related event. Several samples, however, fall just within the WPG field. Some of these samples (eg FA7, MA103, MA132.5) are classified as granites

Figure 6.3: AFM diagram for samples from the Eastern section.

Symbols: open circles = Nd model age outside of the 1.50 Ga to 1.59 Ga age bracket

closed diamonds = Nd model age between 1.50 Ga and 1.59 Ga

open diamonds = Dickin and Higgins, (1992)

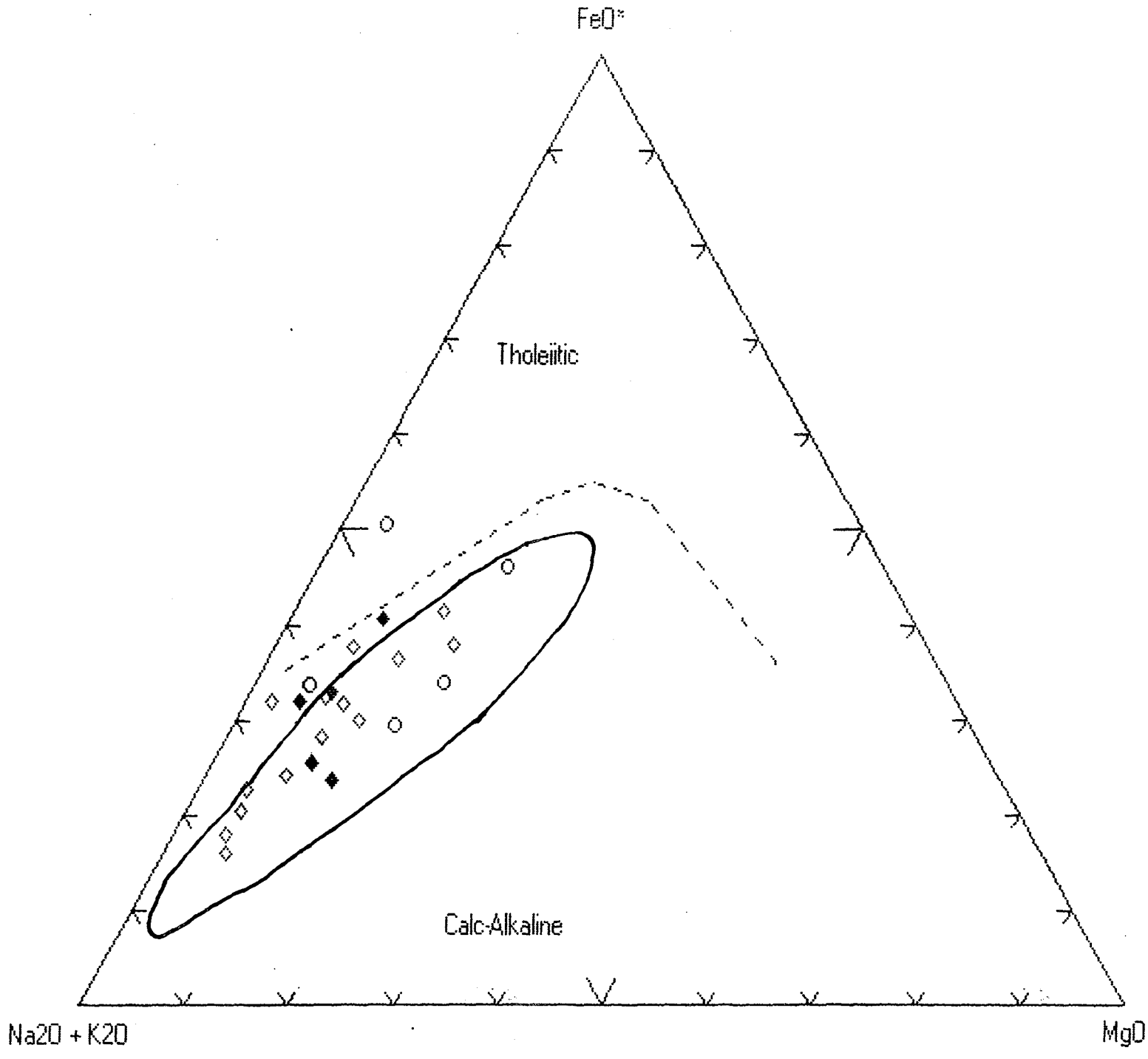
FeO*
Tholeiitic
Calc-Alkaline
Na2O + K2O
MgO

Figure 6.4: Q vs P plot for samples from the Eastern section. Symbols as in Figure 6.3. Numbers as in Figure 4.4.

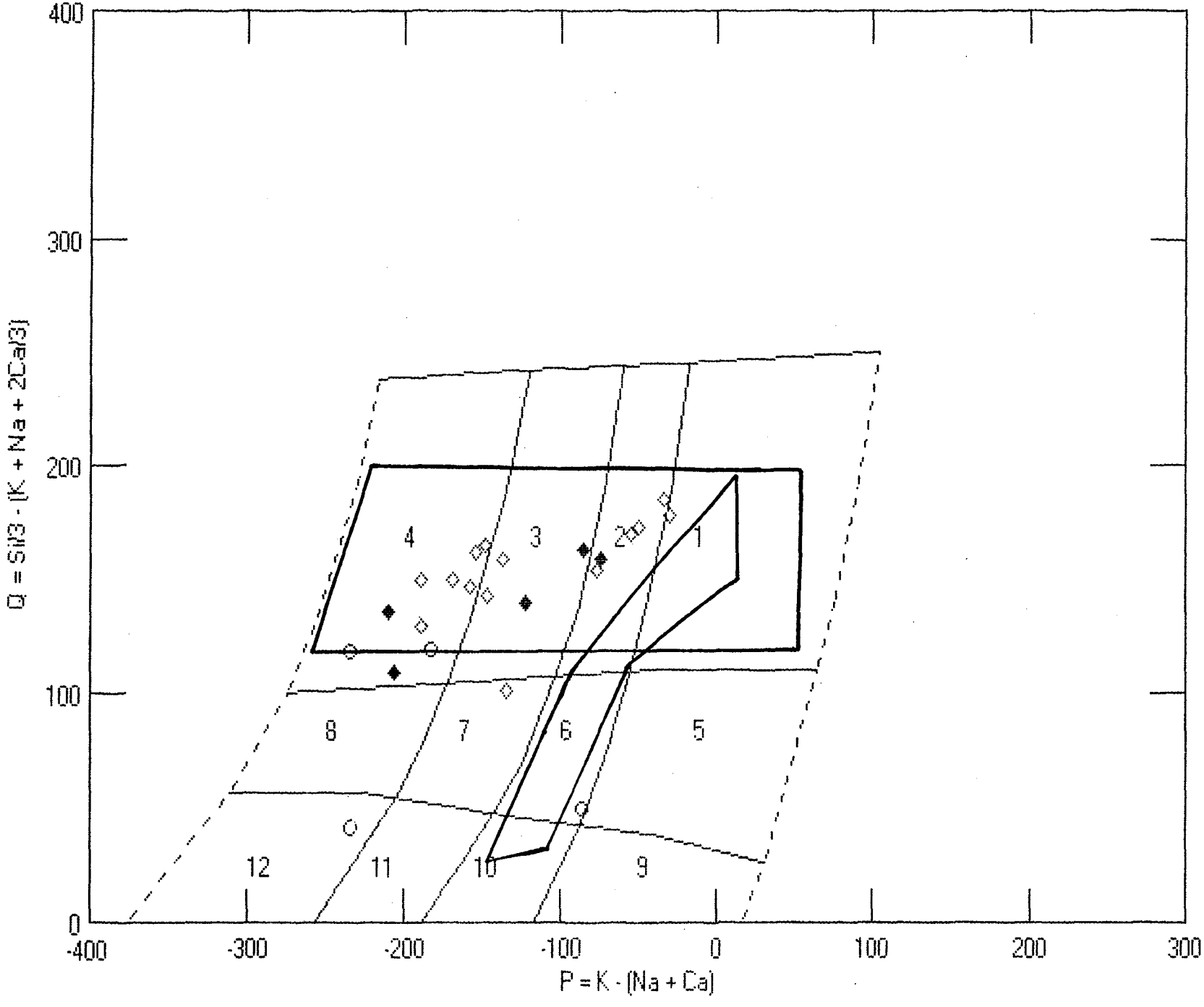
400
300
200
100
0
-400
-300
-200
-100
0
100
200
300
Q = Si/3 - (K + Na + 2Ca/3)
P = K - (Na + Ca)
4
3
2
1
8
7
6
5
12
11
10
9

Figure 6.5: Y vs Nb for samples from the Eastern section. Symbols as in Figure 6.3. WPG = within plate granitoid; ORG = ocean ridge granitoid; VAG = volcanic arc granitoid.

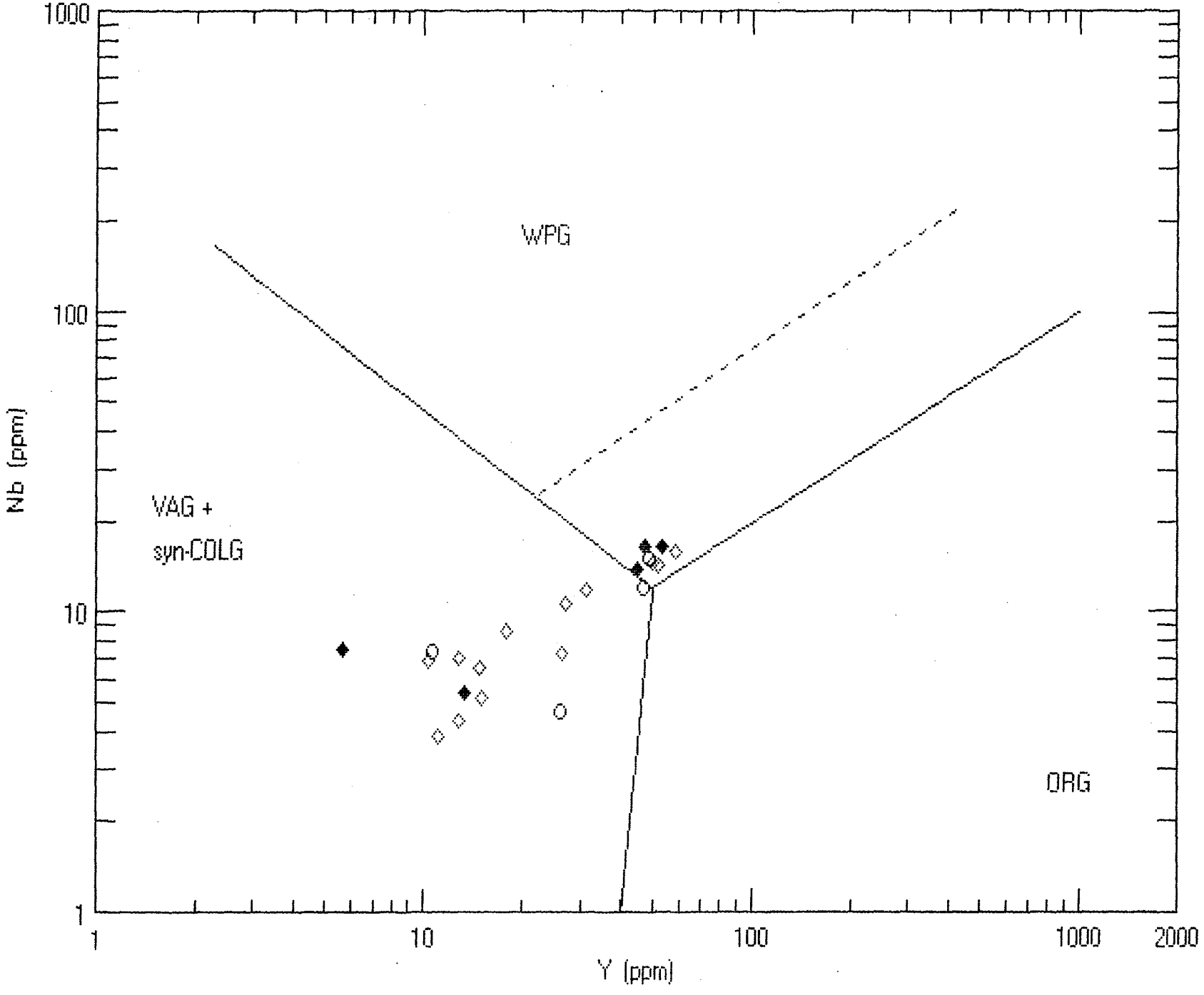
1000
100
10
1
Nb (ppm)
WPG
VAG +
syn-COLG
ORG
1
10
100
1000
2000
Y (ppm)

in Figure 6.4. Perhaps these granitic gneisses represent a differentiated core of the island arc. The arc may have been large enough to allow Y concentrations to increase in the evolving granitic core. A few samples (eg LU12, MS6) also fall in the WPG field. However, neither of these samples are of the tonalite-granite suite (Figure 6.4).

Figure 6.6 represents a Sm-Nd isochron of all ca. 1.5 Ga gneisses. The solid symbols represent data from this study whereas open symbols are taken from Dickin and Higgins (1992). Four samples have been excluded from the Sm-Nd isochron: MS6 and LU12 were excluded because they did not represent rocks from the tonalite suite (MS6 = quartz monzonite; LU 12 = gabbro; stars on Figure 6.6). The other two samples were excluded because their model ages are far outside the 1.5 to 1.59 Ga age bracket (CDP4 = 1.36; LU5 = 1.40). CDP4 and LU5 are likely a product of younger plutonism, and therefore do not represent the ca. 1.5 Ga crust-forming event. The isochron produces an age of 1.50 +/- 0.071 Ga (2σ) with an initial $^{143}Nd/^{144}Nd$ ratio of 0.510900, corresponding to an Epsilon-Nd value of +3.8 which is close to the Epsilon-Nd of DePaolo's Depleted Mantle Model at 1.50 GA (+4.6).

Figure 6.7 represents a QAP diagram for a modern version of an ensialic arc: The Blanco Batholith of Peru. The diagram illustrates the large range of lithologies caused, in part, by variable mixing of subduction-related magmas with existing

Figure 6.6: Sm-Nd isochron for all samples with ca. 1.5 Ga Nd model age. Symbols: open = data from Dickin and Higgins (1992); closed = this study; triangles = granite; squares = adamellite; circles = granodiorite; diamonds = tonalite; * = not included in isochron.

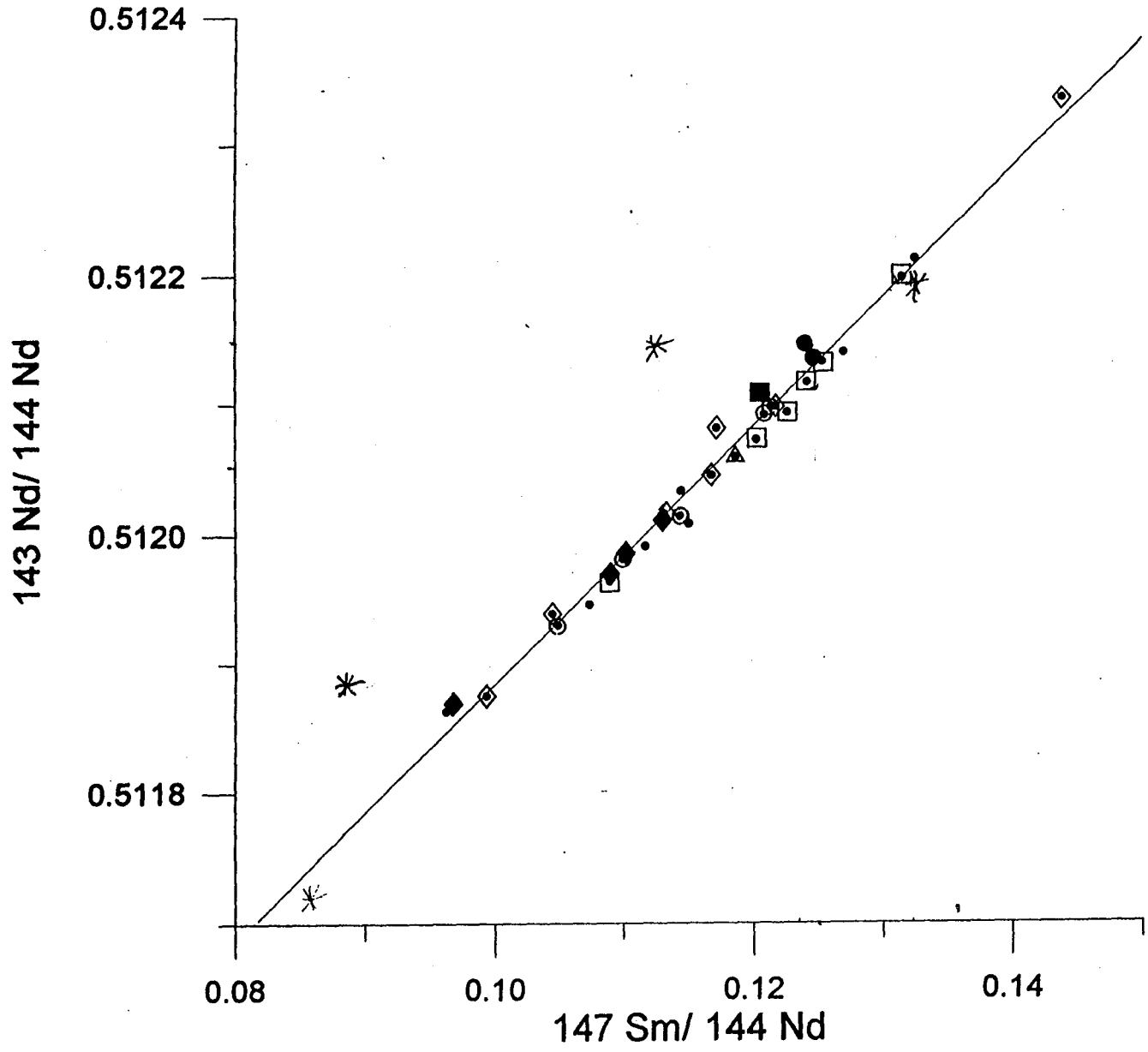
0.5124
0.5122
0.5120
0.5118
143 Nd/ 144 Nd
0.08
0.10
0.12
0.14
147 Sm/ 144 Nd

Figure 6.7: QAP diagram for the Lima (closed circles) and Arequipa (open circles) segments of the Peruvian Coastal Batholith. (after Atherton et al., 1979) Numbers as in Figure 5.5.

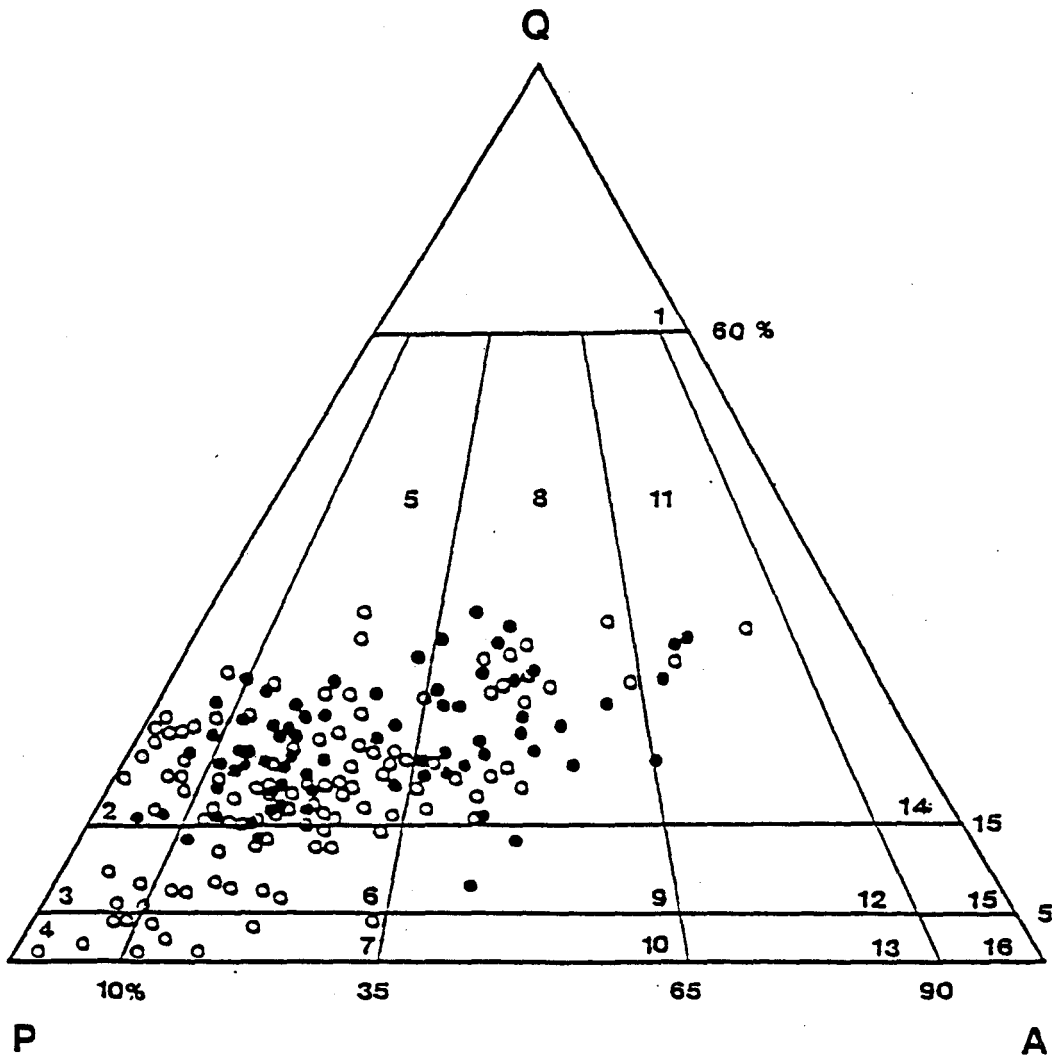
Q
1
60 %
5
8
11
2
14
15
3
6
9
12
15
5
4
7
10
13
16
10%
35
65
90
P
A

continental margin, as well as magma body differentiation during slow diapiric rise through a thickened crust. Rocks of the proposed island arc, on the other hand, are far more restricted in lithology. These gneisses lie only in the tonalitic-granodioritic field (Figure 6.4). It should also be noted, however, that these gneisses probably represent a much deeper crustal level than the Peruvian rocks because of uplift and erosion caused by the Grenville orogeny.

However, rocks representing the proposed ensialic arc from the Central section do represent a deep crustal level. Comparison of Figure 6.4 with Figure 5.4 reveals that samples from the Central section contain a much wider lithological range that exemplify intermediate conditions between orogenic (tonalite-granite suite) and anorogenic monzonite and quartz monzonite. An ensialic arc is expected to have a much wider temporal and spatial range of model ages due to variable mixing of rising diapirs with the existing continental margin. Not only would such mixing produce a wide range of Nd model ages, it would also produce highly variable $^{143}Nd/^{144}Nd$ and $^{147}Sm/^{144}Nd$ ratios and hence an isochron of poor quality. The spread of isotopic ratios in an ensialic arc regime could be caused by mixing of rocks of different age.

However, for the Eastern section of the field area, the tectonic discrimination diagrams suggest that the area analyzed both by Dickin and Higgins (1992) and the new

samples north and west of the previous study represent the roots of a volcanic arc. The large geographical distribution of gray gneisses with approximately the same Nd model age, and the excellent fit of these samples on the Sm-Nd isochron implies that these rocks represent an accreted island arc rather than an ensialic continental arc.

Pb isotopic data for a selection of the new samples are shown in Table 6.2. In general, samples from the Eastern section contain more radiogenic Pb than samples from the rest of the field area because they are younger. Figure 6.8 is a Pb isochron plot for the thirteen analyzed samples from the Eastern section. The best-fit curve for the data produces a slope of 0.1077 +/- 0.014. This $^{207}Pb/^{206}Pb$ ratio corresponds to a single-stage apparent age of approximately 1.76 +/- 0.220 Ga. Two samples have been excluded from the isochron: MS6, and LU12. MS6 and LU12 are excluded because they do not represent rocks from the tonalite-granite suite. The single stage apparent Pb age is not the same as the Sm-Nd isochron age, or the Nd model ages. Thus, this suggests that a single stage model is inapplicable to these rocks.

As in chapters 4 and 5, the Pb data was recalculated assuming a 1.1 Ga metamorphic event caused depleted, uniform U/Pb ratios. However, the age produced from the slope of the new array only produced an age of 1100 Ma, suggesting that Pb isotopes for the Eastern section do not represent a simple

Table 6.2: Pb data for samples from the Eastern section

Sample Name	Grid Refer.	$^{206}Pb/^{204}Pb$	$^{207}Pb/^{204}Pb$	$^{208}Pb/^{204}Pb$	Lithology
TD 1	XK 645263	17.309	15.406	36.283	nd
CDP 1	CF 279185	16.722	15.365	nd	nd
CDP 5	CF 265475	17.200	15.438	36.407	nd
LU 3	CF 358102	17.265	15.426	36.414	GR
LU 6	CF 448215	17.700	15.436	34.807	GR
LU 11	CF 279420	16.902	15.389	36.330	TN
LU 12*	CF 528575	17.048	15.327	35.963	GO
RA 1	XK 939752	17.473	15.463	36.602	nd
RA 4	XK 908854	17.156	15.392	36.245	nd
MS 6*	YK 163317	17.711	15.421	36.967	QM
MS 8	YL 865540	16.985	15.388	36.163	nd
MS 9	YL 150230	18.115	15.525	37.142	nd
FA 7	CE 635590	17.665	15.472	36.613	AD

Notes: nd = not determined
Lithology determined from Q-P plot
GR = granodiorite; TN = tonalite; GO = gabbro; QM = quartz monzonite
* = not included in Pb isochron

Figure 6.8: Pb isochron diagram for samples from the Eastern section

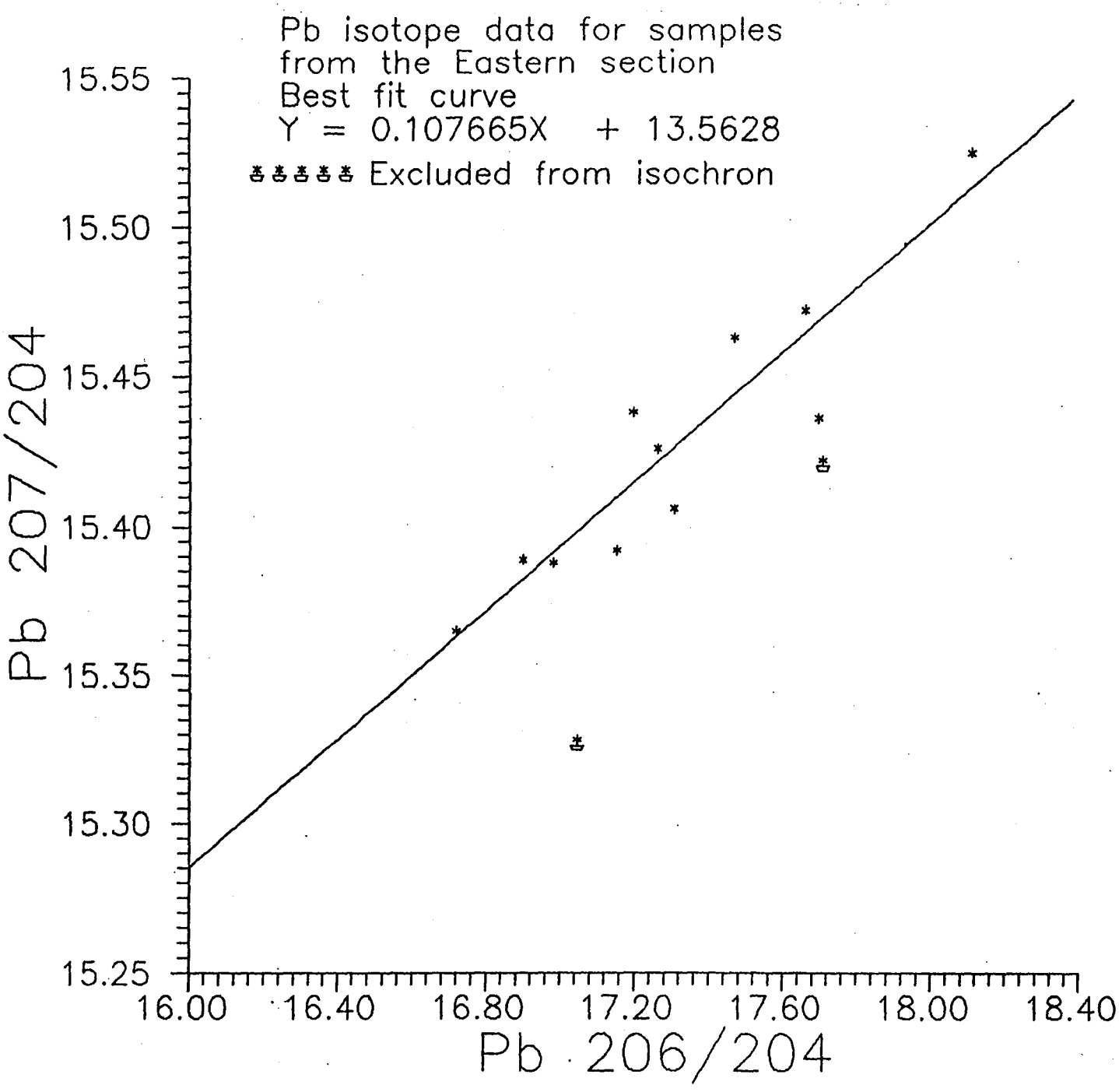
Pb isotope data for samples
from the Eastern section
Best fit curve
Y = 0.107665X + 13.5628
Excluded from isochron
15.55
15.50
15.45
15.40
15.35
15.30
15.25
Pb 207/204
16.00
16.40
16.80
17.20
17.60
18.00
18.40
Pb 206/204

transposed palaeoisochron (shown graphically in Figure 6.9). However, the anomalously old common Pb-Pb age still suggests that there may have been at least partial resetting of U/Pb ratios, and it is quite likely that the Grenville event was responsible. Thus, as a rough estimate for the extent of U/Pb resetting, several calculations were done using different values of t (instead of 1100 Ma) to determine which could produce a slope age of approximately 1.5 Ga. A value of 400 Ma for t produced an age of 1498 Ma (+ 462 Ma, - 662 Ma). This suggests that the U/Pb ratios of these samples were only partially reset.

The samples with the highest radiogenic Pb (FA7, LU3, and LU6) that had major element chemistry determined and represented rocks from the tonalite-granite suite (Figure 6.4), all fall in the WPG field on the Y-Nb tectonic discrimination plot (Figure 6.5), while the least radiogenic sample (LU11) lies in the VAG and SYN-COLG field in Figure 6.5. Thus, the undifferentiated, least radiogenic samples are good examples of relatively primitive arc material, while the other samples represent differentiated material. However, the differentiated samples can still be considered " arc-derived " because of their " good fit " on the Sm-Nd isochron plot (Figure 6.6).

Figure 6.9: Pb data from Eastern section plotted with Pb evolution curve of Stacey and Kramers (1975), starting at 3.7 Ga ago (2nd stage). Illustrates that the these rocks do not get U/Pb ratios completely disrupted by the Grenville event (no transposed palaeoisochron).

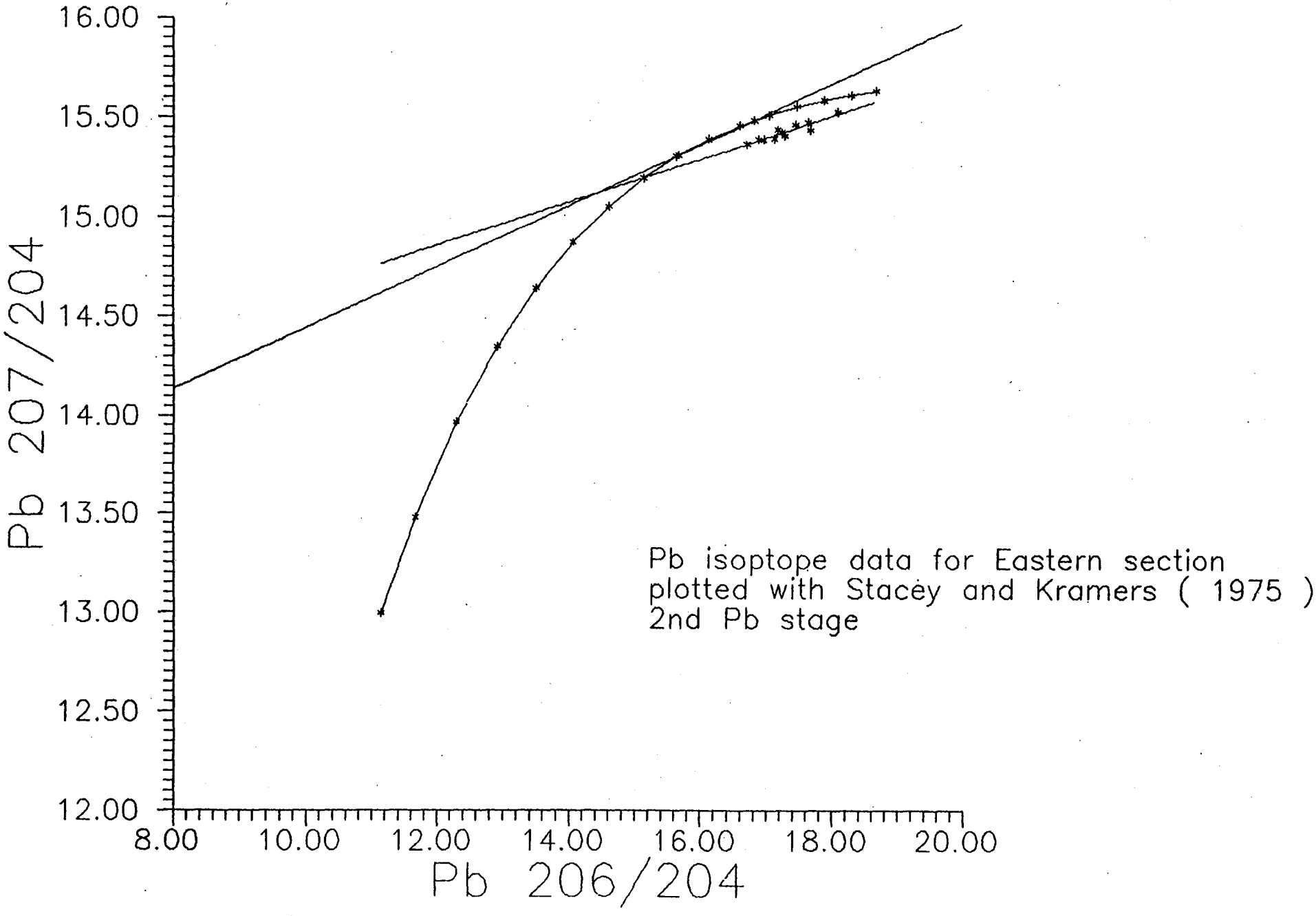
16.00
15.50
15.00
14.50
14.00
13.50
13.00
12.50
12.00
Pb 207/204
8.00
10.00
12.00
14.00
16.00
18.00
20.00
Pb 206/204
Pb isoptope data for Eastern section
plotted with Stacey and Kramers (1975)
2nd Pb stage

6.1 ZIRCON DATING

Zircon Pb-Pb dating was done on four samples collected the Eastern section: FA7, LU6, NS45, and CS20. Of these four samples, the latter two were taken from, and east of, the area analyzed by Dickin and Higgins, (1992) (NS45: FF 585775, and CS20: FG 063248 respectively), while the former two were taken from the Eastern section of the field area presented in this study (note: CS20 and NS45 are not published in Dickin and Higgins). The Sm-Nd model ages for FA7 and LU6 are 1.53 Ga and 1.52 Ga respectively. Major element analyses of FA7 indicates that this sample represents an adamellite while LU6 represents a granodiorite. The Sm-Nd model age NS45 is 1.60 Ga. The Sm-Nd model age for CS20 was not determined. However, CS20 was close to other samples with Nd model ages of ca. 1.60 Ga. Visual inspection of both of these samples indicates that they are foliated granites.

Nineteen zircons were tested from CS20. Of these nineteen zircons, eight produced usable Pb data. The data are shown graphically in Figure 6.10. Each zircon analyzed is represented by a different symbol. Some zircons had enough Pb to produce four or five data points (each data point represents the average of eight ratios). Concentrations of common Pb were estimated using Stacey and Kramers (1975)

approximation of terrestrial Pb. These common Pb points were then combined with the Pb ratios from the zircons to make " two point isochrons " on $^{207}Pb/^{206}Pb$ vs. $^{204}Pb/^{206}Pb$ plots. The intercept was then used to determine the age of crystallization of the zircon.

The Pb data for CS20 indicate that most of the zircons are approximately 1050 Ma old, with a maximum of approximately 1140 Ma. This age is considerably younger than the Sm-Nd model age. There are two possible explanations for this. Firstly, the zircons may have experienced a metamorphic event just prior to 1110 Ma. The metamorphic event (i.e. the Grenville orogeny) was sufficiently strong enough to cause significant Pb loss from the zircons, thus making the apparent Pb-Pb ages younger. Although the 210 Ma range of crystallization ages suggests partial Pb loss from some zircons, it seems unlikely that all zircons would have been reset. Because most of the zircons thatcrystallized at 1050 Ga were so radiogenic, it would seem that this is the best approximation for the crystallization age. Even though Pb loss did occur, it was not as severe enough to explain the large difference between Nd model age and crystallization age. The second explanation for the difference between Nd model age and crystallization age seems the most plausible. CS20 is a pink granite, and thus represents a well differentiated rock. The melting event that formed CS20 was efficient enough that

Figure 6.10: Pb data for zircons from CS20.

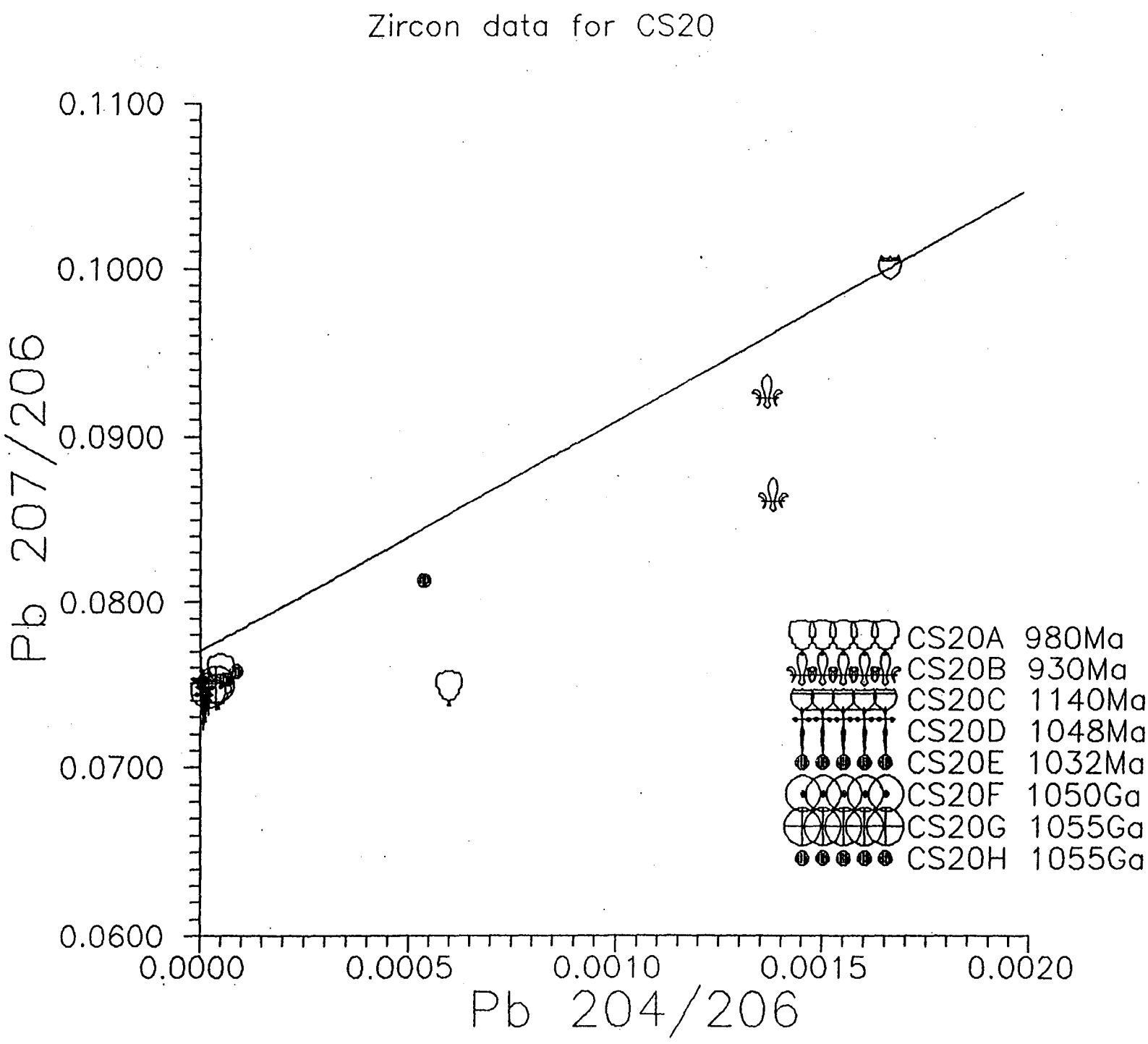
Zircon data for CS20
0.1100
0.1000
0.0900
0.0800
0.0700
0.0600
Pb 207/206
0.0000
0.0005
0.0010
0.0015
0.0020
Pb 204/206
CS20A 980Ma
CS20B 930Ma
CS20C 1140Ma
CS20D 1048Ma
CS20E 1032Ma
CS20F 1050Ga
CS20G 1055Ga
CS20H 1055Ga

any older zircons were completely melted. Later, the melt cooled sufficiently to allow recrystallization of zircons approximately 1100 years ago. However, the Sm-Nd isotope ratio was not affected by this melting event and still indicates the time of crustal extraction from the mantle. This explanation is the most satisfactory because it can explain the difference between Nd model age and crystallization age. Thus, the protolith to CS20 separated from the mantle approximately 1.5 Ga ago, but was remelted during the Grenville event, and recrystallized approximately 1100 years ago.

The data for NS45, FA7, and LU6 are shown in Figures 6.11, 6.12, and 6.13 respectively. Of the thirty-five zircons extracted from NS45, only three produced suitable Pb ion beams. For the twenty-eight FA7 zircons, only six contained sufficient Pb. Similar misfortune occurred when only 1 out of twenty-nine performed satisfactorily for LU6.

Zircons from FA7 and NS45 where similar in appearance. Several were quite large; approximately 0.8 mm long. Each sample contained zircons that were both transparent and cloudy. Some zircons had dark inclusions while others were free from inclusions. The transparent zircons tended to be euhedral in habit while cloudy zircons were subhedral. The different crystal morphologies suggested two generations of zircons. Initially, the cloudy, subhedral zircons were thought

Figure 6.11: Pb data for zircons from NS45.

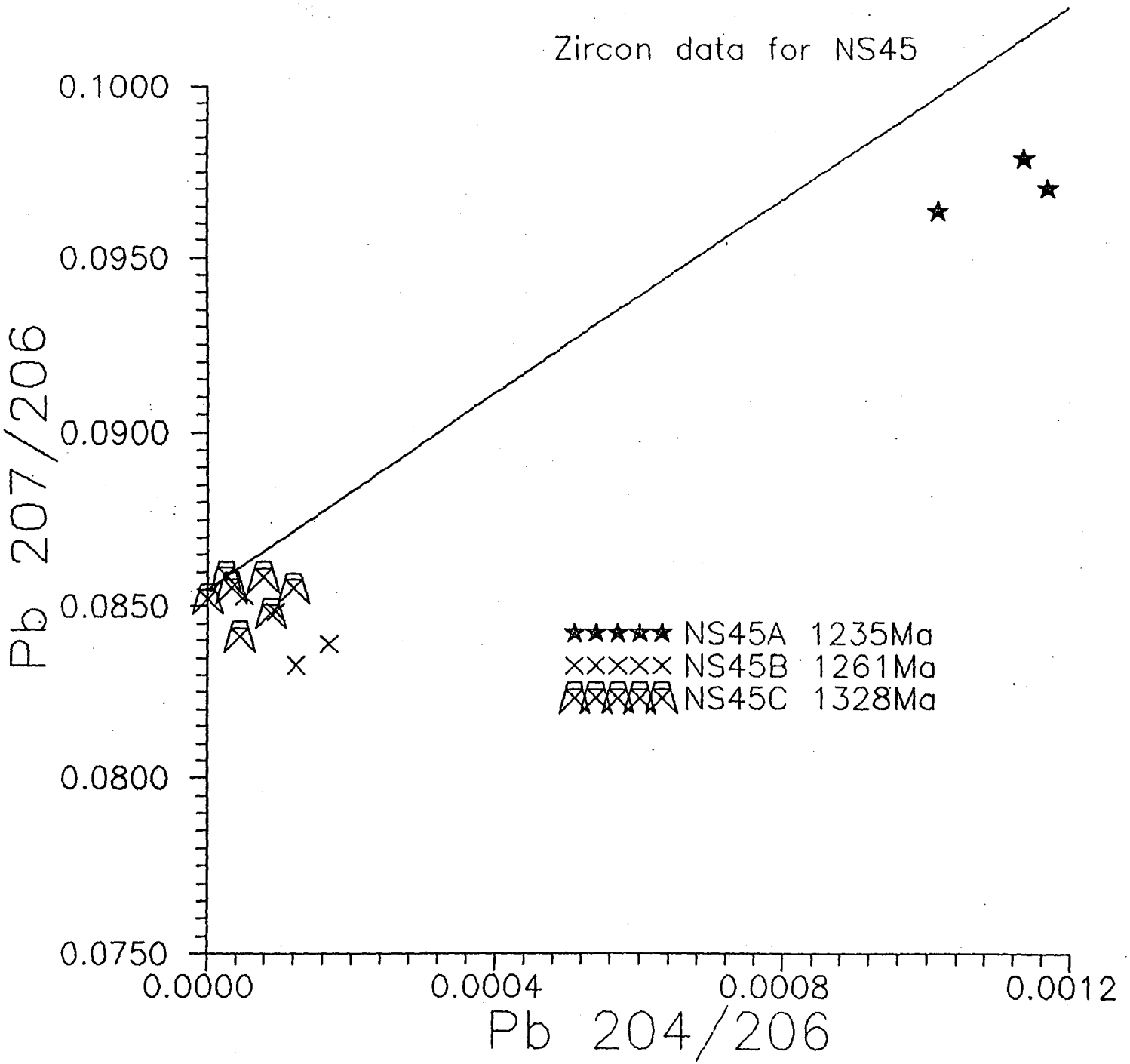
Zircon data for NS45
0.1000
0.0950
0.0900
0.0850
0.0800
0.0750
Pb 207/206
0.0000
0.0004
0.0008
0.0012
Pb 204/206
NS45A 1235Ma
NS45B 1261Ma
NS45C 1328Ma

Figure 6.12: Pb data for zircons from FA7.

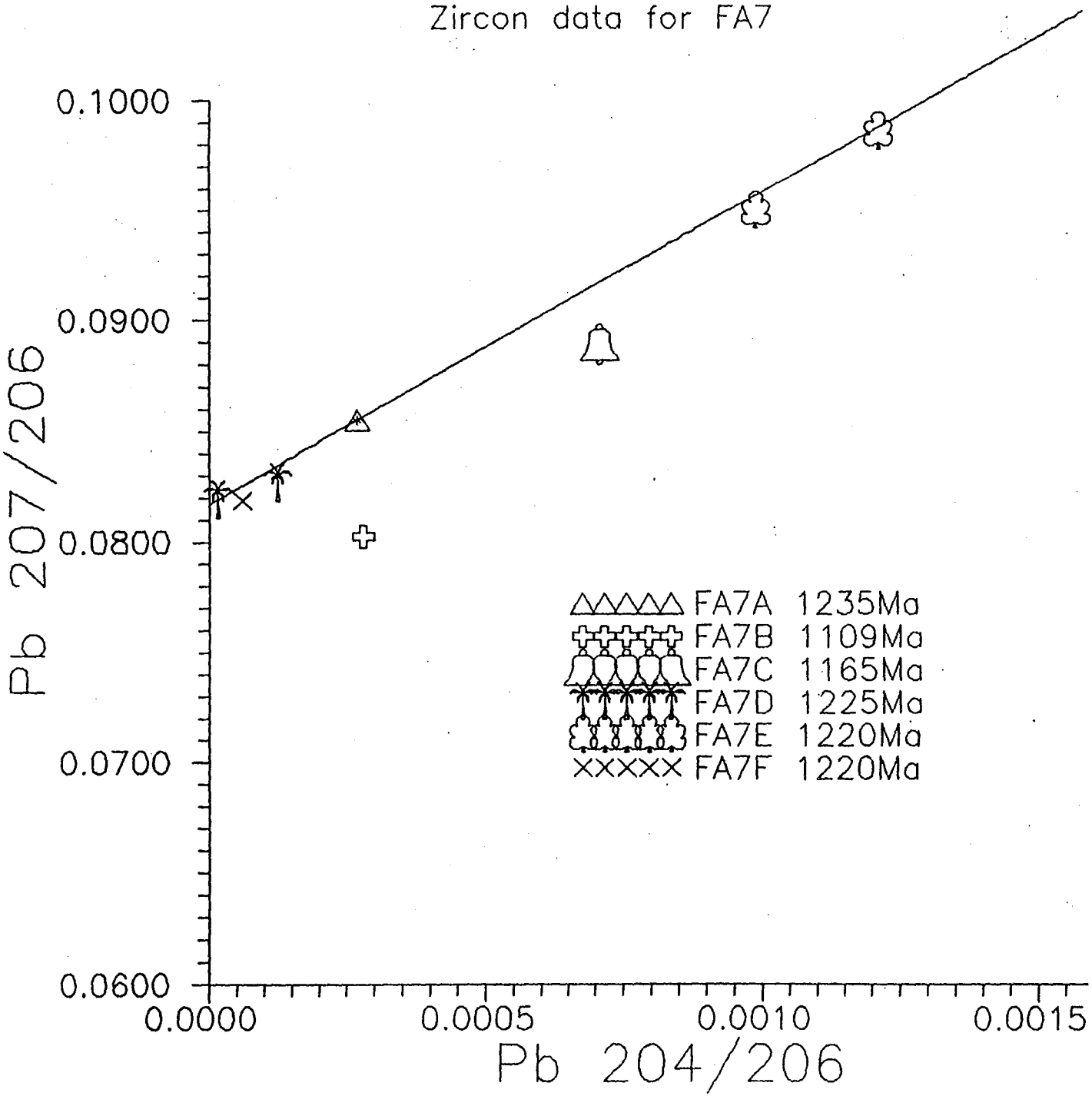
Zircon data for FA7
0.1000
0.0900
0.0800
0.0700
0.0600
Pb 207/206
0.0000
0.0005
0.0010
0.0015
Pb 204/206
FA7A 1235Ma
FA7B 1109Ma
FA7C 1165Ma
FA7D 1225Ma
FA7E 1220Ma
FA7F 1220Ma

Figure 6.13: Pb data for zircon from LU6.

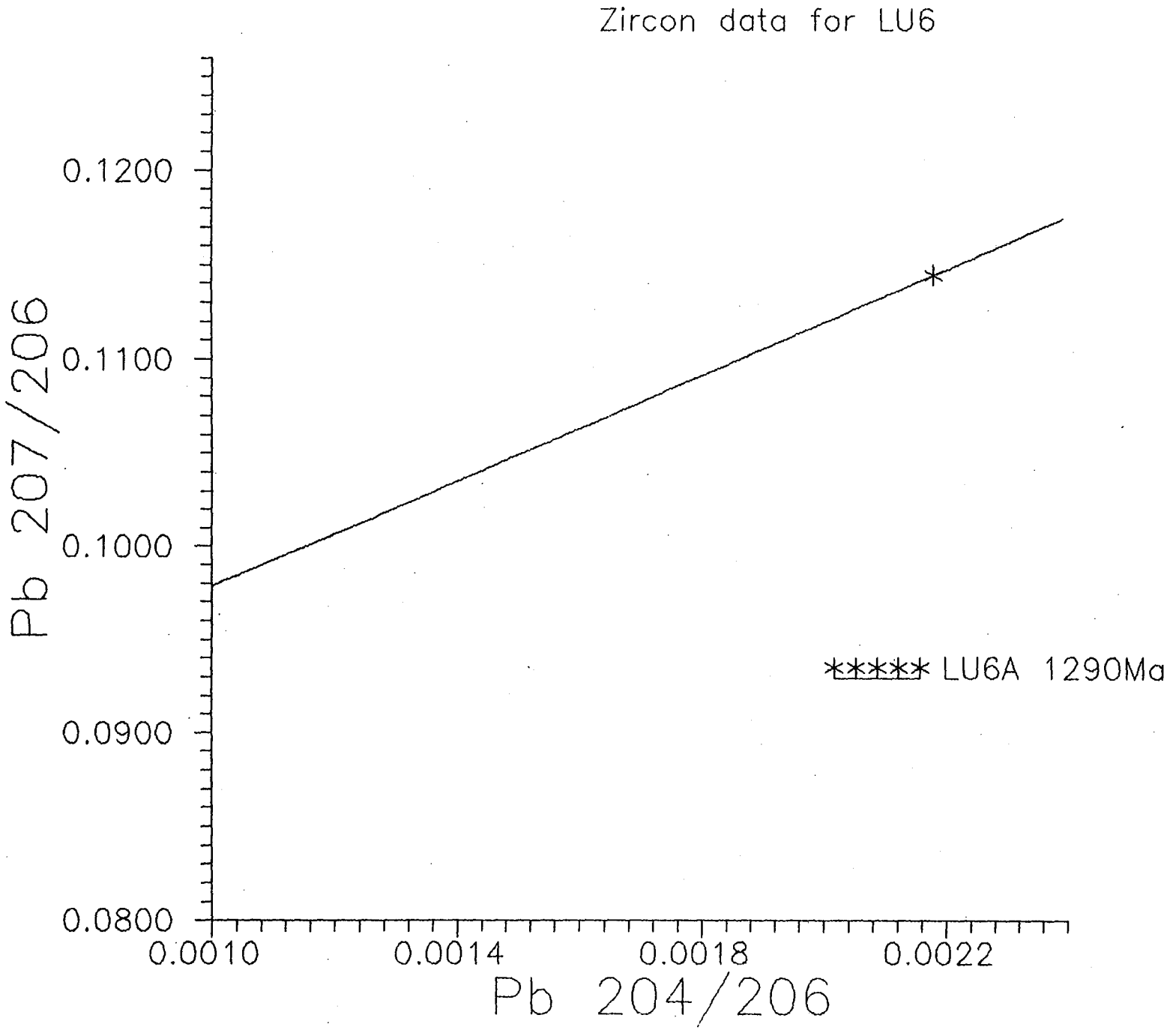
Zircon data for LU6
0.1200
0.1100
0.1000
0.0900
0.0800
Pb 207/206
0.0010
0.0014
0.0018
0.0022
Pb 204/206
***** LU6A 1290Ma

to be older than the euhedral crystals. However, both types yielded similar $^{207}Pb/^{206}Pb$ ages. The zircons extracted from LU6, on the other hand, were smaller than those from NS45 and FA7. LU6 zircons tended to be more transparent and euhedral, with less fractures and inclusions. None of the zircons from any of the samples showed evidence of older cores.

From the three graphs, it is evident that all three samples suffered Pb loss indicated by the range of crystallization ages. However, none of the samples analyzed had a crystallization age close to their Sm-Nd model age. For example, NS45 has a crystallization age approximately 280 Ma younger than the Sm-Nd model age. As was the case for CS20, NS45 is a foliated granite and thus the difference between crystallization age and Nd model age might be a result of melting which eliminated older zircons, but failed to reset the Sm-Nd isotopic system.

Similarly, the oldest crystallization date for FA7 was still approximately 290 Ma younger than the Sm-Nd model age. However, the crystallization ages differ by more than 120 Ma, implying significant Pb loss. Thus, there is a possibility that older zircons may exist.

LU6, like the other samples, did not have a crystallization date and Nd model age within error. Unfortunately, only one zircon produced a large enough Pb beam to allow data collection. This single zircon produced an age

of approximately 1290 Ma. However, the lack of other zircons, and the large volume of common Pb precludes any good estimations of meaningful crystallization ages. Since LU6 represents a granodiorite, thus it has not undergone significant differentiation, and therefore is not likely to be as U rich as the other samples. This would explain the poor results from LU6 zircons.

Although the current study did not produce any minimum crystallization ages old enough to justify the ca. 1.5 Ga Sm-Nd age of the arc terrane, other work has revealed a 1.39 +/- 0.02 Ga U/Pb age for a gabbroic intrusion southeast of the Lac St. Jean anorthosite (Hervet et al., 1990). Thus, further zircon dating may produce conformable zircon/Sm-Nd ages.

CHAPTER 7

DISCUSSION AND CONCLUSIONS

The results described above suggest that the Lac St. Jean region in the central Grenville Province may contain both an ensialic arc (Central section) as well as two island arcs (Western and Eastern sections). This conclusion is derived from three separate lines of evidence: Sm-Nd model age dating, major and trace element geochemistry, and common Pb-Pb whole rock dating.

Isotopic and geochemical analyses for the Western section of the field area have revealed that these rocks represent re-worked Archean material that could be the root of a volcanic arc. The rocks are almost exclusively tonalites, with fairly consistent Nd model ages of ca. 2.7 Ga. The rocks also have a calc-alkaline signature and trace element concentrations indicative of a subduction-related event.

From Figure 4.1, virtually all samples with Archean Nd model ages lie north of the magnetic signature boundary interpreted as the Allochthon Boundary Thrust. However, one sample (TD21 : T_{dm} = 2.50 Ga) falls south of the boundary. Although major element chemistry was not performed on this

sample, visual inspection indicates that it is a pink, foliated granite. Thus, the model age of this sample suggests that it represents a younger pluton that originated by melting of Archean aged rocks beneath the Allochthonous Polycyclic Belt.

All of the other Archean aged samples lie north of the Allochthon Boundary Thrust and thus this aeromagnetic discontinuity does represent a jump in isotopic age.

However, the line drawn that represents the Allochthon Boundary Thrust is only an estimate, traced from aeromagnetic maps. In some areas, the edge of the aeromagnetic discontinuity was obvious, separating subdued magnetic patterns from intense swirling patterns. In other areas, the change from subdued to swirling patterns is much less obvious and appears as a gradual change.

In conclusion, it appears that the Western section may represent the root of an Archean aged arc. Consistency of Nd model age and lithology point towards an island arc precursor rather than an ensialic arc. These conclusions are similar to Ciesielski (1992) who attributes the Parautochthonous Belt to the re-worked Archean substrate of the Abitibi Greenstone Belts.

The Central section of the field area had a distinctly different geology than the Western section. The major and trace element concentrations also point towards an arc

affinity. However, while the Western section had fairly consistent Nd model ages, the Nd model ages for the Central section had a wide range, from 1.45 Ga to 2.18 Ga, with the majority of samples falling between 1.7 and 2.1 Ga. Such a range of Nd model age and lithology is consistent with an ensialic subduction-related arc rather than an island arc. The mixture of lithologies could be produced by variable assimilation of an older component, (represented by the pre-existing continental margin) by a juvenile component, produced by the oceanic slab subducting beneath the continental margin. The diapiric rise of plutons formed in this subduction zone have changed their apparent provenance geochemical signatures typical of island arcs. Such a change could be the result of a thickened continental margin that could be caused by underplating.

The timing and extent of this ensialic arc, however, cannot be precisely discerned. The youngest sample has a model age of 1.63 Ga, suggesting that the arc was active until this time. However, the arc may have had a long-lived history from 1.9 to 1.7 Ga because of the large number of samples in this age bracket. Closer to the Allochthon Boundary Thrust, however, the Nd model ages are greater than 2.0 Ga. This could mean that these rocks represent a mixture of underlying Archean material and juvenile rocks. The larger the Archean component, the older the Nd model age. In an effort to

determine the southern extent of the Archean craton beneath the Allochthonous Polycyclic Belt, a graph of distance (Km) from the trace of the Allochthon Boundary Thrust versus Nd model age was made (Figure 7.1). The diagram indicates that samples within 14 Km of the Allochthon Boundary Thrust may have a significant Archean contribution, shown by the different trend of these samples. Samples younger than ca. 2.0 Ga appear to have a shallower trend, suggesting a smaller Archean component. The small cluster of samples(outlined on Figure 7.1) approximately 20 Km from the Allochthon Boundary Thrust could represent the southern limit of underlying Archean crust because any samples further south of the Allochthon Boundary Thrust have Nd model ages 40 Ma younger. This cluster also corresponds to the change in trend of the two arrays. If this idea that an older Nd model ages is caused by an Archean component is true, then other isotopic systems should also reveal this mixture.

The Pb isotopic data, in part, do suggest the presence of Archean material in the rocks of the Central section. Figure 7.2 is a $^{207}Pb/^{204}Pb$ vs. $^{206}Pb/^{204}Pb$ plot of samples from the Central and Western sections. While the majority of samples in the Western section have much less radiogenic Pb, there is some overlap between Western section samples and Central section samples. The most radiogenic samples from the Western section also tend to have elevated Nd concentrations, implying

Figure 7.1: Plot of Distance (Km) versus Nd model age for samples from the Central section

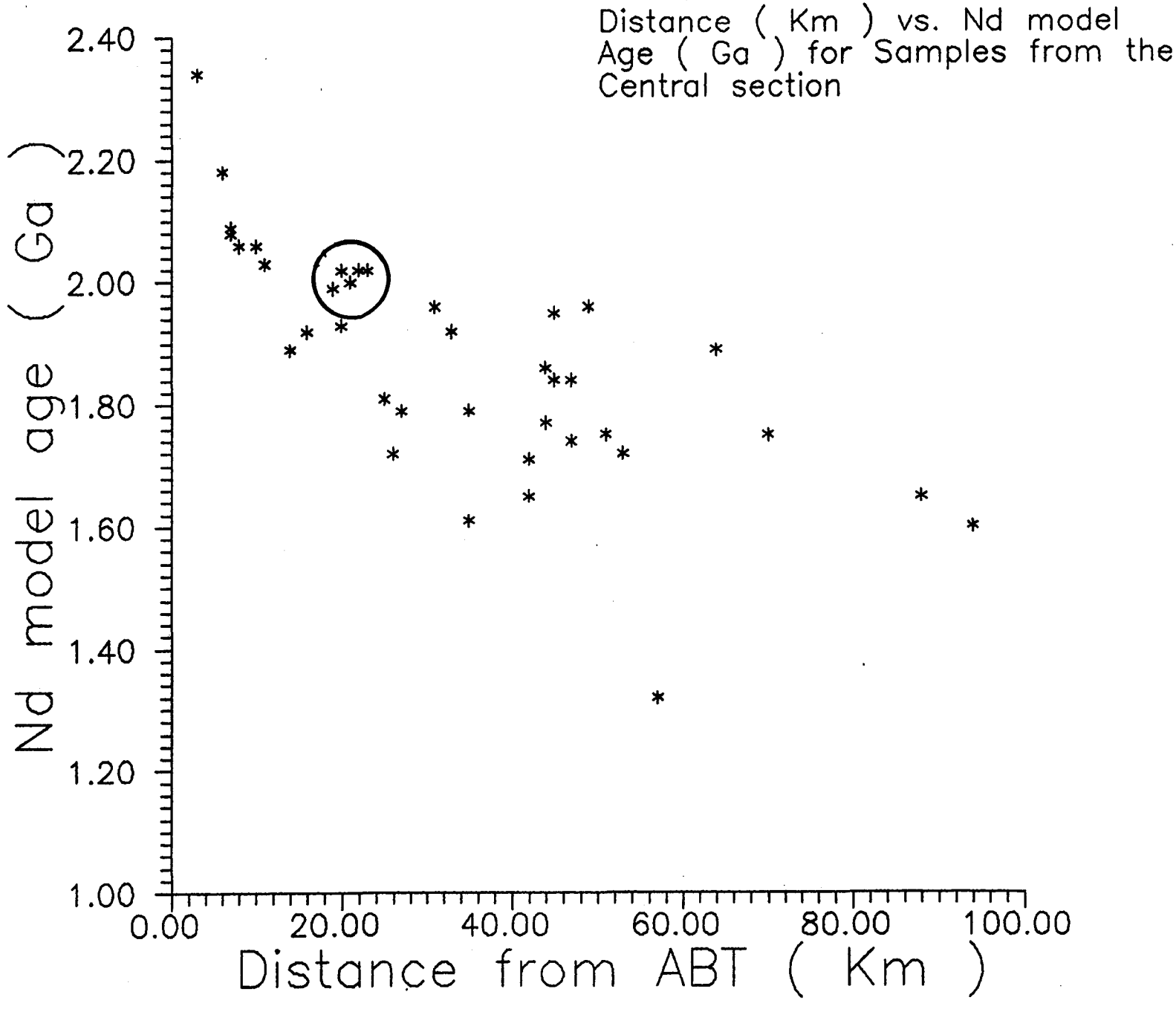
Distance (Km) vs. Nd model Age (Ga) for Samples from the Central section
Nd model age (Ga)
2.40
2.20
2.00
1.80
1.60
1.40
1.20
1.00
0.00
20.00
40.00
60.00
80.00
100.00
Distance from ABT (Km)

Figure 7.2: Pb data from the Western section and the Central section.

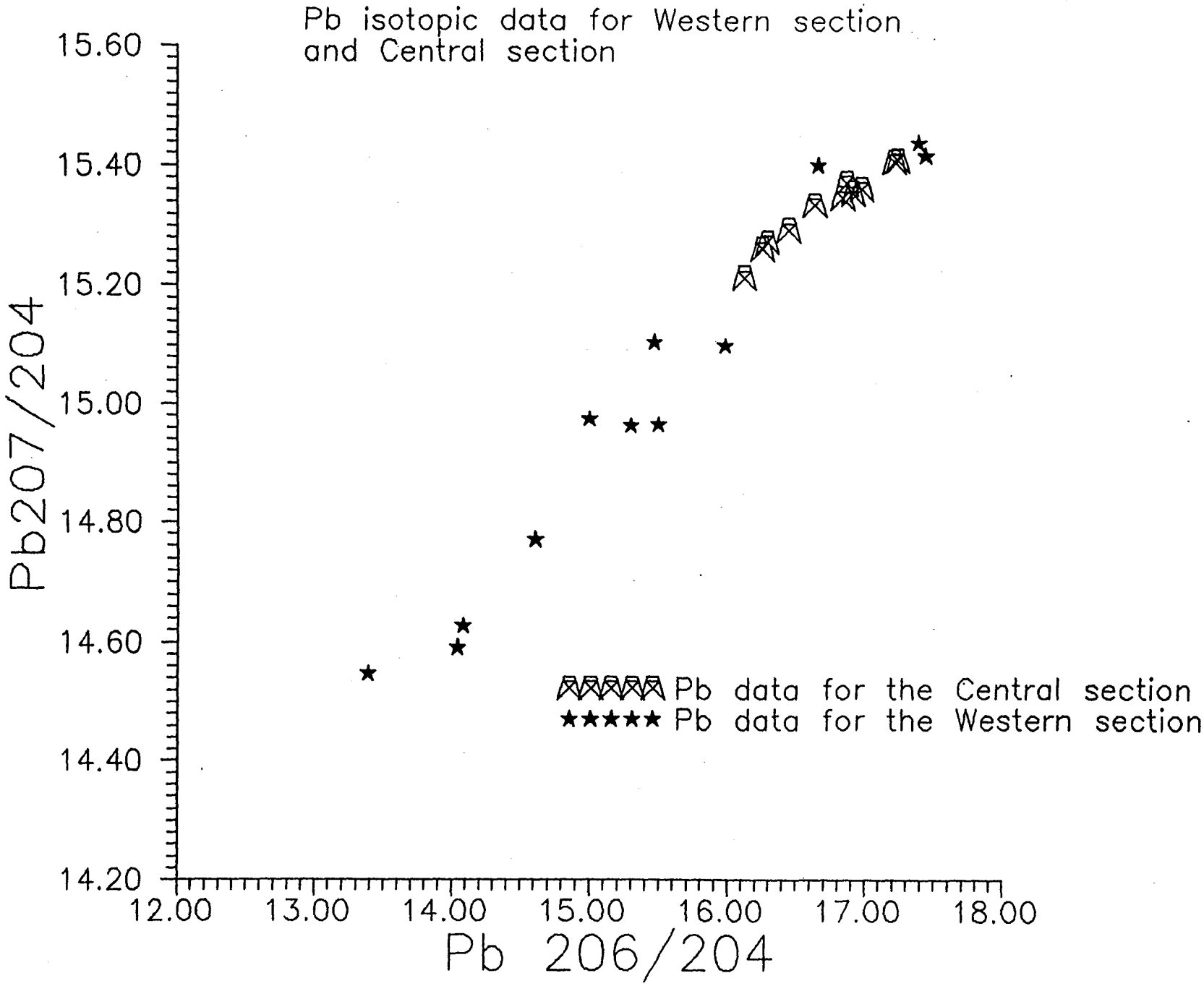
Pb isotopic data for Western section
and Central section
15.60
15.40
15.20
15.00
14.80
14.60
14.40
14.20
Pb207/204
12.00
13.00
14.00
15.00
16.00
17.00
18.00
Pb 206/204
Pb data for the Central section
Pb data for the Western section

that these samples may represent the products of partial melting. Since these samples have similar Pb isotopic ratios as samples from the Central section, then it is possible that some of the rocks in the Central section having older Nd model ages also have a larger Archean component.

The current study has also indicated that more accurate lithological mapping is required for this part of the field area, particularly in the Central section. The large area mapped as " granitic pegmatite " (G19 on map 32H) by MERQ contains significant volumes of other rock types such as granodiorite and quartzmonzodiorite. Although some granites are present in this area, the implication of a batholith-sized granite is unfounded.

In contrast to the variable lithologies and Nd model ages in the Central section, the Eastern section has quite consistent lithologies and Nd model ages. Major and trace element concentrations indicate that the Eastern section represents a subduction-related orogenic event. However, the consistency of lithologies (tonalite-granite suite) coupled with the large geographical distribution of samples all having Nd model ages around 1.5 Ga (> 100,000 km^2 when data from this study is combined with data from Dickin and Higgins, 1992), point towards an island arc precursor rather than a continental ensialic arc. This is best illustrated by comparison with a known version of an ensialic continental

arc: the Blanco Batholith of Peru. Although Nd model age data is not available for the Peruvian Batholith, the variable lithologies for this continental arc strongly contrasts the consistent lithologies of the Eastern section.

The evidence for a ca. 1.5 Ga arc is not restricted to the Central Grenville Province in Quebec using Sm-Nd mapping alone. Other isotopic dating systems have been used on terranes in other parts of the Grenville province. For example, U-Pb crystallization ages of 1.55 Ga have been obtained from a gneiss terrane in Newfoundland (Owen and Erdmer, 1990). Cross cutting intrusions that are contained within the proposed arc can also provide a lower limit to the timing of crustal formation and accretion of the island arc to the Laurentian Foreland. For example, a 1.354 +/- 0.003 Ga U-Pb age obtained for the Pentecote Anorthosite (Machado and Martignole, 1988), and a 1.48 +/- 0.04 Ga Rb-Sr age for the Chamouchouane Monzonite Complex northwest of Lac St. Jean (Frith and Doig, 1973) provide lower age limits to the formation of the proposed arc.

The presence of 1.39-1.46 Ga granitoid plutonism in Ontario, west of the current arc location (Easton, 1986) and southwest of the current geographical location of the arc in Quebec (Nadeau and VanBreeman, 1994), provides evidence for the timing and extent for the accretionary process of the arc. For example, in Ontario, the Britt pluton has a U-Pb zircon

age of approximately 1.450 Ga. This pluton does not have an orogenic signature. In contrast, the La Bostonnais complex in the south-central part of the Grenville Province in Quebec contains igneous zircons with U-Pb ages of 1.39 to 1.41 Ga (Nadeau and VanBreeman, 1994). The rocks of this complex have REE and trace element patterns consistent with arc related magmatism. However, Sm-Nd model ages of the complex have a wide temporal range, from 1.57 Ga to 1.70 Ga (Nadeau, per. comm.) Such a wide range is consistent with a continental ensialic arc, rather than an accreted island arc.

Thus, the 1.45 Ga anorogenic plutons which lie north of gray gneisses with ca. 1.5 Ga Nd model ages analyzed by Dickin and McNutt (1990) in the Muskoka domain of the Ontario Central Gneiss Belt, and the 1.39-1.41 Ga orogenic plutons of the La Bostonnais complex which lie south of the ca. 1.5 Ga gray gneisses in Quebec provide good age brackets for the timing of arc accretion.

A model of the tectonic evolution for the entire study area is shown in Figure 7.3. The model consists of five stages. The first stage corresponds to the formation of the ca. 2.0 Ga to 1.6 Ga ensialic arc. A subduction zone dipping towards the Archean aged cratonic margin produced the lithological and mixed Nd model aged rocks corresponding to the Central section of this study. Evidence for the formation of this continental arc is not just restricted to the Lac

Figure 7.3: 5 stage model for the evolution of rocks in the Lac St. Jean region in Quebec.
light stipple = 1.5 Ga island arc
dark stipple = 1.7 - 1.9 Ga ensialic arc
dark shading = La Bostonnais ensialic arc

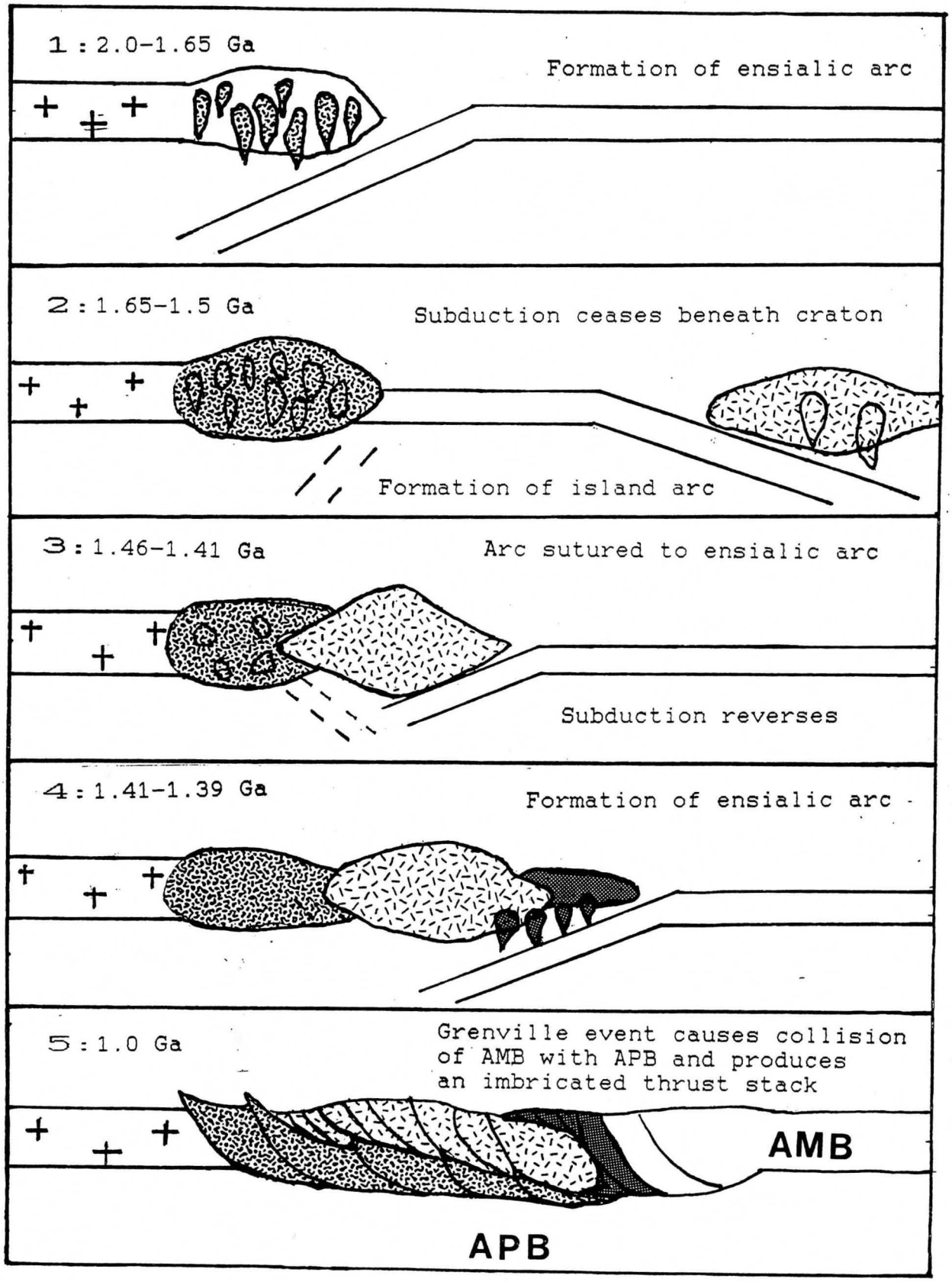
1 : 2.0–1.65 Ga
Formation of ensialic arc
2 : 1.65–1.5 Ga
Subduction ceases beneath craton
Formation of island arc
3 : 1.46–1.41 Ga
Arc sutured to ensialic arc
Subduction reverses
4 : 1.41–1.39 Ga
Formation of ensialic arc
5 : 1.0 Ga
Grenville event causes collision of AMB with APB and produces an imbricated thrust stack
AMB
APB

St.Jean region in Quebec. For example, a Sm-Nd reconnaissance study of rocks in the Bancroft area of Ontario (Martin, 1992) suggested the presence of an ensialic continental arc that was active between 1.86 and 1.65 Ga ago. Similar to the Lac St. Jean region, the wide range of Nd model ages coupled with a large variety of lithologies led to this conclusion. Although the Nd model ages of this ensialic arc in Ontario are slightly younger, this may only be the result of lack of any Archean component associated with the rising diapirs. Further east, in the Kipawa-Mattawa area in Quebec, Guo and Dickin (1992) have also reported early and mid-Proterozoic Nd model ages. They divided the area into three different terranes having Archean (2.6 to 2.7 Ga), early Proterozoic (2.1 to 2.4 Ga) and Penokean (1.86 to 2.0 Ga) Nd model ages. However, Guo and Dickin attributed the 1.86 to 2.0 Ga Nd model ages to a Penokean island arc that had been thrust northwestwards during the Grenville orogeny. However, the variable lithologies and wider range of Nd model ages in the Central section of this study do not indicate the presence of a Penokean island arc, but rather the presence of an early Proterozoic ensialic arc.

The absence of island arc rocks in the Central section doesnot disprove either the interpretation by Guo and Dickin (1992) or the interpretation of the present study. Modern examples of island arcs such as the Aleutian chain of Alaska,

the Philippine islands in the south-west Pacific, or the island arcs of the Lesser Antilles, are typically composed of a series of islands, separated by oceanic crust with less volcanic activity. Similarly, the Canadian Cordillera is composed of a series of arc terranes. Some of the arc terranes that are the same age are separated by hundreds of km. (Samson and Patchett, 1991). One possibility for their distribution has been attributed to a multiple arc model in which smaller penecontemporaneous island arcs were sutured at different parts of the continental margin.

This is not, however, the only possible explanation. For example, there may have been an accreted ca. 1.9 Ga island arc that was thoroughly re-worked by a later ensialic arc. In this scenario, model ages greater than 2.0 Ga could be a result of an Archean contribution. This model would be consistent with previous studies in Ontario (Dickin and McNutt, 1989; Dickin et al., 1990). However, to date, there is no evidence to disprove either theory.

The second stage of the model represents the time period between 1.5 Ga to 1.65 Ga. At this time, there may have been a subduction zone dipping away from the Laurentian craton, above which an island arc formed at approximately 1.5 Ga ago. The subduction zone beneath the Laurentian craton ceased perhaps due to the suturing of allochthonous terranes in the Eastern Grenville province (eg. the Lac Joseph Allochthon and

the Wilson Lake Allochthon: Wardle et al., 1986). These terranes may have prevented further subduction by acting as a wedge and resisting subduction.

The island arc collided with the foreland between 1.46 Ga (age of anorogenic plutonism in Ontario) and 1.41-1.39 Ga (age of ensialic arc in Quebec) (Stage 3). After collision, the subduction zone that produced the 1.5 Ga island arc reversed itself, and began producing the orogenic La Bostonnais plutonic complex (Stage 4). Thus, geochronological constraints imply that the arc was accreted to Laurentia within 120 Ma after its crustal formation.

The final stage represents the collision of the Allochthonous Monocyclic Belt during the Grenville orogeny at approximately 1.0 Ga. The collision of the Allochthonous Monocyclic Belt caused overthrusting and northwestward transport of the 1.5 Ga terrane over the Early-Proterozoic ensialic arc. Sole thrusting may have produced an imbricated stack consisting of a series of northwestward directed thrusts, (the Allochthon Boundary Thrust). This interpretation is the same as Rivers et al's., (1989) definition of the Allochthon Boundary Thrust as a "...locus of major thrust displacements...". A similar model is presented by Rivers et al., (1993) for Molson Lake Terrane in Western Labrador. The collision uplifted the Parautochthonous Belt and erosion produced the present-day location of the

Allochthon Boundary Thrust.

In contrast to Nd model age dates, common Pb-Pb whole rock dating of rocks from all three sections of the field area have revealed two different aspects of the rocks in the Lac St. Jean region of Quebec. Pb analyses from both the Western and Central sections have indicated that these areas are best represented by a two-stage Pb evolution model. Both areas produced much older apparent Pb-Pb ages than Nd model ages. However, if the Grenville orogeny (1.1 Ga) resulted in resetting of the U/Pb ratios, then the Pb isochrons for both areas produce transposed palaeoisochrons whose slope ages are conformable with results from other isotopic dating systems.

Pb data from the Eastern section, on the other hand, do not produce a transposed palaeoisochron. Nor do the Pb data indicate that the area can be modelled by a single stage Pb evolution curve. Instead, the Pb isotopes suggest that these rocks were only partially reset to uniform levels during the Grenville orogeny. It is not known why these rocks are only partially reset. However, because the majority of this arc terrane is located far from the Allochthon Boundary Thrust, then maybe the rocks were affected less by the Grenville orogeny. Alternatively, these rocks may represent higher crustal levels than rocks from the Western and Central sections, and therefore were subjected to lower metamorphism.

While Pb-Pb dating of zircons failed to produce any

inherited Archean zircons for the Central section, dated zircons from the Eastern section did produce a lower age limit on crystallization ages for these rocks.

Thus, in conclusion, a geochemical and isotopic reconnaissance study of the Lac St. Jean region of Quebec in the central Grenville province has revealed the presence of both an ensialic arc and two island arcs. The ensialic arc was active between 1.9 and 1.65 Ga ago. Evidence for this ensialic arc is also present in Ontario. Although the location of the island arc originally proposed by Dickin and Higgins (1992) has been extended northwards to within a few tens of km from the Allochthon Boundary Thrust of Rivers and Chown (1986) and Rivers et al., (1989) in the Eastern section of the field area, the exact location and nature of the northern boundary of the Eastern section is not known. However, the precise location of the Allochthon Boundary Thrust further west has been narrowed down to a few tens of kilometres in certain areas. Structural studies of the geology in this region, coupled with a systematic geochronological study of this area of the Grenville province is required to determine the precise location of the Allochthon Boundary Thrust of Rivers et al., (1989). Similarly, the same techniques are required to determine the location and nature of the northern boundary for the proposed island arc in the Allochthonous Polycyclic Belt.

Appendix

Analytical procedures

1.0 Sm/Nd isotope analyses:

1.01 Introduction: The analytical procedures for Sm/Nd geochronology may be divided up into three main parts: field sampling and rock crushing, dissolution and cation chromatography, and mass spectrometry. The analytical procedures will now be described in chronological order.

1.02 Sampling and rock crushing:

Gneissic samples collected in the field varied from five to ten Kg in mass and were collected at roadside outcrops. All samples collected were as representative of the outcrop as possible and were as homogenous as would allow. The majority of weathered material was removed and care was taken so as not to contaminate the sample with organic material or local soil. The sample locations were pinpointed as accurately as possible on 1:50 000 topographic maps produced by the Surveys and Mapping Branch of the Department of Energy, Mines, and Resources of Canada. Accurate sample locations are very important when trying to determine age boundaries. The

locations are given as grid references on the Sm/Nd data tables and are accurate by +/- 100m. In the rock crushing laboratory, the samples were initially broken down to 1 to 2 Kg pieces with a sledge hammer. The samples were then broken down to smaller sized pieces (approximately 5cm by 5cm) with a hydraulic splitter. The sample fragments were crushed up into gravel less than 1 cm in size using a mechanical jaw crusher. The jaw crusher was first pre-contaminated with some of the sample in order to avoid contamination from previous samples. A table top sample divider was then used several times to split and homogenize the gravel. After splitting, the remaining 100 ml to 200 ml of gravel was loaded into a tungsten carbide disc mill which was then placed in a shatterbox. The sample was then pulverized in the shatterbox for approximately 5 minutes, producing a fine sand. The fine sand was then removed from the shatterbox and poured onto a clean sheet of paper. Approximately one half of the sand was discarded while the other half was put back in the shatterbox for further pulverization. This procedure not only pre-contaminated the shatterbox, but also pre-contaminated the paper which would later come in contact with the sample.

After approximately 5 to 10 minutes, the remaining sample was removed from the shatterbox. The fine powder, approximately 300 mesh size, was transferred from the shatterbox to the pre-contaminated paper. The resulting 80 to

100 ml of fine powder was then poured into a clean 125 ml glass container, ready for dissolution.

Between each sample preparation, all equipment and working surfaces were carefully cleaned with a vacuum, and then wiped clean with disposable paper towels. The jaw crusher was dismantled, and the steel crushing plates were scrubbed with a wire brush. The plates were then vacuumed, along with the rest of the jaw crusher, and finally wiped clean of all remaining dust using disposable paper towels. The disc mill was also disassembled and the ring, puck, and container were thoroughly vacuumed and wiped clean of all remaining grit with paper towels. If the disc mill could not be completely cleaned, then 30 to 40 ml of pure quartz grains were added to the disc mill. This effectively acted as a grinding grit which removed any stubborn powder left from the last sample. Latex gloves were worn at all times, ensuring that no dust-attracting skin oils were deposited on the tungsten carbide ring and puck of the disc mill, as well as the steel plates of the jaw crusher. The table top sample divider was first vacuumed, and then blown clean with an air hose to ensure that the divider chutes were clean, and free of powder from the previous sample. At all times, the volume of airborne particles was kept to a minimum by using an air filtering system. For safety, an air filter mask and goggles were worn at all times.

1.03 Dissolution and Cation Chromatography:

Each sample was accurately weighed with a balance. The balance was first levelled and static was removed. The teflon bombs which were used for dissolution were also freed from static electricity. The empty teflon bombs were twice weighed to ensure that all static had been removed. If the mass was discrepant by more than 0.0002g, then more static was removed from the bombs. When all of the static was satisfactorily removed from the bombs, between 75 mg and 150 mg of sample was added. The amount of sample was accurately weighed and recorded. Approximately 10 ml of concentrated hydrofluoric acid (48 %) was added to each of the teflon bombs. The teflon bombs were tightly sealed and placed in teflon safety jackets. The teflon safety jackets were then put in an oven for 3 days at 140°C.

When the three days had passed, the bombs were removed from the oven and safety jackets, and left to cool. Once cool, the bombs were tapped on a hard surface in order to remove any hydrofluoric acid that had condensed on the inside of the lid. The lids were then removed and the bombs were placed on hot plates contained in laminar flow hoods overnight to evaporate. When the samples were dry, approximately 5 ml of concentrated HNO_3 (16 M) was added to each bomb and then evaporated. 5 ml of 6 M HCL was added to the bombs and the

lids were tightly closed. The bombs were then placed in teflon safety jackets, and put in the oven overnight. The next day, the samples were cooled and diluted with approximately 5 ml of Milli-Q water. If there were no undissolved residues left over, then the samples were ready to be split and spiked.

For the splitting and spiking procedure, each bomb containing dissolved sample, HCL, and Milli-Q water was accurately weighed and the mass recorded. Approximately one half of each sample was poured into separate 15 ml teflon beakers and the bombs were reweighed Approximately 5 drops of a mixed Rare Earth Element spike enriched in ^{149}Sm and ^{150}Nd was added to the teflon beakers. The weight of the spike was determined and recorded for each sample. Both the beakers and the bombs were then evaporated to dryness and re-dissolved in 2 ml of 2.5 M HCl. This spiking procedure is known as Isotope Dilution. Essentially, a known mixture and quantity of Nd and Sm isotopes are added to an unknown mixture of Nd and Sm isotopes in the sample. Thus, simple subtraction of the known isotope ratio in the spike from the ratio measured reveals the concentration of each isotope in the sample.

Once the samples had been redissolved, the aliquots were then transferred to plastic test tubes and centrifuged for ten minutes. The samples were now ready for cation chromatography.

There are actually two steps in column chromatography. The first step involves the separation of major elements such as Na, K, and Ca from the Rare Earth Elements (Cation Exchange Chromatography), while the second step involves separation and concentration of Sm and Nd from the other Rare Earth Elements (Rare Earth Element Chromatography).

1.04 Cation Exchange Chromatography:

One ml of 2.5 M HCl/sample mixture was loaded into glass columns (30 cm by 0.5 cm I.D.) containing approximately 18 cm of Dowex Bio-Rad AG 50W (200 - 400 mesh) resin. The major cations were removed from the sample by eluting a total of 46 ml of 2.5 M HCl followed by 30 ml of 2 M HNO_3 over a polystyrene sulphionic acid resin. The Rare Earth Elements remaining in the columns were then collected with 14 ml of 7.5 M HNO_3. Before the samples were loaded onto the columns, they were cleaned first with 10 ml of Milli-Q water and then with 60 ml of 6 M HCl. The HCl removed any substances that might have remained on the resin from a previous sample, while the water neutralized the 7.5 M HNO_3 used to collect the remaining Rare Earth Elements. Thirty ml of 2.5 M HCl was then added to the columns to prepare them for sample introduction.

The Rare Earth Element solutions, after being evaporated to dryness beneath heat lamps in a laminar flow hood, were redissolved in 1 ml of 0.2 M HCl. The samples were now ready

for Rare Earth Element chromatography.

1.05 Rare Earth Element Chromatography:

The Rare Earth Element chromatography performed is known as the " Reverse Phase Method " because the light Rare Earth Elements (Nd) are collected before the heavy Rare Earth Elements (Sm).

Three different solutions were collected from the Rare Earth Element columns: a spiked Sm solution used in Sm isotope dilution, a spiked Nd solution used in Nd isotope dilution, and an unspiked Nd solution used for the Nd isotope ratio determination.

The isotope dilution procedures are slightly different than the isotope ratio procedure. For the isotope dilution separations, the 1 ml of 0.2 M HCl mixed Sm/Nd spiked sample is loaded onto the Rare Earth Element columns. Then, 21 ml of 0.2 M HCl is added in three steps: 2 ml to wash in the sample, 7 ml to remove unwanted Rare Earth Elements, and 12 ml to collect the Nd isotope dilution solution. Following Nd collection, 4ml of 0.5 M HCl is eluted into the columns and then the Sm isotope dilution solution is collected with 6 ml of 0.5 M HCl.

For the Nd isotope ratio separations, the 1 ml of 0.2 M HCl/sample mixture is added to the columns and then washed in with 2 ml of 0.2 M HCl. 7 ml of 0.2 m HCl is eluted, followed by collection with 12 ml of 0.2 M HCl.

All three solutions were then evaporated down and 2 to 3 drops of 3 M HNO_3 with 1.3% H_3PO_4 was added and partially evaporated again. This helps to redissolve the crystalline residue in 0.3 M H_3PO_4 when the samples are loaded onto filaments for mass spectrometry.

Prior to loading samples onto the Rare Earth Element columns, the columns were thoroughly cleaned with 60 ml of 6 M HCl and 30 ml of 0.2 M HCl. The 30 ml of 0.2 M HCl prepared the resin for the samples.

1.06 Mass Spectrometry:

Before the samples were loaded onto the Tantalum side filaments of a Rhenium-centre, Tantalum side, glass bead, the beads and filaments were outgassed under a vacuum. Thirlwall (1982) gives a complete account of bead preparation.

Approximately 1/2 microlitre of 0.3 M H_3PO_4 was used to dissolve the samples. This acid/sample solution was loaded onto the Tantalum side filament and dried by applying 2.0-2.5 amps to the Tantalum filament.

Sm-Nd isotope analyses were performed on both a VG 354 thermal ionization, solid source, mass spectrometer and a VG Isolab thermal ionization, solid source, mass spectrometer using 4 collector peak switching programs. All analyses were done at source pressures less than 2.0×10^{-7} bars. Nd isotope ratios were normalized against a $^{146}Nd/^{144}Nd$ ratio of 0.7219. 27 runs of the La Jolla standard produced a $^{143}Nd/^{144}Nd$ average

of 0.511846 +/- 0.000017 (2σ) with an average in run precision of 0.000015 +/- .0008 (2σ). No isotope dilution data was accepted with within run standard errors of greater than 0.02%. No Nd isotope ratio data was accepted with within run standard errors of greater than 0.01%. Thus, the resultant uncertainty for the model ages calculated was approximately +/- 20 Ma (2σ).

2.00 Zircon Analysis:

2.01 Introduction:

The analytical procedures for Pb-Pb zircon dating by direct evaporation is divided into three main parts: zircon separation, zircon loading, and mass spectrometry. The analytical procedure will be described in chronological order.

2.02 Zircon Separation:

The samples selected for zircon dating were powdered using a ceramic disc mill in order to obtain a grain size between 24 and 100 mesh. To prevent contamination of samples, the disc mill was vacuumed clean, wiped with disposable paper towels, and blown free of dust with an air hose. The sand sized particles obtained from the disc mill were then processed using a shaker table. The shaker table vibrated in such a way as to remove the majority of lighter, less dense grains such as quartz and feldspar, while heavier, denser grains such as magnetite, biotite, amphibole, and zircon, were collected at the end of the shaker table. The shaker table's frequency of vibration and water flow could be adjusted so as to maximize the volume of heavy fraction minerals collected. The heavy fraction grains were then dried down with a heat lamp. Once the sample was dry, a hand magnet was used to

remove the highly magnetic grains such as magnetite and biotite. In some cases, zircons were also removed by this step. However, these zircons generally had a large number of dark inclusions, presumed to be magnetite and biotite, and were also very cloudy. These " magnetic " zircons were not used in any analyses because they represent highly metamict grains that may have lost substantial volumes of Pb or U and/or have been contaminated with common Pb (^{204}Pb).

Further separation of zircons from the remaining grains was achieved by using the heavy liquid CH_2I_2 (Diiodomethane 99%). CH_2I_2 has a density of 3.325 g/cm^3 which is just slightly less than that of zircon grains. However, it is significantly different than some of the remaining mineral grains that had not been removed by the shaker table. The apparatus used to separate the zircons is shown in Figure 1.

Only a few mg of mineral grains could be added to the Diiodomethane holding reservoir at a time. If too much sample was added, then " rafts " of sediment that contained significant volumes of zircons formed. To prevent any zircons from eluding collection, the holding reservoir was constantly stirred with a glass pipette. The zircons accumulated at the bottom of the holding reservoir and once there was a sufficient volume, the stop cock was rotated backwards and forwards, allowing the zircons to flow downwards and be collected in filter paper below.

Figure 1.1: apparatus for zircon separation.

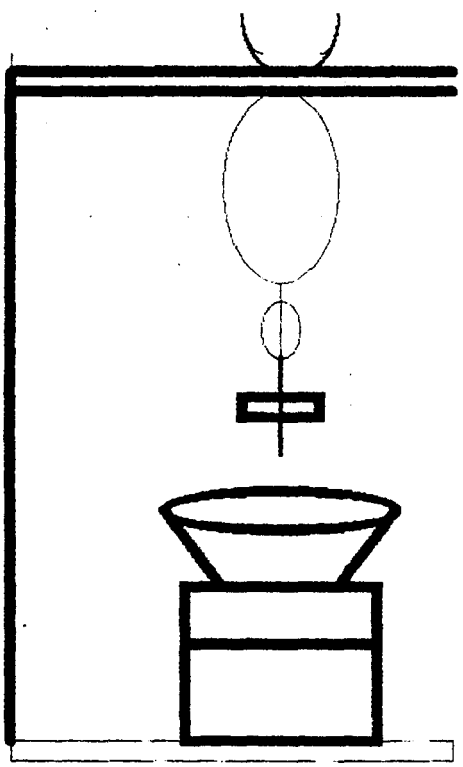

CLAMP

HOLDING CONTAINER FOR DIIODOMETHATE

STOPCOCK APPARATUS

COLLECTING FUNNEL AND FILTER PAPER

WASTE BEAKER

STAND

This valve had to be rotated rapidly so that no other grains from above could exit the holding reservoir.

Due to the carcinogenic hazard associated with Diiodomethane, the entire separation procedure was carried out behind the glass door of a fume hood and latex gloves were worn at all times.

Once the majority of zircons had been collected in the filter paper, the filter paper and apparatus were thoroughly cleaned with acetone. The waste products were carefully disposed of in an appropriate manner. The zircons collected in the filter paper were now ready to be loaded onto glass beads for analysis.

2.03 Zircon Loading :

The zircons were loaded onto the side filament of a zone refined (99.5% pure), wide (0.05") Rhenium filament welded onto standard triple filament glass beads. Each zircon was wrapped securely in the side filament by firstly making a trough-like shape in the filament, and secondly, crimping the top of the filament with the zircon grain inside the trough. A second zone refined, wide (0.05") filament was welded in a vertical position to the centre posts. The centre filament acts as a deposit site for Pb evaporated from the side filament (Figure 2). The centre and side filament posts were then brought as close as possible to each other (0.5 mm to 1.0 mm). This would cause the majority of Pb that had

Figure 1.2: Diagram of the beads used for zircon dating (after Mueller, 1990)

a)

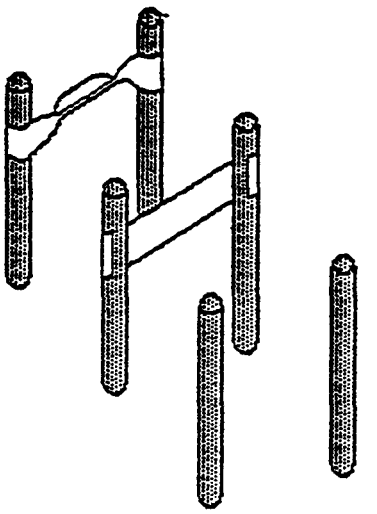

b)

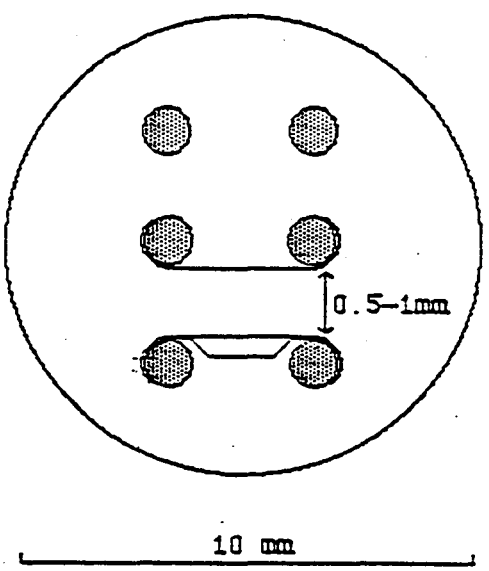

been evaporated from the side filament to be deposited on the centre filament. The zircon beads were now ready for mass spectrometry.

2.04 Mass Spectrometry :

The procedure for analyzing zircons by direct evaporation was as follows:

1) The centre filament was cleaned of any Pb by passing a 7.0 to 8.0 amp current through it. Similarly, the side filament was turned up to approximately 5.0 amps so as to drive off any loose Pb.

2) Once the filaments were satisfactorily cleaned, the side filament was heated for 10 to 30 minutes by running 4.0 to 6.0 amps through it. During this stage, the Pb contained in the zircon was being evaporated and deposited on the cool centre filament. Although the time of deposition varied, 15 minutes seemed to be enough to remove all of the Pb contained in the zircon.

3) The centre filament was then turned up slowly, and the computer program began to focus the beam of Pb that had been deposited by the side filament. The beam emitted from the centre filament tended to be much more stable than the beam emitted directly from the side filament. Throughout the procedure, the current was controlled manually.

4) If the beam was sufficiently large enough (approximately 10^{-20} amps), and the ^{204}Pb was low enough (1 part per 10000 of ^{206}Pb), then the data was collected for as long as possible.

5) When the zircon was finished, the filaments were cleaned by passing a high current through them so that the beads could be used again.

Used beads seemed to produce a much larger and more stable beam. Perhaps this is caused by an increase in surface area of the centre filament. After a bead had been used once, close examination of the centre filament revealed a surface that was much rougher than the new filament. This roughened surface might allow Rhenium atoms, which ionize the Pb atoms, a larger " spread " in direction, thereby ionizing more Pb atoms. Re-used beads were also much more ductile and therefore it was much easier to wrap the zircon in the side filament.

To avoid collecting Pb data from metamorphic rims that may have been present on the zircons, the computer program was paused at the start of the focusing procedure for each sample. The side filament was then turned up so as to allow enough time to drive off the metamorphic Pb. The centre filament was then briefly heated to remove this Pb.

3.0 Pb Isotopic Analyses

3.01 Introduction: The sampling and rock crushing procedures for Pb isotopic analyses are the same as those for Sm-Nd isotope analyses. However, the sample dissolution and cation chromatography steps are slightly different.

3.02 Sample Dissolution:

Day 1: Between 200 and 400 mg of sample is placed in a teflon bomb. The bomb is filled approximately half full with 6M HCl. The lid is tightened on the bomb, and the bomb is placed on a hotplate overnight.

Day 2: On the second day, the bomb is removed from the hotplate and allowed to cool. The lid is carefully opened so as not to stir up the sample that lies on the bottom of the bomb. Almost all of the 6M HCl is poured off, taking care not to lose any sample. The bomb is then filled with Milli-Q water and left for approximately half an hour. The purpose of these decantation procedures is to remove loosely bound atoms and iron. The bomb is then placed on the hotplate and dried down. 5 to 15 ml of HF is added to the bomb, and the bomb is placed into a teflon safety jacket and put into an oven for 3 days at 140 °C after the bomb lids have been securely tightened.

Day 6: The bomb in the teflon safety jacket is removed from the oven and left to cool. The bomb is removed from the teflon safety jacket and any HF that had condensed on the inside of the bomb lid is carefully removed by taping the bomb on a solid surface. The bomb is then placed on a hotplate enclosed in a laminar flow hood, and the HF is evaporated. This usually takes about 4 to 6 hours, depending on how much HF was added to the bomb.

After the HF has evaporated, about 5 ml to 10 ml of concentrated HNO_3 (16 M) is added to the bomb, and the bomb is put back into the teflon safety jacket and into the oven overnight.

Day 7: On the seventh day, the bomb is removed from the oven and placed on a hotplate to evaporate the 6 M HCl. 2 ml of HBr is then added to the bomb and the bomb is left standing overnight.

Day 8: The contents of the bomb is poured into disposable plastic test tubes and centrifuged for 10 minutes. The sample is now ready for cation exchange chromatography.

3.03 Anion Exchange Chromatography:

There are a large number of sources in the environment that can cause Pb contamination. For this reason, it is imperative that the columns used for Pb isotope separations are extremely clean.

Column Production and Anion exchange Chromatography:

The columns used in anion exchange chromatography are made from plastic 4 ml volume pipettes. The tops of the pipettes are cut off, and the ends are cut and heated. The heating process not only allows the pipette end to be pulled apart approximately 2 to 3 cm below the funnel, but also restricts the exit hole at the bottom of the column. The columns that are produced measure 7 to 8 cm in total length; 2 to 3 cm of this representing the thin portion below the funnel. The thin portion, which will hold the exchange resin, is approximately 4 to 5 mm with the exit hole approximately 2 to 3 mm wide. Once the columns are produced, they are now ready to receive the exchange resin.

Before the exchange resin is added to the columns, a frid must be made and placed in each column just above the exit hole at the bottom of the column. The purpose of this frid is to prevent the exchange resin from leaving the column. The frid is made of cotton rolled up into a small ball. This cotton ball is pushed down the neck of the column with a plastic tube. Care must be taken when making the frid because if the frid is too loose, then the sample and resin will leak out. If the frid is too tight, then this will prevent the passage of liquid past the frid. When the frid is in place, it is now time to add the exchange resin.

The resin used is anion exchange resin BIO RAD AG 1-X8 in

the chloride form, 200 to 400 mesh size. The resin is stored in Milli-Q water to prevent the resin from drying out. Now that the column is made, it is now ready for the cleaning procedure and anion exchange chromatography.

There are a large number of sources in the environment that can cause Pb contamination. For this reason, it is important that the columns used in Pb isotope separation are extremely clean. There are 6 steps in the cleaning procedure. They are as follows: First, 3 ml of Milli-Q water is added. Once this has dripped through the column, 3 ml of 6 M HCl is added. The acid helps to remove any elements that may be on the inner walls of the column or on the resin surface. This acid is followed by 3 more ml of Milli-Q water. The water helps to wash out the acid, and further clean the resin. This is followed by 3 more ml of 6 M HCl. This acid step fully removes any anions still adhering to the resin. Another 3 ml of Milli-Q water is added to dilute and wash out the HCl. The final step is the addition of 3 ml of 0.7 M HBr. This last step prepares the column for the addition of the sample which has already been concentrated in 0.7 M HBr. Note that each of the 3 ml steps in the cleaning procedure takes about 2 hours, depending upon how dirty the column was. The column is now ready to receive the sample.

Approximately 1 ml of sample dissolved in 0.7 M HBr is added to the column. Once this has dripped through, 2 ml of

0.7 M HBr is washed in to ensure that no sample is left on the inner walls of the upper portion of the column. 3 more ml of 0.7 M HBr is added to the column. At this point, most of the Pb has adhered to the resin, while a majority of the waste has been washed through the column and discarded. The sample is then collected in an 8 ml teflon beaker by washing 6 ml of 6 M HCl through the column. The beaker is placed beneath heat lamps in a laminar flow hood and allowed to evaporate overnight. Once the sample has evaporated, the residue is examined to determine whether or not the sample needs to be run through the column again. If the residue appears very black and in clumps rather than a thin, evenly spread out greyish residue, then the sample still contains too much waste and therefore must be put through the anion exchange process again. Prior to adding the sample, which is redissolved in 0.7 M HBr, to the column, the column must once again be cleaned as outlined in the cleaning procedure above. Normally a second wash through the column is sufficient to prepare the sample for the mass spectrometer. If the sample does not have a large amount of Pb present, it is possible that the third column procedure will not leave sufficient Pb in the sample to be measured. The sample is now ready for loading and mass spectrometry.

3.04 Sample loading:

The Pb samples are loaded on Rhenium single filament glass beads. A pipet was used to add approximately 1/2ul of H_3PO_4 to the filament surface. This was followed by the addition of approximately 1 ul of Si gel to the filament. The Si gel is thought to act as a blanket and prevent the rapid and sporadic release of Pb from the sample. Approximately 1/2 ul of H_3PO_4 is added to the teflon beaker containing the sample. The H_3PO_4 was swirled around inside the teflon beaker with the pipette tip. The sample was then drawn into the pipette tip and deposited onto the Rhenium filament. In order to dry down the sample, approximately 1.5 Amps of current was passed through the Rhenium filament. During this drying procedure, the sample/Si gel/H_3PO_4 mixture slowly decreases in size and transforms into a lumpy mass. At this point the filament current is reduced to approximately 1 Amp because at higher temperatures, the sample could be blown off. After approximately 1 minute, the sample mixture turns to a black liquid, at which point, the filament current is turned up slowly until the sample smokes. The bead is now ready for mass spectrometry.

3.05 Mass Spectrometry:

Pb isotope measurements were done on a VG 354 thermal ionization, solid source mass spectrometer operated at source pressures $< 2.0 \times 10^{-7}$ bars. The samples were run at

approximately 1320 °C. This temperature was regulated by a pyrometer. The mass spectrometer measured masses 204, 205, 206, 207, and 208. 205 was used as an indicator of background noise. The computer program calculated the $^{206}Pb/^{204}Pb$, $^{207}Pb/^{204}Pb$, and $^{208}Pb/^{204}Pb$ ratios and determined their mean in blocks of 15. A total of 10 blocks, consisting of 15 analyses/block were measured for each sample. In most cases, the standard error for samples did not exceed 0.05% for any of the ratios. Because of disolving a little more sample than was required, there was always high Pb concentrations which translated into very low standard errors for $^{206}Pb/^{204}Pb$ and $^{207}Pb/^{204}Pb$ ($< 0.005\%$). NBS 981 was the standard used to make sure that the Pb data collected from the samples was correct. At least 2 standards were run with each barrel: one at the start and one at the end. If the $^{206}/Pb^{204}Pb$ and $^{207}Pb/^{204}Pb$ ratios were not close to 16.89 and 15.43 respectively, then this indicated that there had been some drift of the high voltage, and samples had to be run again. However, the samples could not be run several times over because the Pb isotopes may experience fractionation with several heating episodes. A fractionation correction of 0.1%/amu was applied to the final Pb data in order to correct for any fractionation effects.

BIBLIOGRAPHY

Arndt, N.T., Goldstein, S.L., 1987, Use and abuse of crust-formation ages: Geology, v. 15, p. 893-895.

Atherton, M.P., McCourt, W.J., Sanderson, L.M., and Taylor, W.P., 1979, The geochemical character of the segmented Peruvian Coastal Batholith and associated volcanics, in Atherton, M.P., and Tarney, J., eds., Origin of Granite Batholiths: Geochemical Evidence

Barovich, K.M., PAtchett, J.P., 1992, Behaviour of isotopic systematics during deformation and metamorphism: a Hf, Nd and Sr isotopic study of mylonitized granite: Contrib. Mineral Petrol., v. 109, p. 386-393.

Ciesielski, A., 1992, Tonalitic orthogneisses in the central Grenville Province: a reworked Archean substrate to the Abitibi Greenstone Belt, eastern Superior Province, Quebec, in Glover, J.E., and Ho, S.E., eds., The Archean: Terrains, Processes and Metallogeny, Geology Department (Key Centre) & University Extension, The University of Western Australia Publication No.22.

Culshaw, N., Jamieson, R., Corrigan,D., Ketchum, J., Reynolds, P., Wodicka, N., Heaman, L., Krough, T., 1990, History of Central Gneiss Belt, Grenville province, along Georgian Bay in Abitibi/Grenville project, Lithoprobe Workshop Report 3, Oct. 1990, Montreal.

Davidson, A., 1986, New interpretations in the southwestern Grenville Province, in Moore, J.M., Davidson, A., Baer, A.J., eds., The Grenville Province: Geological Association of Canada Special Paper #31, p. 61-74.

Davidson, A., and Grant, S.M., 1986, Reconnaissance geology of western and central Algonquin Park and detailed study of coronitic olivine metagabbro, Central Gneiss Belt, Grenville Province of Ontario, in Current Research, Part B, Geological Survey, Paper 86-1B, p. 837-848.

Debon,F., LeFort,P., 1983, A chemical-mineralogical classification of common plutonic rocks and associations: Royal Society of Edinburgh Transactions, Earth Sciences, v. 73, p. 135-149.

DePaolo, D.J., Wasserburg, G.J., 1976b, Inferences about magma sources and mantle structure from variations of $^{143}Nd/^{144}Nd$. Geophys. Res. Lett., v. 3, p. 743-746.

DePaolo, D.J., 1981c, Neodymium isotopes in the Colorado Front Range and crust-mantle evolution in the Proterozoic: Nature, V. 291, p. 193-196.

DePaolo, D.J., 1988, Neodymium Isotope Geochemistry: an Introduction, Springer-Verlag, Germany, pp. 187.

Dickin, A., McNutt, R., 1989, Nd model age mapping of the southeast margin of the Archean foreland in the Grenville Province of Ontario: Geology, v. 17, p. 299-302.

Dickin, A.P., McNutt, R.H., and Clifford, P.M., 1990, A neodymium isotope study of plutons near the Grenville Front in Ontario: Chemical Geology, v. 83, p. 315-324.

Dickin, A.P., and McNutt, R.H., 1990, Nd model-age mapping of Grenville Lithotectonic domains: Mid-Proterozoic crustal evolution in Ontario in Gower, C.F., Rivers, T., and Ryan, B., eds., Mid-Proterozoic Laurentia-Baltica: Geological Association of Canada, Special Paper #38, p. 79-94.

Dickin, A.P., and Higgins,M.D., 1992, Sm/Nd evidence for a major 1.5 Ga crust-forming event in the Central Grenville Province: Geology, v. 20, p. 137-140.

Easton, R.M., 1986, Geochronology of the Grenville Province in Moore, J.M., Davidson, A., Baer, A.J., eds., The Grenville Province: Geological Association of Canada Special Paper #31, p. 127-173.

Faure, G., Principles of Isotope Geology. John Wiley & Sons, 589p.

Frith, R.A., and Doig, R., 1973, Rb-Sr isotopic ages and petrologic studies of the rocks in the Lac St. Jean area, Quebec: Canadian Journal of Earth Sciences, V. 10, p. 881- 899.

Frith, R.A., and Doig, R., 1975, Pre-Kenoran tonalitic gneisses in the Grenville province: Canadian Journal of Earth Sciences, v. 12, p. 844-849.

Goldstein, S.L., O'Nions, R.K., Hamilton, P.J., 1984, A Sm-Nd isotopic study of atmospheric dusts and particulates from major river systems: Earth Planet. Sci. Lett., v. 7 p. 93-98.

Guo, A., and Dickin, A., 1992, Tectonic significance of Nd model age mapping in the Grenville province of western Quebec, Lithoprobe, Abitibi/Grenville Transect, Report No. 25.

Hamner, S., 1988, Ductile thrusting at mid-crustal level, southwestern Grenville Province: Can. J. Earth Sci., v. 25, p. 1049-1059.

Heaman, L., McNutt, R., Krogh, T., 1986, Geological significance of U-Pb and Rb-Sr ages for two pre-tectonic granites from the Central Metasedimentary Belt, Ontario:in Moore, J.M., Davidson, A., and Baer, A.J., eds., The Grenville Province: Geological Association of Canada Special Paper # 31, p. 209-221.

Hervet,M., Higgins, M., VanBreemen, O., Dickin, A., 1990, U-Pb age and Nd constraints on the Chicoutimi gneissic complex (CGC) at the southeast border of the Lac St. Jean anorthosite complex (LSJAC), Grenville province, Quebec, Canada: Eos (Transactions, American Geophysical Union), v. 71, p. 661-662.

Holmden, C., Dickin, A., 1995, Early Proterozoic evolution of the Grenville belt: Evidence from Nd isotopic mapping, North Bay, Ontario (Submitted to Can. Journal of Earth Sci.)

Holmes, A., 1946, An estimation of the age of the Earth: Nature, v. 157, p. 680-684.

Houtermanns, F., 1946, Die Isotopenhaufigkeiten im naturlichen Blei und das Alter des Urans: Naturwissenschaften, v. 33, p. 185-186.

Irvine T.N., and Barager, W.R.A., 1971, A guide to the chemical classification of common volcanic rocks: Canadian Journal of Earth Sciences, v. 8, p. 523-548.

Jacobsen, S., Wasserburg, G., 1978a, The interpretation of Nd, Sr, and Pb isotope data from archean migmatites in Loften-Versteraalen, Norway: Earth and Planetary Sci. Lett., v. 41 p. 245-253.

Ketchum, J., Culshaw, N., Jamieson, R., Krogh, T., 1994, Extensional reactivation of the Allochthon Boundary Thrust, southwest Grenville orogen: Geological association of Canada, Mineralogical association of Canada Program with Abstracts, v. 19, p. A56.

Krogh, T., 1982b, Improved accuracy of U/Pb zircon ages by the creation of more concordant systems using an air abrasion technique: Geochim. Cosmochim. Acta, v. 46, p. 637-649.

Krogh, T., Heaman, L., Tucker, R., 1990, Terrane identification in the Grenville province using igneous, metamorphic, and detrital U-Pb mineral ages in Proceedings of the Abitibi/Grenville Workshop, Oct. 1990, Montreal, unpaginated.

Kober, B., 1987, Single zircon evaporation combined with Pb^+ emitter bedding for $^{207}Pb/^{206}Pb$-age investigations using thermal ion mass spectrometry, and implications to zirconology: Contrib. Mineral Petrol., v. 96, p. 63-71.

Kober, B., Pidgeon, R.T., and Lippolt, H.J., 1989, Single zircon dating by stepwise Pb-evaporation constrains the Archean history of detrital zircons from the Jack Hills, Western Australia; Earth Planet. Sci. Lett., v. 91, p. 286-296.

Machado, N., and Martignole, J., 1988, First U-Pb age for magmatic zircon in anorthosites: The case of the Pentecote intrusion in Quebec: Geological Association of Canada Program with Abstracts, v. 13, p. A76.

Martin, C.L., 1992, Mid-proterozoic evolution of the Grenville Belt: evidence from Neodymium isotopic mapping, Bancroft, Ontario, unpublished B.Sc. Thesis, McMaster University, Hamilton, Ontario, pp.75.

Moorbath, S., Welke, H., Gale, N., 1969, The significance of Pb isotopes in ancient, high-grade metamorphic basement complexes, as typified by the Lewisian rocks of northwest Scotland, Earth and Planet. Sci. Lett., v. 6, p. 245-256.

Moorbath, S., Taylor, P., 1985, Precambrian geochronology and the geological record in N.J. Snelling, The chronology of the Geological record, Geol. Soc. London, Mem. No 10, p. 10-28.

Moore, J.M., 1986, Introduction: The "Grenville Problem", then and now, in Moore, J.M., Davidson, A., and Baer, A.J., eds., The Grenville Province: Geological Association of Canada Special Paper #31, p. 1-11.

Mueller, E.L., 1991, Pb-Pb zircon dating by direct evaporation: Method development and selected geological applications, unpublished M.Sc. Thesis, McMaster University, Hamilton, Ontario, pp. 158.

Nadeau, L., and VanBreeman, O., 1994, Do the 1.45-1.39 Ga Montauban Group and the La Bostonnais complex constitute a Grenvillian accreted terrane? : Geological Association of Canada, Mineralogical Association of Canada v. 19, p. A81.

Nelson, B.K., and DePaolo, D.J., 1985, Rapid production of continental crust 1.7-1.9 b.y. ago: Nd isotope evidence from the basement of the North American mid-continent: Geological Society of America Bulletin, v. 96, p. 746-754.

Owen, J., Erdmer, P., 1990, Middle Proterozoic geology of the Long Range Inlier, Newfoundland: Regional significance and tectonic implications in C.F. Gower, T. Rivers, and A.B. Ryan, eds., Mid-Proterozoic Laurentia-Baltica: Geological Association of Canada Special Paper 38, p. 215-231.

Pearce, J., Harris, N., Tindle, A., 1984, Trace element discrimination diagram for the tectonic interpretation of granitic rocks: J. Petrol., v. 25, p. 956-983.

Rivers, T., Chown, E., 1986, The Grenville orogen in eastern Quebec and western Labrador - Definition, identification and tectonometamorphic relationships of autochthonous, parautochthonous and allochthonous terranes in Moore, J.M., Davidson, A., and Baer, A.J., eds., The Grenville Province: Geological Association of Canada Special Paper

31, P. 31-50.

Rivers, T., Martignole, J., Gower, C., Davidson, A., 1989, New tectonic divisions of the Grenville province, southeastern Canadian Shield: Tectonics, v. 8, p. 63-84.

Rivers,T., van Gool, J., Connelly, J., 1993, Contrasting tectonic styles in the northern Grenville Province: implications for the dynamics of orogenic fronts: Geology, v. 21, p. 1127-1130.

Samson, S., Patchett, P., 1991, The Canadian cordillera as a modern analogue of Proterozoic crustal growth: Australian J. Earth Sci., v. 38, p. 595-611.

Stacey, J., Kramers, J., 1975, Approximation of terrestrial Pb isotope evolution by a two-stage model: Earth Planet. Sci. Lett., v. 26, p. 207-221.

Thomas, A., Nunn, G., 1986, The Labradorian orogeny: evidence for a newly identified 1600 to 1700 Ma orogenic event in Grenville province crystalline rocks from central Labrador in Moore, J.M., Davidson, A., and Baer, A.J., eds., The Grenville Province: Geological Association of Canada Special Paper # 31, p. 175-189.

Thirwall, M., 1982, A triple filament method for rapid and precise analysis of rare-earth elements by isotope dilution: Chemical Geology, v. 35, p. 155-166.

VanBreemen, O., Davidson, A., Loveridge, W., Sullivan, R., 1986, U/Pb zircon geochronology of Grenville tectonites, granulites, and igneous precursors, Parry Sound, Ontario, in Moore, J.M., Davidson, A., and Baer, A.J., eds., The Grenville Province: Geological Association of Canada Special Paper # 31, p. 191-207.

Wardle, R., Rivers, T., Gower, C., Nunn, G., Thomas, A., 1986, The northeastern Grenville Province: new insights in Moore, J.M., Davidson, A., Baer, A.J., eds., The Grenville Province: Geological Association of Canada Special Paper # 31, p. 13-29.

White, W., Dupre, B., 1986, Sediment subduction and magma genesis in the Lesser Antilles: Isotopic and trace element constraints: J. Geophys. Res., v. 91, p. 5927-5941.

Whitehouse, M., 1990, Isotopic evolution of the southern Outer Hebridean Lewisian gneiss complex: constraints on late Archean source regions and the generation of transposed Pb-Pb palaeoisochrons: Chemical Geology (Isotope Geoscience Division), v. 86, p. 1-20.

Windley, B., Tarney, J., 1986, The structural evolution of orogenic belts, present and past in Dawson, J.B., Carswell, D.A., Hall, J., and Wedepohl, K.H., eds., The Nature of the Lower Continental Crust: Geological Society Special Publication # 24, p. 221-230.

Wynne-Edwards, H., 1972, The Grenville Province, in Price, R.A., and Douglas, R.J.W., eds., Variations in Tectonic Styles in Canada: Geological Association of Canada Special Paper # 11, p. 263-334.

	GV5	GV6	LU11	DO16	DO13	DO14	DO17	DO18	DO6	DO9
SIO2	65.55	62.85	67.39	64.41	69.98	68.42	66.18	67.06	63.76	60.87
TIO2	0.60	0.80	0.41	0.39	0.34	0.39	0.53	0.38	0.72	0.89
AL2O3	15.96	16.48	17.35	17.85	15.90	16.50	16.07	16.29	17.22	17.03
FE2O3	4.81	6.27	2.70	3.84	2.41	3.28	4.97	3.54	5.22	7.36
FEO	nd	nd	nd	nd	nd	nd	nd	nd	nd	nd
MNO	0.09	0.11	0.04	0.07	0.03	0.05	0.09	0.08	0.08	0.19
MGO	1.76	2.07	1.28	1.47	0.77	1.15	1.60	1.43	2.00	0.66
CAO	4.04	4.43	4.05	4.22	2.89	3.76	4.97	5.17	4.16	2.90
NA2O	3.75	3.66	5.01	5.66	5.69	5.02	4.59	5.08	4.74	5.52
K2O	3.17	2.99	1.54	1.82	1.83	1.25	0.77	0.77	1.84	4.26
H2O+	nd	nd	nd	nd	nd	nd	nd	nd	nd	nd
H2O-	nd	nd	nd	nd	nd	nd	nd	nd	nd	nd
P2O5	0.29	0.34	0.21	0.26	0.16	0.17	0.24	0.21	0.26	0.32
TOTAL	100.00	100.00	100.00	100.00	100.00	100.00	100.00	100.00	100.00	100.00
Y	24.00	24.00	6.00	10.00	7.00	5.00	17.00	9.00	18.00	35.00
Nb	11.40	11.60	7.50	6.50	5.50	5.60	8.80	6.30	14.70	20.30

	LSJ27	LSJ4	LSJ5	LSJ6	LSJ7	LSJ9MA178.	MA182.	LSJ10	LSJ13	
SIO2	66.63	69.80	55.41	70.21	62.77	64.16	72.05	72.05	60.87	74.79
TIO2	0.83	0.40	1.99	0.50	0.64	0.80	0.33	0.33	0.98	0.27
AL203	17.03	15.68	16.97	15.11	17.63	16.60	15.46	15.46	16.42	13.55
FE203	6.21	2.95	8.65	2.92	5.33	5.45	2.35	2.35	6.92	1.63
FEO	nd	nd	nd	nd	nd	nd	nd	nd	nd	nd
MNO	0.13	0.05	0.17	0.06	0.12	0.01	0.06	0.06	0.22	0.03
MGO	1.62	0.86	2.46	0.94	1.61	1.67	0.55	0.55	2.13	0.13
CAO	1.88	2.75	3.90	2.35	4.16	4.13	1.46	1.46	4.97	0.94
NA20	2.92	4.90	4.76	3.42	5.83	4.37	3.17	3.17	4.69	3.15
K20	2.70	2.51	4.72	4.35	1.71	2.62	4.46	4.46	2.55	5.48
H20+	nd	nd	nd	nd	nd	nd	nd	nd	nd	nd
H20-	nd	nd	nd	nd	nd	nd	nd	nd	nd	nd
P205	0.05	0.11	0.96	0.15	0.19	0.19	0.10	0.10	0.26	0.02
TOTAL	100.00	100.00	100.00	100.00	100.00	100.00	100.00	100.00	100.00	100.00
Y	nd	nd	nd	nd	nd	nd	18.00	27.00	nd	nd
Nb	nd	nd	nd	nd	nd	nd	8.60	10.50	nd	nd

	LSJ15	LSJ17	LSJ19	LSJ24	LSJ26	MA132.	MA153.	NS20	NS32A	NS32B
SIO2	62.19	64.71	64.76	60.29	57.51	71.40	70.64	68.98	67.82	73.04
TIO2	0.47	0.51	0.66	0.66	0.60	0.57	0.31	0.28	0.73	0.28
AL2O3	19.51	17.79	16.51	17.32	21.77	13.90	16.26	17.01	16.36	14.83
FE2O3	3.83	4.77	5.66	6.53	4.52	4.15	2.39	1.92	4.16	2.08
FEO	nd	nd	nd	nd	nd	nd	nd	nd	nd	nd
MNO	0.05	0.08	0.08	0.10	0.15	0.07	0.06	0.04	0.08	0.03
MGO	1.50	2.11	2.95	3.21	1.37	0.32	0.47	0.67	1.13	0.54
CAO	5.58	4.30	4.17	6.08	6.06	1.81	2.88	2.56	2.59	1.10
NA2O	5.47	3.82	3.63	4.34	5.68	3.49	4.39	5.33	4.70	3.41
K2O	1.27	1.78	1.38	1.28	2.07	4.20	2.53	3.15	2.27	4.66
H2O+	nd	nd	nd	nd	nd	nd	nd	nd	nd	nd
H2O-	nd	nd	nd	nd	nd	nd	nd	nd	nd	nd
P2O5	0.13	0.12	0.20	0.19	0.27	0.09	0.07	0.06	0.15	0.03
TOTAL	100.00	100.00	100.00	100.00	100.00	100.00	100.00	100.00	100.00	100.00
Y	nd	nd	nd	nd	nd	50.00	15.00	13.00	31.00	27.00
Nb	nd	nd	nd	nd	nd	14.50	5.10	7.00	11.80	7.20

	LT3	LSJ1	NS9	NS29MA199.		RT3	RT2	TD10	TD11	TD16
SIO2	68.17	65.79	67.09	63.35	67.87	69.30	68.78	61.23	59.55	69.75
TIO2	0.56	0.46	0.36	0.65	0.37	0.61	0.22	0.71	0.78	0.36
AL203	14.60	16.83	17.63	18.11	17.68	14.97	15.57	18.00	16.78	16.14
FE203	5.29	5.78	3.43	5.17	3.01	4.22	3.77	5.39	6.90	2.88
FEO	nd	nd	nd	nd	nd	nd	nd	nd	nd	nd
MNO	0.07	0.10	0.08	0.06	0.01	0.10	0.07	0.13	0.12	0.04
MGO	1.65	1.79	1.22	2.07	0.89	1.26	1.11	1.83	2.66	0.87
CAO	2.79	3.43	4.01	4.86	3.98	2.98	2.32	4.24	5.27	3.55
NA20	2.66	3.94	4.22	4.11	4.60	3.46	4.64	5.39	4.22	5.19
K20	4.04	1.61	1.78	1.43	1.44	2.88	3.29	2.70	3.36	1.06
H20+	nd	nd	nd	nd	nd	nd	nd	nd	nd	nd
H20-	nd	nd	nd	nd	nd	nd	nd	nd	nd	nd
P205	0.17	0.27	0.17	0.19	0.16	0.22	0.22	0.39	0.36	0.16
TOTAL	100.00	100.00	100.00	100.00	100.00	100.00	100.00	100.00	100.00	100.00
Y	nd	59.00	10.00	13.00	11.00	41.00	11.00	28.00	26.00	5.00
Nb	nd	15.90	6.90	4.40	3.90	19.90	11.90	10.70	14.10	4.80

	TD18	TD19	MA103	MA121	LU12	LU14	LU3	LU4	LU5	LU6
SIO2	66.65	70.49	67.61	68.44	57.88	66.45	69.24	66.04	63.88	65.99
TIO2	0.45	0.30	0.86	0.27	0.77	0.41	0.70	0.51	0.67	0.92
AL203	16.47	16.07	14.94	17.08	18.20	17.36	14.29	16.34	16.64	14.81
FE203	4.29	2.39	5.41	3.42	9.34	3.28	4.54	3.99	5.10	6.25
FEO	nd	nd	nd	nd	nd	nd	nd	nd	nd	nd
MNO	0.05	0.03	0.08	0.14	0.18	0.05	0.08	0.05	0.07	0.10
MGO	1.42	0.71	0.97	0.71	0.70	1.11	0.95	1.91	2.44	1.22
CAO	4.48	3.16	2.88	4.17	5.10	3.57	2.61	4.28	4.33	3.37
NA20	4.77	5.07	3.28	3.71	5.49	5.50	3.57	5.42	4.43	3.85
K20	0.97	1.63	3.78	1.98	2.02	2.03	3.77	1.33	2.12	3.17
H20+	nd	nd	nd	nd	nd	nd	nd	nd	nd	nd
H20-	nd	nd	nd	nd	nd	nd	nd	nd	nd	nd
P205	0.45	0.16	0.19	0.09	0.30	0.24	0.25	0.13	0.32	0.31
TOTAL	100.00	100.00	100.00	100.00	100.00	100.00	100.00	100.00	100.00	100.00
Y	6.00	nd	52.00	15.00	47.00	13.00	45.00	nd	11.00	47.00
Nb	5.30	3.50	14.30	6.50	11.90	5.40	13.90	nd	7.30	16.30

	MS6	MS8	RT1	GA4	GA5	GA6	GA7	GA8	GA9	GV4
SIO2	60.46	50.91	66.94	65.97	59.16	65.26	58.86	64.14	59.90	63.86
TIO2	0.71	0.84	0.79	0.50	0.78	0.55	0.80	0.67	0.68	0.65
AL2O3	18.97	21.21	15.03	16.76	18.05	15.59	17.47	15.87	16.88	17.49
FE2O3	5.87	8.68	5.73	3.76	6.66	4.91	6.56	5.00	6.56	4.25
FEO	nd	nd	nd	nd	nd	nd	nd	nd	nd	nd
MNO	0.12	0.12	0.14	0.09	0.15	0.09	0.13	0.09	0.12	0.07
MGO	0.83	3.06	0.80	1.28	2.33	2.08	2.68	2.12	2.97	1.39
CAO	3.27	8.58	2.87	3.27	5.02	4.14	5.60	4.23	5.69	3.57
NA2O	4.24	5.01	3.66	4.82	5.40	3.66	5.02	3.56	3.95	5.12
K2O	5.30	1.06	3.76	3.27	2.03	3.46	2.41	4.04	2.89	3.29
H2O+	nd	nd	nd	nd	nd	nd	nd	nd	nd	nd
H2O-	nd	nd	nd	nd	nd	nd	nd	nd	nd	nd
P2O5	0.24	0.54	0.29	0.29	0.42	0.27	0.47	0.29	0.35	0.31
TOTAL	100.00	100.00	100.00	100.00	100.00	100.00	100.00	100.00	100.00	100.00
Y	49.00	26.00	69.00	nd	34.00	23.00	24.00	22.00	22.00	26.00
Nb	15.10	4.70	20.70	nd	17.70	12.70	10.30	12.90	10.00	13.10

	D05	FA7
SIO2	63.38	69.92
TIO2	0.67	0.67
AL203	17.28	14.02
FE203	4.61	4.38
FEO	nd	nd
MNO	0.11	0.08
MGO	1.50	0.66
CAO	3.74	2.24
NA2O	4.42	3.70
K2O	4.03	4.09
H2O+	nd	nd
H2O-	nd	nd
P2O5	0.26	0.23
TOTAL	100.00	100.00
Y	39.00	53.00
Nb	13.70	16.50